arXiv:hep-ph/9211255v1 16 Nov 1992

Relativistic constituent quark model for baryons

Inaugural-Dissertation
zur
Erlangung der Philosophischen Doktorwürde
vorgelegt der
Philosophischen Fakultät II
der
Universität Zürich

von
Felix Schlumpf
aus Zürich ZH

Begutachtet von den Herren
Prof. Dr. G. Rasche und Prof. Dr. W. Jaus

Zürich 1992

Dedicated to Priska

Now we are seeing a dim reflection in a mirror;
but then we shall be seeing face to face.
The knowledge that I have now is imperfect;
but then I shall know as fully as I am known.
1. Cor. 13.12

Abstract

The electroweak properties of nucleons and hyperons are calculated in a relativistic constituent quark model. The baryons are treated as three quark bound states, and the diagrams of perturbation theory are considered on the light front. The electroweak properties of the baryons are of nonperturbative nature and can be represented by one-loop diagrams. We consider different extensions of the simplest model:

- Quark form factors.
- Configuration mixing of the wave function.
- Asymmetric wave function.
- Wave function different from the one of a harmonic oscillator valid up to energies of more than 30 GeV^2.

A comprehensive study of various baryonic properties is given:

- Elastic form factors of the nucleon.
- Magnetic moments of the baryon octet.
- Semileptonic weak form factors.

This analysis also gives the Kobayashi-Maskawa matrix element V_{us} and a sound symmetry breaking scheme for the Cabibbo theory (see Sec. 4.4).

A consistent physical picture appears in this work. The nucleon consists of an unmixed, symmetric three quark state, the wave function of the hyperons is however asymmetric with a spin-isospin-0 diquark. Only for the strangeness-changing weak decay do we need nontrivial form factors.

Contents

Abstract **iii**

1 Introduction **1**

2 Light-front formalism for baryons **5**
2.1 Relativistic three-body equation 5
2.2 Current matrix element 8
2.3 Wave function 10
2.4 Extensions of the model 13
2.4.1 Minimal quark model 13
2.4.2 Quark structure 13
2.4.3 Configuration mixing 13
2.4.4 Asymmetric wave function 15
2.5 Discussion of the wave function 16

3 Electromagnetic properties **19**
3.1 Nucleon electromagnetic form factors 19
3.1.1 Calculation of nucleon form factors 19
3.1.2 Results and conclusions 20
3.2 Magnetic moment of the baryon octet 27
3.2.1 $F_2(0)$ in the quark model 27
3.2.2 Results and conclusions 29

4 Hyperon semileptonic beta decay **31**
4.1 Hyperon semileptonic decay 31
4.2 The form factors in the quark model 36
4.3 Results 39
4.3.1 The rates and $f_1(0), g_1(0)$ 39
4.3.2 $f_2(0)$ and $g_2(0)$ 42
4.3.3 K^2-dependence of the form factors 43
4.4 Cabibbo fit and V_{us} 44
4.5 Conclusions 47

5 Asymmetric wave functions **49**
5.1 The diquark model 49
5.2 Results and discussions 51

6 Discussion and conclusions **55**

A Computational methods **57**
A.1 Symbolic calculation 58
A.2 Numerical calculation 62
A.3 Fitting procedures 63
A.4 Program listing 64

Acknowledgments **69**

Bibliography **71**

Index **75**

List of Figures

2.1 Feynman diagrams for the elastic form factor of baryons. 8
2.2 Feynman diagrams for the elastic form factor. 8
2.3 Feynman diagrams that represent the transition of the baryon state. 10
2.4 Different wave functions used by other authors and used in this work. . . . 18

3.1 Parameter space for the nucleon sector. 21
3.2 The proton form factor $F_{1p}(K^2)$. 22
3.3 The proton form factor $F_{2p}(K^2)$. 23
3.4 The proton form factor $F_{1p}(K^2)$. 24
3.5 The proton form factor $F_{2p}(K^2)$. 24
3.6 The neutron form factor $F_{1n}(K^2)$. 25
3.7 The neutron form factor $F_{2n}(K^2)$. 25
3.8 Proton form factor $G_{Mp}(K^2)$. 26

4.1 The axial vector form factor $g_1(K^2)$ for the np-transition. 43

5.1 Parameter space of the asymmetric wave function fit. 52

A.1 Flow chart of the basic steps for this thesis. 58
A.2 Example of a density plot for the magnetic moments of the baryon octet. . 64

List of Tables

2.1 Parameters for the configuration mixing of the baryon octet. 14

3.1 The parameters of the constituent quark model. 22
3.2 The quantity $F'(0)$ for the nucleons. 22
3.3 Magnetic moments of the baryon octet and transition moment for $\Sigma^0 \to \Lambda\gamma$ in units of the nuclear magneton. 30

4.1 Ratio of the rate to the rate with vanishing lepton mass. 34
4.2 Radiative corrections to the semileptonic decay rates. 34
4.3 Matrix elements for weak beta decay. 36
4.4 Parameters in Eq. (4.20). 37
4.5 Parameters in Eq. (4.22). 38
4.6 Results for $\Delta S = 0$ weak beta decay. 40
4.7 Results for $\Delta S = 1$ weak beta decay. 41
4.8 The parameters M_V and M_A for various models. 44
4.9 Fits to the Cabibbo model. 45
4.10 Symmetry breaking for f_1. The ratio $f_1/f_1^{\mathrm{SU(3)}}$ is shown. 45
4.11 Symmetry breaking for g_1. The ratio $g_1/g_1^{\mathrm{SU(3)}}$ is shown. 46

5.1 The parameters of the asymmetric constituent quark model. 51
5.2 Electroweak properties of the baryon octet. 53
5.3 Comparison with other models for the electroweak properties of the baryon octet. 54

Chapter 1

Introduction

The purpose of this thesis is to present the results of comprehensive calculations of electromagnetic and weak form factors of the baryon octet in a relativistic constituent quark model. Ever since the proposal of the quark model in the early sixties by Gell-Mann [1], the modeling of the hadrons has been a very active area of theoretical research. There are many interesting current questions, which can only be answered by quark model calculations. New high-statistics data from hyperon beta decay raise questions about SU(3) breaking [2, 3] and the related controversy about the meson and baryon derived values for the Kobayashi-Maskawa matrix element V_{us} has not been solved yet [4]. This value is important for studying the unitarity of the Kobayashi-Maskawa matrix. There are also many recent papers on the magnetic moments of the baryon octet, which are a hard testing ground for various hadronic models.

In this thesis we consider a relativistic constituent quark model on the light front that was first formulated by Terent'ev and Berestetskii [5, 6]. It has been applied to various hadronic processes by Aznauryan et al. [7, 8, 9]. Recently, new studies have been carried out by Jaus in the meson sector [10, 11, 12] and by Chung and Coester on the electromagnetic form factors of the nucleons [13]. Dziembowski et al. [14, 15, 16] and Weber et al. [17, 18] treat the Melosh transformation of the quark spin in a "weak-binding approximation" of questionable validity.

Nonrelativistic constituent quark models are successful in describing the mass spectrum of baryons (for a review, see Refs. [19, 20, 21]). The dominant effects of the gluonic degrees of freedom are absorbed into constituent quark masses and into an effective confining potential. In addition, effective dynamics inspired by QCD has been considered in Refs. [22, 23]; but this is inconsistent for light quarks. A review in Ref. [24] gives an estimate of the r.m.s. radius of the nucleon from 0.8 fm (derived from the charge radius) to 0.4 fm (obtained from hyperon decays). Considering the uncertainty principle these values of the r.m.s. radius imply a quark momentum in the range 250–500 MeV, which has to be compared with the light constituent quark mass in the range 210–360 MeV. The use of nonrelativistic quantum mechanics is therefore inconsistent, even for static properties of the hadrons, because the relativistic corrections are of the order $\langle p^2 \rangle / m^2$ and must be expected to be large.

In a relativistic theory the Poincaré invariance has to be respected; this means, on the quantum level, the fulfillment of the commutation relations between the generators of the

Poincaré group. Dirac [25] has given a general formulation of methods to simultaneously satisfy the requirements of special relativity and Hamiltonian quantum mechanics. An extension of the Dirac classes of dynamics can be found in Ref. [26]. The light front scheme is in particular distinguished from the other Dirac classes. Among the ten generators of the Poincaré group, there are in the light front approach seven (the maximal number) generators of kinematical character, and only the remaining three generators contain interaction, which is the minimal possible number. The light front dynamics is therefore the most economical scheme for dealing with a relativistic system. If we introduce the light front variables $p^{\pm} \equiv p^0 \pm p^3$, the Einstein mass relation $p_\mu p^\mu = m^2$ is linear in p^- and linear in p^+, in contrast to the quadratic form in p^0 and $\vec{p}$ in the usual dynamical scheme. A consequence is a single solution of the mass shell relation in terms of p^-, in contrast to two solutions for p^0:

$$p^- = (p_\perp^2 + m^2)/p^+ \,, \qquad p^0 = \pm\sqrt{\vec{p}^{\,2} + m^2} \,. \tag{1.1}$$

The quadratic relation of p^- and $p_\perp \equiv (p^1, p^2)$ in Eq. (1.1) resembles the nonrelativistic scheme [27], and the variable p^+ plays the role of "mass" in this nonrelativistic analogy. It is therefore a good idea to introduce relative variables like the Jacobi momenta when dealing with several particles. As in the nonrelativistic scheme such variables allow us to decouple the center of mass motion from the internal dynamics. Hence we do not have the problems with the center of mass motion which occur in the bag model. The light front scheme shows another attractive feature that it has in common with the infinite momentum technique [28]. In terms of the old fashioned (Heitler type, time ordered, pre-Feynman) perturbation theory, the diagrams with quarks created out of or annihilated into the vacuum do not contribute. The usual qqq quark structure is therefore conserved as in the nonrelativistic theory. It is, however, harder to get the hadron states to be eigenfunctions of the spin operator [29].

In this thesis we describe the baryon as a three quark bound state with relativistic Faddeev equations and a Bethe-Salpeter interaction kernel. Using the quasiparticle method these equations can be reduced to a relativistic Schrödinger equation with an effective potential. We could either start with an Ansatz for the effective potential and derive the wave function or else start with the wave function itself. For simplicity we take the latter approach and work with an Ansatz for the wave function. In addition to the standard Gauss shaped wave function we also investigate a Lorentz shaped one that fits the nucleon form factors up to more than 30 GeV^2. In addition to the minimal quark model (MQM), which uses the smallest number of parameters, we also consider some extensions to the MQM: structure of the constituent quark, several different radial wave functions, and asymmetry in the wave function. For the MQM we have five parameters: the quark masses $m_u = m_d \equiv m_{u/d}$ and m_s, and the wave function parameters β for the nucleons, the Σs and the Ξs respectively, which essentially determine the confinement scale. For the asymmetric model we have three additional parameters: instead of β we have β_q and β_Q. In the configuration mixing case there are some more parameters that determine the mixing and the confinement scale of the various radial wave functions. For the structure of the constituent quarks there are seven additional parameters, i.e. the anomalous quark moments f_{2u}, f_{2d}, f_{2s}, and the vector and axial weak form factors f_{1ud}, f_{1us}, g_{1ud}, and g_{1us} at zero momentum transfer. Our goal is to keep the number of parameters as small

as possible in order to have a model with predictive power. On the other hand the MQM is not able to fit all electroweak properties of the baryons. The parametric dependence on the data is highly nonlinear, so it is not obvious that even 15 parameters may fit two experimental data. Our analysis gives a physical picture of a baryon, which is an asymmetric three quark state with quark form factors in the weak sector.

This thesis is organized as follows:

Chapter 2 In this Chapter we present the light front formalism for bound states of three quarks. We start with the light front variables, elaborate on the quasipotential reduction of the Bethe-Salpeter equation, and calculate the one loop diagram. We also study the wave function and compare it with the one given by Chernyak and Zhitnisky [30], and Lepage and Brodsky [31].

Chapter 3 In Sec. 3.1 we give the details of our calculation of the electromagnetic form factors. We fit the mass $m_{u/d}$ and the scale parameter β to the data of the magnetic moments of the proton and neutron, and the weak axial form factor $g_1(n \to p)$. We not only examine the Gauss shaped wave function, but also a Lorentz shaped one. With the latter it is possible to fit the data in the whole experimentally accessible energy region up to more than 30 GeV^2. In Sec. 3.2 we derive the explicit formulae for the magnetic moments. The MQM is not able to give a reasonable fit, even with non-zero quark anomalous moments. Only an asymmetric wave function can fit all magnetic moments of the baryon octet as is shown in Chapter 5. The mass m_s and the range parameters $\beta_{\Sigma/\Lambda}$ and β_Ξ can be fixed in Chapter 3.

Chapter 4 Semileptonic beta decay of hyperons is an active area of current research, both experimentally with high-statistic data and theoretically with the problem of the Kobayashi-Maskawa matrix element V_{us} [2, 3]. In addition to the calculation of the weak form factors and their derivatives we present a Cabibbo fit that gives almost the same value for V_{us} as the one recently published [4].

Chapter 5 The smallest extension to the MQM is to use an asymmetric wave function, in which the scale parameter β is replaced by two scales β_Q and β_q corresponding to the quark-diquark binding and the quark-quark binding within the diquark. In the limit of two particles this extended MQM reduces to a MQM of the meson, which is successfully used in Refs. [10, 12].

Chapter 6 summarizes our investigation. We discuss the physical picture derived from our analysis and draw some conclusions.

Appendix A describes in detail the symbolic and numerical methods used in this thesis.

Appendix ?? contains all formulae for the spin matrix elements to all orders of the momentum transfer.

The index at the end of this thesis should give quick access to special topics.

Chapter 2

Light-front formalism for baryons

2.1 Relativistic three-body equation

To specify the dynamics of a many-particle system one has to express the ten generators of the Poincaré group P_μ and $M_{\mu\nu}$ in terms of dynamical variables. The kinematic subgroup is the set of generators that are independent of the interaction. There are five ways to choose these subgroups [32]. Usually a physical state is defined at fixed x_0, and the corresponding hypersurface is left invariant under the kinematic subgroup.

We shall use the light-front formalism which is specified by the invariant hypersurface $x^+ = x^0 + x^3 =$ constant. The following notation is used: The four-vector is given by $x = (x^+, x^-, x_\perp)$, where $x^\pm = x^0 \pm x^3$ and $x_\perp = (x^1, x^2)$. Light-front vectors are denoted by an arrow $\vec{x} = (x^+, x_\perp)$, and they are covariant under kinematic Lorentz transformations [33]. The three momenta $\vec{p}_i$ of the quarks can be transformed to the total and relative momenta to facilitate the separation of the center of mass motion [34].

$$\begin{aligned} \vec{P} &= \vec{p}_1 + \vec{p}_2 + \vec{p}_3, \quad \xi = \frac{p_1^+}{p_1^+ + p_2^+} , \quad \eta = \frac{p_1^+ + p_2^+}{P^+} , \\ q_\perp &= (1-\xi)p_{1\perp} - \xi p_{2\perp} , \quad Q_\perp = (1-\eta)(p_{1\perp} + p_{2\perp}) - \eta p_{3\perp} . \end{aligned} \tag{2.1}$$

Note that the four-vectors are not conserved, i.e. $p_1 + p_2 + p_3 \neq P$. In the light-front dynamics the Hamiltonian takes the form

$$H = \frac{P_\perp^2 + \hat{M}^2}{2P^+} , \tag{2.2}$$

where $\hat{M}$ is the mass operator with the interaction term W

$$\begin{aligned} \hat{M} &= M + W , \\ M^2 &= \frac{Q_\perp^2}{\eta(1-\eta)} + \frac{M_3^2}{\eta} + \frac{m_3^2}{1-\eta}, \\ M_3^2 &= \frac{q_\perp^2}{\xi(1-\xi)} + \frac{m_1^2}{\xi} + \frac{m_2^2}{1-\xi} , \end{aligned} \tag{2.3}$$

with m_i being the masses of the constituent quarks. To get a clearer picture of M we transform to q_3 and Q_3 by

$$\begin{aligned} \xi &= \frac{E_1+q_3}{E_1+E_2}\,, \quad \eta = \frac{E_{12}+Q_3}{E_{12}+E_3}\,, \\ E_{1/2} &= (\mathbf{q}^2+m_{1/2}^2)^{1/2}\,, \quad E_3=(\mathbf{Q}^2+m_3^2)^{1/2}\,, \quad E_{12}=(\mathbf{Q}^2+M_3^2)^{1/2}\,, \end{aligned} \tag{2.4}$$

where $\mathbf{q}=(q_1,q_2,q_3)$, and $\mathbf{Q}=(Q_1,Q_2,Q_3)$. The expression for the mass operator is now simply

$$M = E_{12}+E_3\,, \quad M_3 = E_1+E_2\,. \tag{2.5}$$

We shall assume only two-particle forces interacting in a ladder-type pattern so that the dynamics of the three-body system is governed by the Bethe-Salpeter (BS) interaction kernel for the two body system and the relativistic Faddeev equations.

Using the Faddeev decomposition for the vertex function $\Gamma=\Gamma^{(1)}+\Gamma^{(2)}+\Gamma^{(3)}$, we can write down a BS equation for the various components in operator notation

$$\Gamma^{(1)} = T^{(1)}G_2G_3(\Gamma^{(2)}+\Gamma^{(3)}) \tag{2.6}$$

with

$$G_i = \not{p}_i - m_i, \quad T^{(1)} = (1-VG_2G_3)^{-1}V\,, \tag{2.7}$$

and similarly for $\Gamma^{(2)}$ and $\Gamma^{(3)}$. V is the one gluon exchange kernel between two quarks, and T is already the ladder sum to all orders. It is useful to consider the second iteration of the vertex equation, which is given by:

$$\mathbf{\Gamma} = UG_1G_2G_3\mathbf{\Gamma}\,, \tag{2.8}$$

where $\mathbf{\Gamma}=(\Gamma^{(1)},\Gamma^{(2)},\Gamma^{(3)})$ and U is the matrix

$$U_{ij} = \begin{cases} T^{(i)}G_jT^{(k)} & \text{for } i\neq j \text{ with } k\neq i,j\,, \\ T^{(i)}(G_kT^{(l)}+G_lT^{(k)}) & \text{for } i=j \text{ with } k\neq l\neq i\,. \end{cases} \tag{2.9}$$

The four-dimensional Eq. (2.8) can be reduced to a three-dimensional equation

$$\mathbf{\Gamma} = Wg_3\mathbf{\Gamma}\,, \quad W=(1-UR_3)^{-1}U \tag{2.10}$$

by writing $G_1G_2G_3=g_3+R_3$ where g_3 has only three-particle singularities. We choose a g_3 which puts the quarks on their mass shells:

$$g_3 = (2\pi i)^2\int ds\frac{1}{P^2-s}\prod_{i=1}^{3}\delta^+(p_i^2-m_i^2)(\not{p}_i+m_i)\,, \tag{2.11}$$

where P is the total momentum of the bound state, $s=(p_1+p_2+p_3)^2$ and p_i are restricted by $p_i^+\geq 0$. We get

$$g_3 = (2\pi i)^2\delta(p_2^2-m_2^2)\delta(p_3^2-m_3^2)\Theta(\xi)\Theta(1-\xi)\Theta(\eta)\Theta(1-\eta)\frac{\Lambda^+(p_1)\Lambda^+(p_2)\Lambda^+(p_3)}{\xi\eta(P^2-M^2)} \tag{2.12}$$

with the spin projection operator

$$\Lambda^+(p_i) = \sum_\lambda u(p_i,\lambda)\bar{u}(p_i,\lambda) \ . \tag{2.13}$$

Writing

$$\begin{aligned}
\hat{g}_3 &= \frac{1}{P^2 - M^2} \ , \\
\hat{\Gamma}^{(i)} &= \left(\frac{M_3 M}{E_1 E_2 E_3 E_{12}}\right)^{1/2} \Gamma^{(i)} u(p_1\lambda_1)u(p_2\lambda_2)u(p_3\lambda_3) \ , \\
\hat{W}_{ij} &= \left(\frac{M_3 M_3' M M'}{E_1 E_1' E_2 E_2' E_3 E_3' E_{12} E_{12}'}\right)^{1/2} u(p_1\lambda_1)u(p_2\lambda_2)u(p_3\lambda_3) W_{ij} \bar{u}(p_1'\lambda_1')\bar{u}(p_2'\lambda_2')\bar{u}(p_3'\lambda_3')
\end{aligned} \tag{2.14}$$

we are led to the integral equation

$$\begin{aligned}
\hat{\Gamma}^{(i)}(\mathbf{q},\mathbf{Q},\lambda_1,\lambda_2,\lambda_3) &= \frac{1}{(2\pi)^6} \sum_{\lambda_1'\lambda_2'\lambda_3' j} \int d^3q' d^3Q' \hat{W}^{ij}(\mathbf{q},\mathbf{q}',\mathbf{Q},\mathbf{Q}',\lambda_1,\lambda_1',\lambda_2,\lambda_2',\lambda_3,\lambda_3') \\
&\quad \times \hat{g}_3(\mathbf{q}',\mathbf{Q}')\hat{\Gamma}^{(j)}(\mathbf{q}',\mathbf{Q}',\lambda_1',\lambda_2',\lambda_3') \ .
\end{aligned} \tag{2.15}$$

We can write this equation in terms of the wave function Ψ. The Faddeev decomposition is $\Psi = \Psi^{(1)} + \Psi^{(2)} + \Psi^{(3)}$, the relation to the vertex function is $\Psi^{(i)} = \hat{g}_3\hat{\Gamma}^{(i)}$, and writing $\mathbf{\Psi} = (\Psi^{(1)}, \Psi^{(2)}, \Psi^{(3)})$ we get

$$(M_B^2 - M^2)\mathbf{\Psi} = \hat{W}\mathbf{\Psi} \tag{2.16}$$

with M_B being the mass of the baryon. If we put $\hat{W} = MW + WM + W^2$ we see that the wave function is an eigenfunction of the mass operator $\hat{M}^2$, given in Eq. (2.3):

$$\hat{M}^2\Psi = M_B^2\Psi \tag{2.17}$$

which is equivalent to the equation usually used in constituent quark models [19]

$$(E_{12} + E_3 + W)\Psi = M_B\Psi \ . \tag{2.18}$$

This last equation is the starting point for an explicit calculation of the wave function, which has been done for the meson sector [35, 36].

2.2 Current matrix element

We would like to calculate the current matrix element $M^\mu = \langle B'|\bar{q}\gamma^\mu q|B\rangle$ corresponding to the Feynman diagram of Fig. 2.1 (a).

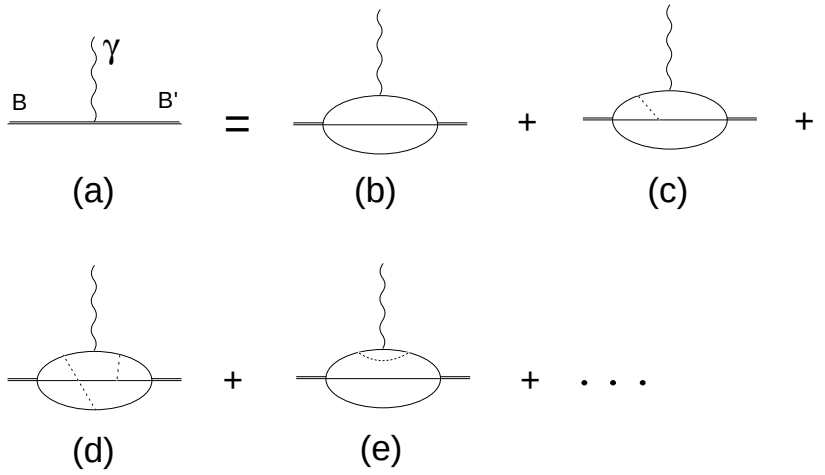

Figure 2.1: Feynman diagrams for the elastic form factor of baryons. Only the three quark core of the baryon is considered.

We restrict ourselves to the three quark core of the baryon. The diagrams of Fig. 2.1 (c+d), and (e) can be absorbed into the wave function and quark form factors, respectively. We are left with the diagram Fig. 2.1 (b).

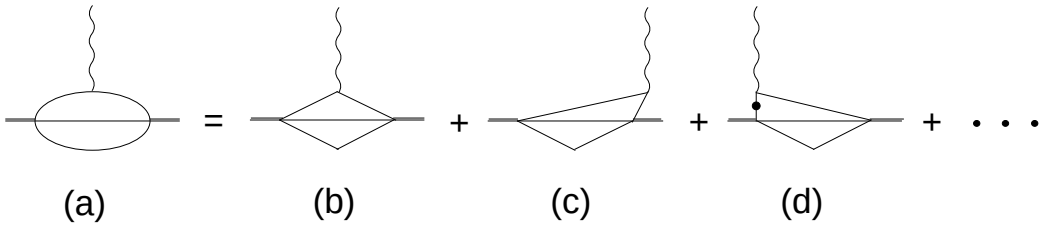

Figure 2.2: (a) Feynman diagram for the elastic form factor. (b)–(d) Time x^+-ordered diagrams corresponding to (a). Pointed lines represent instantaneous quark propagators.

In Fig 2.2, the Feynman diagram (a) is equivalent to the sum of diagrams (b) – (d) in the old-fashioned perturbation theory. If we consider x^+-ordering and put $K^+ = 0$, diagram (c) drops out because of conservation of +-momentum. The x^+-instantaneous propagator in diagram (d) is proportional to γ^+, and gives no contribution for $K^+ = 0$

since $(\gamma^+)^2 = 0$. We are left with diagram (b) which can be expressed with the help of the vertex function Γ (N_c is the number of colors):

$$\begin{aligned} M^+ &= \frac{N_c}{(2\pi)^8}\int d^4k\, d^4l \sum_{\text{indices}} \Gamma_{ijk}\frac{u^i(p_1\lambda_1)\bar{u}^l(p_1\lambda_1)}{(p_1^2-m_1^2+i\epsilon)}\gamma^+_{lm}\frac{u^m(p_1'\lambda_1')\bar{u}^n(p_1'\lambda_1')}{(p_1'^2-m_1'^2+i\epsilon)} \\ &\quad \times\Gamma^\dagger_{nop}\frac{u^j(p_2\lambda_2)\bar{u}^o(p_2\lambda_2)u^k(p_3\lambda_3)\bar{u}^p(p_3\lambda_3)}{(p_2^2-m_2^2+i\epsilon)(p_3^2-m_3^2+i\epsilon)} + \text{permutations}\,, \\ \vec{p}_1 &= \frac{1}{3}\vec{P}+\vec{k}+\frac{1}{2}\vec{l}\,, \quad \vec{p}_2 = \frac{1}{3}\vec{P}-\vec{k}+\frac{1}{2}\vec{l}\,, \quad \vec{p}_3 = \frac{1}{3}\vec{P}-\vec{l}\,, \\ \vec{p}_1{}' &= \vec{p}_1 - \vec{K}\,, \quad K = P - P'\,. \end{aligned} \tag{2.19}$$

On the light front, we have exact correspondence with the choice of the Greens function in Eq. (2.12). If the vertex function Γ is assumed to be independent of the components k^- and l^-, we can calculate M^+ by contour methods in the k^- and l^- planes. M^+ is given by the residua of the two noninteracting quark poles. Replacing vertex functions by wave functions we get

$$\begin{aligned} M^+ &= \frac{N_c}{(2\pi)^6}\int d^3q d^3Q \left(\frac{E_1'E_2'E_3'E_{12}'M_3M}{E_1E_2E_3E_{12}M_3'M'}\right)^{1/2}\sum_{\text{spin}}\Psi^\dagger(\mathbf{q}',\mathbf{Q}',\lambda_1',\lambda_2',\lambda_3') \\ &\quad \times(O_1+O_2+O_3)\Psi(\mathbf{q},\mathbf{Q},\lambda_1,\lambda_2,\lambda_3)\,, \\ O_1 &= \frac{1}{\xi\eta}\bar{u}(\vec{p}_1{}'\lambda_1')\gamma^+u(\vec{p}_1\lambda_1)\,, \\ O_2 &= \frac{1}{(1-\xi)\eta}\bar{u}(\vec{p}_2{}'\lambda_2')\gamma^+u(\vec{p}_2\lambda_2)\,, \\ O_3 &= \frac{1}{(1-\eta)}\bar{u}(\vec{p}_3{}'\lambda_3')\gamma^+u(\vec{p}_3\lambda_3)\,. \end{aligned} \tag{2.20}$$

The O_is correspond to the ith diagram in Fig. 2.3. For O_1 the primed variables are

$$q_\perp' = q_\perp - (1-\xi)K_\perp, \quad Q_\perp' = Q_\perp - (1-\eta)K_\perp\,, \tag{2.21}$$

for O_2

$$q_\perp' = q_\perp + \xi K_\perp\,, \quad Q_\perp' = Q_\perp - (1-\eta)K_\perp\,, \tag{2.22}$$

and for O_3

$$q_\perp' = q_\perp\,, \quad Q_\perp' = Q_\perp + \eta K_\perp\,. \tag{2.23}$$

For pointlike quarks the matrix element of the current is

$$\begin{aligned} \bar{u}(\vec{p}_1{}'\lambda_1')\gamma^+u(\vec{p}_1\lambda_1) &= 2\xi\eta P^+\delta_{\lambda_1\lambda_1'}\,, \\ \bar{u}(\vec{p}_2{}'\lambda_2')\gamma^+u(\vec{p}_2\lambda_2) &= 2(1-\xi)\eta P^+\delta_{\lambda_2\lambda_2'}\,, \\ \bar{u}(\vec{p}_3{}'\lambda_3')\gamma^+u(\vec{p}_3\lambda_3) &= 2(1-\eta)P^+\delta_{\lambda_3\lambda_3'}\,. \end{aligned} \tag{2.24}$$

After factoring out color the wave function is totally symmetric and we have $\sum_i\langle O_i\rangle = 3\langle O_j\rangle$ for any j. Since primed variables take a simple form for O_3 we choose $3\langle O_3\rangle$. We arrive at the form

$$M^+ = 2P^+\frac{N_c}{(2\pi)^6}\int d^3q d^3Q\left(\frac{E_3'E_{12}'M}{E_3E_{12}M'}\right)^{1/2}\sum_{\text{spin}}\Psi^\dagger(\mathbf{q}',\mathbf{Q}',\lambda_3')3\delta_{\lambda_3\lambda_3'}\Psi(\mathbf{q},\mathbf{Q},\lambda_3)\,. \tag{2.25}$$

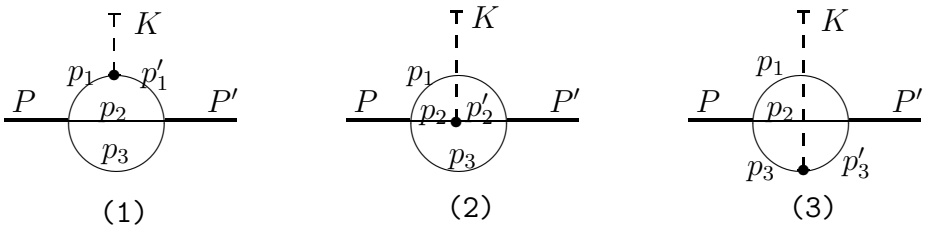

Figure 2.3: Feynman diagrams that represent the transition of the baryon state with four-momentum P to the baryon state with four-momentum P'. $K = P - P'$. The photon or the W boson is coupled either to the first, second or third quark line, corresponding to the diagrams (1),(2) and (3), respectively.

2.3 Wave function

In light front variables one can separate the center of mass motion from the internal motion. The wave function Ψ is therefore a function of the relative momenta $\mathbf{q}$ and $\mathbf{Q}$. The product $\Psi = \Phi\chi\phi$, with Φ = flavor, χ = spin, and ϕ = momentum distribution, is a symmetric function. This is consistent with Fermi statistics since the color wave function is totally antisymmetric.

The angular momentum $\mathbf{j}$ can be expressed as a sum of orbital and spin contributions

$$\mathbf{j} = i\nabla_{\mathbf{p}} \times \mathbf{p} + \sum_{j=1}^{3} \mathcal{R}_{Mj}\mathbf{s}_j \ , \tag{2.26}$$

where $\mathcal{R}_M$ is a Melosh rotation acting on the quark spins $\mathbf{s}_j$, which has the matrix representation (for two particles)

$$\langle\lambda'|\mathcal{R}_M(\xi, q_\perp, m, M)|\lambda\rangle = \left[\frac{m + \xi M - i\sigma\cdot(\mathbf{n}\times\mathbf{q})}{\sqrt{(m+\xi M)^2 + q_\perp^2}}\right]_{\lambda'\lambda} \tag{2.27}$$

with $\mathbf{n} = (0, 0, 1)$. In previous works [14, 15, 16, 17, 18] this rotation has been approximated by putting $M = M_B$. This corresponds to a weak-binding limit which cannot be justified for a bound state in QCD. In this limit our model has a close connection to many other relativistic quark models as shown by Koerner et al. [37].

The operator $\mathbf{j}$ commutes with the mass operator $\hat{M}$; this is necessary and sufficient for Poincaré-invariance of the bound state.

In terms of the relative momenta the angular momentum takes the form

$$\begin{aligned} \mathbf{j} &= i\nabla_{\mathbf{Q}} \times \mathbf{Q} + \mathcal{R}_M(\eta, Q_\perp, M_3, M)\mathbf{j}_{12} + \mathcal{R}_M(1-\eta, -Q_\perp, m_3, M)\mathbf{s}_3 \ , \\ \mathbf{j}_{12} &= i\nabla_{\mathbf{q}} \times \mathbf{q} + \mathcal{R}_M(\xi, q_\perp, m_1, M_3)\mathbf{s}_1 + \mathcal{R}_M(1-\xi, -q_\perp, m_2, M_3)\mathbf{s}_2 \ . \end{aligned} \tag{2.28}$$

We can drop the orbital contribution.

$$\mathbf{j} = \sum \mathcal{R}_i \mathbf{s}_i \ ,$$

$$\begin{aligned}
\mathcal{R}_1 &= \frac{1}{\sqrt{a^2+Q_\perp^2}\sqrt{c^2+q_\perp^2}} \begin{pmatrix} ac-q_RQ_L & -aq_L-cQ_L \\ cQ_R+aq_R & ac-q_LQ_R \end{pmatrix} , \\
\mathcal{R}_2 &= \frac{1}{\sqrt{a^2+Q_\perp^2}\sqrt{d^2+q_\perp^2}} \begin{pmatrix} ad+q_RQ_L & aq_L-dQ_L \\ dQ_R-aq_R & ad+q_LQ_R \end{pmatrix} , \\
\mathcal{R}_3 &= \frac{1}{\sqrt{b^2+Q_\perp^2}} \begin{pmatrix} b & Q_L \\ -Q_R & b \end{pmatrix} ,
\end{aligned} \tag{2.29}$$

with

$$\begin{aligned}
a &= M_3+\eta M , \quad b = m_3+(1-\eta)M , \\
c &= m_1+\xi M_3 , \quad d = m_2+(1-\xi)M_3 , \\
q_R &= q_1+iq_2 , \quad q_L = q_1-iq_2 , \\
Q_R &= Q_1+iQ_2 , \quad Q_L = Q_1-iQ_2 .
\end{aligned} \tag{2.30}$$

The momentum wave function ϕ is normalized according to [38]

$$\frac{N_c}{(2\pi)^6}\int d^3q d^3Q|\phi|^2 = 1 , \tag{2.31}$$

and can be chosen as a function of M to fulfill the spherical and permutation symmetry. That is the same as to express it in terms of the off-shell energy $\mathcal{E}$ since

$$\mathcal{E} = P^+(P^- - p_1^- - p_2^- - p_3^-) = M_B^2 - M^2 . \tag{2.32}$$

The S-state orbital function $\phi(M)$ is approximated by either

$$\phi(M) = N\exp\left[-\frac{M^2}{2\beta^2}\right] \qquad \text{or} \qquad \phi(M) = \frac{N'}{(M^2+\beta^2)^{3.5}} , \tag{2.33}$$

which depend on two free parameters, the constituent quark mass and the confinement scale parameter β. The first function is the conventional choice used in spectroscopy, but it has a too strong falloff for high K^2. Both functions give nearly the same result for low values of K^2, the second one performs obviously better for high K^2. This independence of the wave function ϕ for low K^2 suggests that the static properties are mainly given by the flavor and spin part of the wave function.

The total wave functions for the baryon octet are [1]

$$\begin{aligned}
p &= \frac{-1}{\sqrt{3}}\left(uud\chi^{\lambda 3}+udu\chi^{\lambda 2}+duu\chi^{\lambda 1}\right)\phi , \\
n &= \frac{1}{\sqrt{3}}\left(ddu\chi^{\lambda 3}+dud\chi^{\lambda 2}+udd\chi^{\lambda 1}\right)\phi , \\
\Lambda &= \frac{-1}{\sqrt{6}}\left[(uds-dus)\chi^{\rho 3}+(usd-dsu)\chi^{\rho 2}+(sud-sdu)\chi^{\rho 1}\right]\phi , \\
\Sigma^+ &= \frac{1}{\sqrt{3}}\left(uus\chi^{\lambda 3}+usu\chi^{\lambda 2}+suu\chi^{\lambda 1}\right)\phi ,
\end{aligned} \tag{2.34}$$

[1] The overall sign for Σ^+,Λ and Ξ^0 has to be changed in Ref. [39, p. 46].

$$
\begin{aligned}
\Sigma^0 &= \frac{-1}{\sqrt{6}}\left[(uds+dus)\chi^{\lambda 3}+(usd+dsu)\chi^{\lambda 2}+(sud+sdu)\chi^{\lambda 1}\right]\phi\,,\\
\Sigma^- &= \frac{-1}{\sqrt{3}}\left(dds\chi^{\lambda 3}+dsd\chi^{\lambda 2}+sdd\chi^{\lambda 1}\right)\phi\,,\\
\Xi^0 &= \frac{-1}{\sqrt{3}}\left(ssu\chi^{\lambda 3}+sus\chi^{\lambda 2}+uss\chi^{\lambda 1}\right)\phi\,,\\
\Xi^- &= \frac{1}{\sqrt{3}}\left(ssd\chi^{\lambda 3}+sds\chi^{\lambda 2}+dss\chi^{\lambda 1}\right)\phi\,,
\end{aligned}
$$

with

$$
\begin{aligned}
\chi^{\lambda 3}_{\uparrow} &= \frac{1}{\sqrt{6}}(\downarrow\uparrow\uparrow+\uparrow\downarrow\uparrow-2\uparrow\uparrow\downarrow),\\
\chi^{\lambda 3}_{\downarrow} &= \frac{1}{\sqrt{6}}(2\downarrow\downarrow\uparrow-\downarrow\uparrow\downarrow-\uparrow\downarrow\downarrow)\,,\\
\chi^{\rho 3}_{\uparrow} &= \frac{1}{\sqrt{2}}(\uparrow\downarrow\uparrow-\downarrow\uparrow\uparrow)\,,\\
\chi^{\rho 3}_{\downarrow} &= \frac{1}{\sqrt{2}}(\uparrow\downarrow\downarrow-\downarrow\uparrow\downarrow)\,.
\end{aligned}
\tag{2.35}
$$

The spin wave functions $\chi^{\lambda 2}$ and $\chi^{\lambda 1}$ are the appropriate permutations of $\chi^{\lambda 3}$, and $\chi^{\rho 2}$ and $\chi^{\rho 1}$ are the appropriate permutations of $\chi^{\rho 3}$. The spin-wave function of the ith quark is given by

$$
\uparrow = \mathcal{R}_i\begin{pmatrix}1\\0\end{pmatrix} \text{ and } \downarrow = \mathcal{R}_i\begin{pmatrix}0\\1\end{pmatrix}\,. \tag{2.36}
$$

2.4 Extensions of the model

As already mentioned in the introduction we are also considering some extensions to the minimal quark model (MQM), because the MQM is not able to fit experimental data for both the electromagnetic and weak sector with the same parameters. We give an overview of the different models in this Section. Questions concerning particular experimental data are discussed in the appropriate Chapters.

2.4.1 Minimal quark model

The MQM uses the wave function presented in Eq. (2.33) with structureless quarks. It is called minimal because it uses the smallest number of parameters. These are the mass of the up and down quark $m_u = m_d \equiv m_{u/d}$, the mass of the strange quark m_s, and the wave function parameter β for the nucleons, the Σs and the Ξs; this β essentially determines the confinement scale. With these five parameters we either fit the electromagnetic properties (parameter set 4 of Table 3.1 on page 22) or the semileptonic weak decays (parameter set 6). The contrary statement in Ref. [9] has to be questioned, since their numerical results for the magnetic moments of the baryon octet are wrong.

2.4.2 Quark structure

One extension to the MQM is the introduction of nontrivial quark form factors. This would give us three new parameters in the electromagnetic sector (quark anomalous magnetic moments), and four new parameters in the weak sector (axial and vector quark form factors at zero momentum transfer). Chung and Coester [13] investigate the nucleon sector of the same model, and favor quark anomalous magnetic moments and a modified axial coupling for quarks. There are two reasons why we think that the quarks should be structureless in the electromagnetic sector:

1. Whatever the nature of this form factor is, whether it be due to a composite model or to radiative corrections, one expects the quark form factors to fall off for large K^2 in a different way from that used in Ref. [13].

2. There exists no parameter set of the anomalous magnetic moments that can improve the magnetic moments of the baryon octet (see Sec. 3.2).

2.4.3 Configuration mixing

Another extension of the MQM is the admixture of different radial wave functions. The configuration mixing suggested by spectroscopy reads:

$$|\text{Baryon}\rangle = \text{A}\ [56,0^+][8\times 2] + \text{B}\ [56,0^+]^*[8\times 2] + \text{C}\ [70,0^+][8\times 2], \tag{2.37}$$

in the notation $[\text{SU}(6),\text{L}^p][\text{SU}(3)_{\text{flavour}}\times\text{SU}(2)_{\text{spin}}]$, where $\text{A}^2+\text{B}^2+\text{C}^2=1$, L denotes the angular momentum, and p is the parity of the nucleon. The values for A, B, C are listed in Table 2.1 for different references.

Table 2.1: Parameters for the configuration mixing of the baryon octet given in Eq. (2.37) for two different references.

	A	B	C
Ref. [40]	0.93	–0.29	–0.23
Ref. [22]	0.90	–0.34	–0.27

In principle no additional parameters are required, if we use the same scale parameter β for every wave function, but in practice, it is convenient to choose different βs or admixture parameters. The wave functions in Eq. (2.37) are as follows:

$$\begin{aligned}
[56,0^+][8\times 2] &= \frac{1}{\sqrt{2}}\left(\chi^\rho\Phi^\rho+\chi^\lambda\Phi^\lambda\right)\phi_s\ ,\\
[56,0^+]^*[8\times 2] &= \frac{1}{\sqrt{2}}\left(\chi^\rho\Phi^\rho+\chi^\lambda\Phi^\lambda\right)\phi_s^*\ ,\\
[70,0^+][8\times 2] &= \frac{1}{2}\left(\chi^\rho\Phi^\lambda+\chi^\lambda\Phi^\rho\right)\phi_\rho+\frac{1}{2}\left(\chi^\rho\Phi^\rho-\chi^\lambda\Phi^\lambda\right)\phi_\lambda\ .
\end{aligned} \tag{2.38}$$

The spin functions χ^ρ and χ^λ are the same as in Eq. (2.35), the flavor wave functions Φ^ρ and Φ^λ correspond to χ^ρ and χ^λ with spin up and down exchanged with the appropriate flavors of the baryon. For the momentum wave functions ϕ_s, ϕ_s^*, ϕ_ρ, and ϕ_λ we first define

$$M_i=\frac{k_{i\perp}^2+m_i^2}{x_i}\ ,\quad x_i=p_i^+/P^+\ ,\quad k_{i\perp}=p_{i\perp}-x_iP_\perp\ . \tag{2.39}$$

With these functions M_i it is easier to build wave functions with special symmetries. Note that $M=M_1+M_2+M_3$, the combination $M_1+M_2-2M_3$ is symmetric in the particles (12), and M_1-M_2 is antisymmetric in the same particles. We therefore write:

$$\begin{aligned}
\phi_s &= N_s e^{-M^2/2\beta^2}\ ,\\
\phi_s^* &= N_s^*(M^2/\beta^2-c)\phi_s\ ,\\
\phi_\lambda &= N_\lambda(M_1+M_2-2M_3)\phi_s\ ,\\
\phi_\rho &= N_\rho(M_1-M_2)\phi_s\ .
\end{aligned} \tag{2.40}$$

The constant c in ϕ_s^* is evaluated from the orthogonality of ϕ_s and ϕ_s^*:

$$c=\frac{\int\phi_s^2M^2/\beta^2}{\int\phi_s^2}\ , \tag{2.41}$$

and the constants N_s, N_s^*, N_λ, and N_ρ are given by the normalization in Eq. (2.31). These wave functions in Eq. (2.40) go over into the nonrelativistic ones [41, 39] in the limit, where the masses m_i go to zero and the ξ and η to their nonrelativistic values.

Unfortunately, the mixing configuration does not improve the fit, it is even worse for the crucial ratio in Eq. (4.27). A rough estimate gives

$$\frac{g_1/f_1(\Lambda\to pe^-\bar\nu_e)}{g_1/f_1(\Sigma^-\to ne^-\bar\nu_e)}\simeq -3\left(1+\frac{8}{3}\mathrm{C}^2\right)=-3.5\pm 0.1\ , \tag{2.42}$$

to be compared with the MQM value -3, and the experimental data -2.11 ± 0.15. Other values like the ratio $\mu(p)/\mu(n)$ also get worse. We therefore do not consider this extension any further.

2.4.4 Asymmetric wave function

The extension to the MQM with a two quark clustering in the light front wave function is minimal in the sense that there is no difference between the extension and MQM in the meson sector. Instead of one scale parameter β, we have two of them, β_q for the scale between the two spin-isospin-zero quarks and β_Q for the scale between the third quark and the diquark. We devote the entire Chapter 5 to the asymmetric wave function, because it improves the fit dramatically in many details and it provides a comprehensive fit of both the electromagnetic and weak sectors.

2.5 Discussion of the wave function

An analysis of the baryon spectrum based on Eq. (2.18) could in principle determine the wave function, but we restrict ourselves to the two approximations in Eq. (2.33). It is therefore important to compare our Ansatz with the wave function of other authors. Usually the transverse momenta are integrated out up to a scale μ, and the wave function is expressed in light front fractions $x_i = p_i^+/P^+$, written in our variables as

$$\begin{aligned} x_1 &= \xi\eta \,, \\ x_2 &= \eta(1-\xi) \,, \\ x_3 &= 1-\eta \,. \end{aligned} \tag{2.43}$$

The valence quark distribution amplitude $\phi(x_1, x_2, x_3, \mu^2)$ is

$$\phi(x_i, \mu^2) = \int^{|q_\perp^2|<\mu^2} \int^{|Q_\perp^2|<\mu^2} \phi(x_i, q_\perp, Q_\perp) d^2q_\perp d^2Q_\perp \,. \tag{2.44}$$

This amplitude is well known in two limits, which are unfortunately not interesting. In the static, symmetric SU(6) quark model, the variables x_i take on only discrete values:

$$\phi_{\rm NR}(x_i) = \delta\left(x_1 - \frac{1}{3}\right)\delta\left(x_2 - \frac{1}{3}\right)\delta\left(x_3 - \frac{1}{3}\right) = \delta\left(\xi - \frac{1}{2}\right)\delta\left(\eta - \frac{2}{3}\right) \tag{2.45}$$

and the asymptotic amplitude $\phi_{\rm as}$ for large K^2 is known as [31]

$$\phi_{\rm as}(x_i) = \phi(x_i, \mu^2 \to \infty) = 120 x_1 x_2 x_3 \,, \tag{2.46}$$

with a normalization such that

$$\int \phi(x_i, \mu^2)\delta(\sum x_i - 1) dx_1 dx_2 dx_3 = 1 \,. \tag{2.47}$$

Notice that this is not the same normalization as the one used in Eq. (2.31). Unfortunately the knowledge of both forms is not very useful since they contradict experimental data [42].

Using the QCD sum rule technique, Chernyak and Zhitnitsky [30] suggest the quark distribution amplitudes for the proton as follows:

$$\begin{aligned} &\phi_{\rm CZ}(x_i, \mu \approx 1 \text{ GeV}) = \\ &\quad 120 x_1 x_2 x_3 \left[11.35(x_1^2 + x_2^2) + 8.82 x_3^2 - 1.68 x_3 - 2.94 - 6.72(x_2^2 - x_1^2)\right] \,. \end{aligned} \tag{2.48}$$

For the Gauss shaped wave function $\phi_{\rm G}$ and the Lorentz shaped one $\phi_{\rm L}$ in Eq. (2.33) we can write

$$\begin{aligned} &\phi_{\rm G} = N e^{-M^2/2\beta^2} \,, \qquad \phi_{\rm L} = \frac{N'}{(M^2/\beta^2 + 1)^n} \,, \\ &\int_{-\infty}^{\infty}\int_{-\infty}^{\infty} \phi_{\rm G}\, d^2q_\perp d^2Q_\perp = \\ &\quad \tilde{N}\beta^4 \xi\eta^2(1-\eta)(1-\xi) \exp\left(-\frac{m_1^2}{2\beta^2\eta\xi} - \frac{m_2^2}{2\beta^2(1-\xi)} - \frac{m_3^2}{2\beta^2(1-\eta)}\right) \,, \\ &\int_{-\infty}^{\infty}\int_{-\infty}^{\infty} \phi_{\rm L}\, d^2q_\perp d^2Q_\perp = \\ &\quad \frac{\tilde{N}'\beta^{2n}(1-\eta)^{n-1}\eta^n(1-\xi)^{n-1}\xi^{n-1}}{[m_1^2(1-\xi)(1-\eta) + m_2^2\xi(1-\eta) + m_3^2\xi\eta(1-\xi) + \beta^2\eta\xi(1-\xi)(1-\eta)]^{n-2}} \,. \end{aligned} \tag{2.49}$$

Letting the quark masses m_i go to zero the amplitudes both converge to the asymptotic form (2.46):

$$\begin{aligned} \phi_{\rm G}(x_i) &\xrightarrow{m_i\to 0} \tilde{N}\beta^4\xi\eta^2(1-\eta)(1-\xi) = \tilde{N}\beta^4 x_1x_2x_3 \ , \\ \phi_{\rm L}(x_i) &\xrightarrow{m_i\to 0} \tilde{N}'\beta^4\xi\eta^2(1-\eta)(1-\xi) = \tilde{N}'\beta^4 x_1x_2x_3 \ . \end{aligned} \tag{2.50}$$

The differences between these various wave functions are best seen in a plot. In Fig. 2.4 we show $\phi_{\rm as}$ (a), $\phi_{\rm CZ}$ (b), $\phi_{\rm G}$ (c+d), and $\phi_{\rm L}$ (e+f). The plots (c) and (e) are the symmetric wave functions (parameter set 6), (d) and (f) are the asymmetric ones (parameter set 8 for hyperons). The broad, unstructured distribution in the asymptotic limit gets sharper and more structured for the phenomenological amplitudes. The wave function in (c) usually used in quark models is close to the asymptotic function (a).

The important difference between ϕ_G and ϕ_L is their large momentum behavior. For $|K^2| \to \infty$ the wave functions behave as:

$$\phi_G \to e^{-|K^2|/2\beta^2} \ , \qquad \phi_L \to \left[\frac{|K^2|}{\beta^2}\right]^{-n} \ . \tag{2.51}$$

The exponential falloff for ϕ_G becomes too strong at a momentum scale of about 2 GeV^2 (see Fig. 3.8).

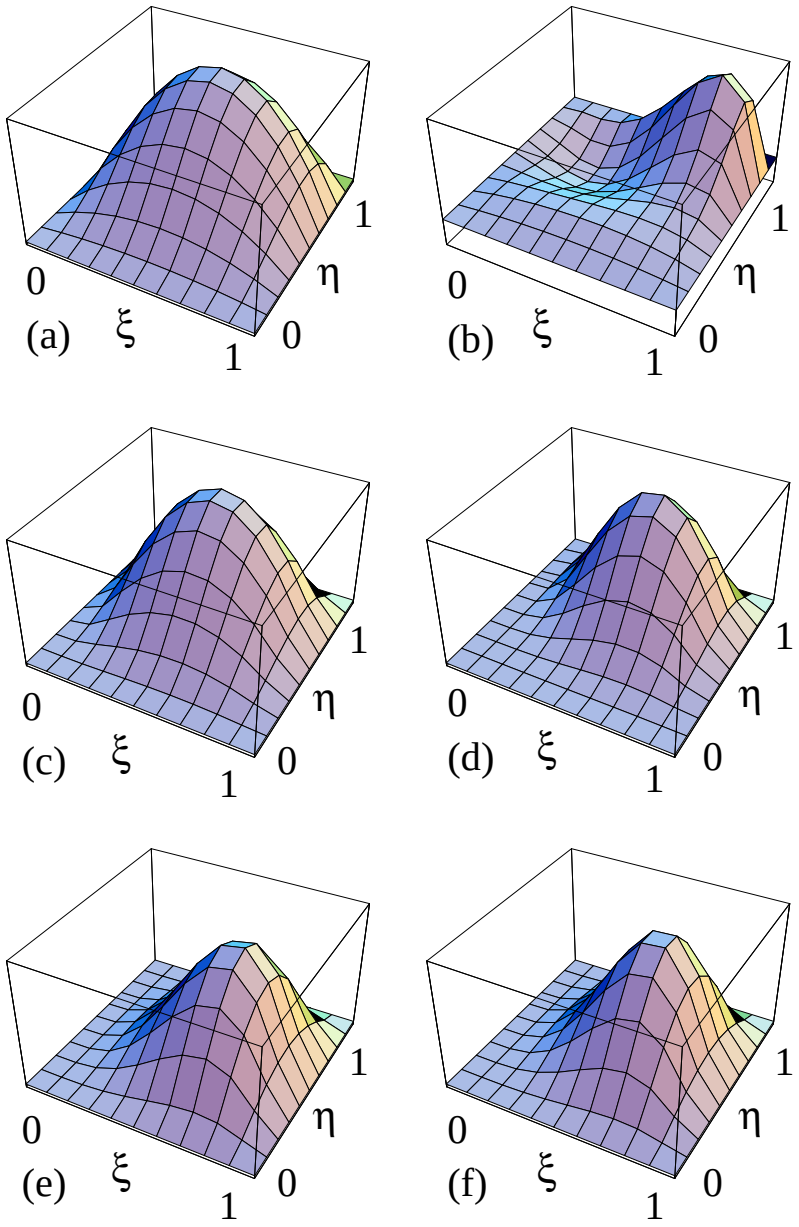

Figure 2.4: Different wave functions used by other authors and used in this work. (a) asymptotic quark distribution [31]; (b) amplitude derived by QCD sum-rule technique [30]; Gauss shaped wave function with parameter set 6 (c) and set 8 for hyperons (d); Lorentz shaped wave function with parameter set 6 (e) and set 8 for hyperons (f). A trend to more structured, asymmetric wave functions can be seen.

Chapter 3

Electromagnetic properties

3.1 Nucleon electromagnetic form factors

3.1.1 Calculation of nucleon form factors

The electromagnetic current matrix element can be written in terms of two form factors taking into account current and parity conservation:

$$\langle N, \lambda' p' \left| J^\mu \right| N, \lambda p \rangle = \bar{u}_{\lambda'}(p') \left[F_1(K^2)\gamma^\mu + \frac{F_2(K^2)}{2M_N} i\sigma^{\mu\nu} K_\nu \right] u_\lambda(p) \tag{3.1}$$

with momentum transfer $K = p' - p$ and $J^\mu = \bar{q}\gamma^\mu q$. For $K^2 = 0$ the form factors F_1 and F_2 are respectively equal to the charge and the anomalous magnetic moment in units e and e/M_N, and the magnetic moment is $\mu = F_1(0) + F_2(0)$. The Sachs form factors are defined as

$$G_E = F_1 + \frac{K^2}{4M_N^2} F_2 \ , \quad \text{and} \quad G_M = F_1 + F_2 \ , \tag{3.2}$$

and the charge radii of the nucleons are

$$\left\langle r_i^2 \right\rangle = 6 \frac{dF_i(K^2)}{dK^2}\bigg|_{K^2=0} , \quad \text{and} \quad \left\langle r_{E/M}^2 \right\rangle = \frac{6}{G_{E/M}(0)} \frac{dG_{E/M}(K^2)}{dK^2}\bigg|_{K^2=0} . \tag{3.3}$$

The form factors can be expressed in terms of the + component of the current:

$$\begin{aligned} F_1(K^2) &= \frac{1}{2P^+} \left\langle N, \uparrow \left| J^+ \right| N, \uparrow \right\rangle \ , \\ K_\perp F_2(K^2) &= -\frac{2M_N}{2P^+} \left\langle N, \uparrow \left| J^+ \right| N, \downarrow \right\rangle \ . \end{aligned} \tag{3.4}$$

Therefore Eq. (2.25) can be used to calculate the form factors. In addition, the Dirac quark current $\bar{q}\gamma^\mu q$ can be generalized to include the quark structure in the following way:

$$\bar{q} \left(F_{1q}\gamma^\mu + \frac{F_{2q}}{2m_q} i\sigma^{\mu\nu} K_\nu \right) q \ . \tag{3.5}$$

We get

$$\begin{aligned} F_1(K^2) &= \frac{N_c}{(2\pi)^6}\int d^3q d^3Q \left(\frac{E_3' E_{12}' M}{E_3 E_{12} M'}\right)^{1/2} \phi^\dagger(M')\phi(M) \\ &\quad \times \sum_{i=1}^{3}\left[F_{1i}(K^2)\left\langle \chi_\uparrow^{\lambda i}|\chi_\uparrow^{\lambda i}\right\rangle + \frac{K_\perp}{2m_i}F_{2i}(K^2)\left\langle \chi_\uparrow^{\lambda i}|O_3|\chi_\uparrow^{\lambda i}\right\rangle\right] \\ K_\perp F_2(K^2) &= -2M_N\frac{N_c}{(2\pi)^6}\int d^3q d^3Q \left(\frac{E_3' E_{12}' M}{E_3 E_{12} M'}\right)^{1/2} \phi^\dagger(M')\phi(M) \\ &\quad \times \sum_{i=1}^{3}\left[F_{1i}(K^2)\left\langle \chi_\uparrow^{\lambda i}|\chi_\downarrow^{\lambda i}\right\rangle + \frac{K_\perp}{2m_i}F_{2i}(K^2)\left\langle \chi_\uparrow^{\lambda i}|O_3|\chi_\downarrow^{\lambda i}\right\rangle\right] \end{aligned} \tag{3.6}$$

with $O_3 = \begin{pmatrix} 0 & -1 \\ 1 & 0 \end{pmatrix}$, $i = (uud)$ for the proton and $i = (ddu)$ for the neutron. The form factors $F_{1u}(0)$ and $F_{1d}(0)$ are the charges, $F_{2u}(0)$ and $F_{2d}(0)$ are the anomalous magnetic moments of the u and d quarks, respectively. Only the F_{1i}-terms contribute for $K^2 = 0$, and $\left\langle \chi_\uparrow^{\lambda i}|\chi_\uparrow^{\lambda i}\right\rangle = 1$. The matrix elements $\left\langle \chi_\uparrow^{\lambda i}|\chi_\uparrow^{\lambda i}\right\rangle$ and $\left\langle \chi_\uparrow^{\lambda i}|O_3|\chi_\downarrow^{\lambda i}\right\rangle$ are given in the next Subsection. The expressions for $K^2 \neq 0$ are quite long, we therefore give only F_1 for the proton with vanishing quark anomalous moment and $F_{1u} = \frac{2}{3}$, $F_{1d} = -\frac{1}{3}$:

$$\sum_{i=1}^{3} F_{1i}\left\langle \chi_\uparrow^{\lambda i}|\chi_\uparrow^{\lambda i}\right\rangle = \frac{\text{Num}}{(a'^2+Q_\perp'^2)(a^2+Q_\perp^2)\sqrt{(b'^2+Q_\perp'^2)}\sqrt{(b^2+Q_\perp^2)}(c^2+q_\perp^2)(d^2+q_\perp^2)} \tag{3.7}$$

$$\begin{aligned} \text{Num} &= (a'^2+Q_\perp'^2)(a^2+Q_\perp^2)(b'b+Q_\perp'\cdot Q_\perp)(c^2d^2+q_\perp^4) \\ &\quad +(c^2+d^2)q_\perp^2\Big\{a^2a'^2(bb'+Q_\perp'\cdot Q_\perp)+(aa'+\frac{1}{2}Q_\perp'\cdot Q_\perp) \\ &\quad \times[2bb'(Q_\perp'\cdot Q_\perp)+Q_\perp'^2Q_\perp^2+(Q_\perp'\cdot Q_\perp)^2]\Big\} \\ &\quad +cdq_\perp^2\Big\{4aa'bb'(Q_\perp'\cdot Q_\perp)-2(a^2Q_\perp'^2+a'^2Q_\perp^2)(bb'+Q_\perp'\cdot Q_\perp) \\ &\quad +2aa'[Q_\perp'^2Q_\perp^2+(Q_\perp'\cdot Q_\perp)^2]+(2bb'+Q_\perp'\cdot Q_\perp)[(Q_\perp'\cdot Q_\perp)^2-Q_\perp'^2Q_\perp^2]\Big\} \end{aligned}$$

For $K^2 = 0$, Eq. (3.7) reduces to 1 and we get $F_{1p}(0) = 1$, the charge of the proton in units of e.

3.1.2 Results and conclusions

Appendix A describes how the formulae were generated and integrated. The exponential function $\phi(M)$ in Eq. (2.33) falls off too fast, it can only be valid for low K^2. In general ϕ has to be just a function decreasing with M. We try

$$\phi(M) = \frac{N}{(M^2+\beta^2)^{3.5}}\ , \tag{3.8}$$

and N is chosen so that Eq. (2.31) is fulfilled. The wave function $\phi(M)$ does correspond to a confining potential in the sense that we need more energy to ionize the bound state than to produce a new quark pair. This guarantees that no free quark appears. Figures 3.2 and 3.3 show that the low K^2 behavior is the same for both wave functions.

We plot the parameter β against $m_{u/d}$ for the different experimental data. In Fig. 3.1 the fits for the Gauss shaped wave function (a) and for the Lorentz shaped one (b) are given. We see that it is not possible to exactly fit the three data, since the three lines should ideally meet in one single point. Figure 3.1 shows for case (a) that the proton and

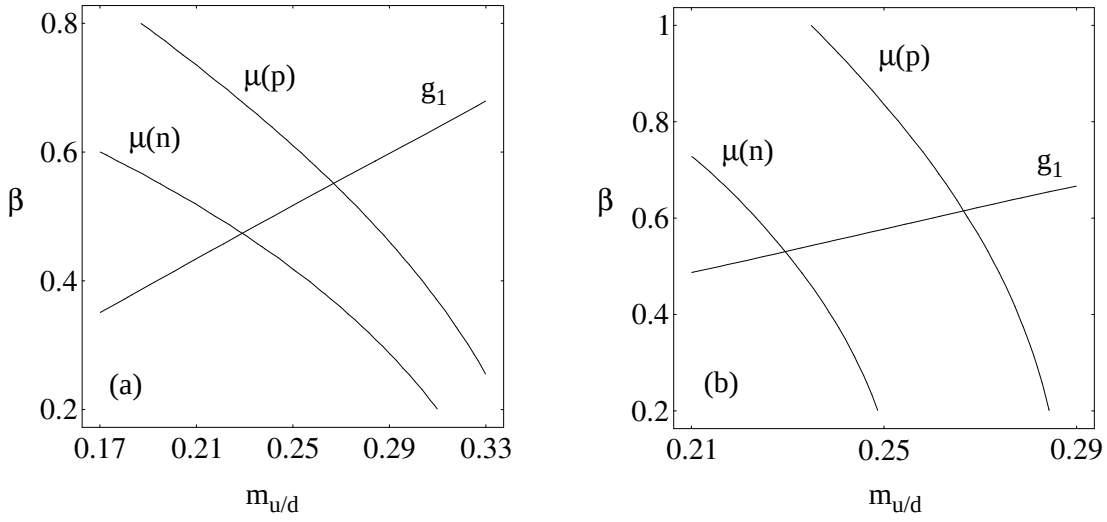

Figure 3.1: The lines represent a set of parameters β and $m_{u/d}$, which reproduce respectively the experimental data for the magnetic moments of the proton and neutron, and for $g_1(n \to pe^-\bar{\nu})$. (a) Parameters for the Gauss shaped wave function; (b) parameters for the Lorentz shaped wave function.

neutron magnetic moments alone tend to a large quark mass $m_{u/d} \simeq 0.33$ GeV, whereas g_1 of the neutron beta decay together with the neutron magnetic moment favors a small $m_{u/d} \simeq 0.23$ GeV. We compromise and fit to the proton magnetic moment and to g_1 of the neutron decay , which yields $m_{u/d} \simeq 0.267$ GeV. The anomalous moments of the u and d quarks are fitted to $F_1'(0)$ of the neutron. To analyze the results we have chosen two sets of parameters given in Table 3.1 on page 22, set 1 with quark anomalous magnetic moments and set 2 without them. The situation for case (b) in Fig 3.1 is similar, with the exception that the proton and neutron magnetic moments do not favor a large mass. We use parameter set 3 for the Lorentz shaped wave function.

Figures 3.2 – 3.7 show F_1 and F_2 for the proton and neutron for the various versions of the model. If we neglect the quark anomalous magnetic moments, only the form factor F_{1n} (Fig 3.6) changes and F_{2n} (Fig 3.7) gets shifted by a small amount. Both changes are welcome but only of minor importance. F_{1n} is very small and therefore sensitive to any

Table 3.1: The parameters of the constituent quark model. All numbers are given in units of GeV. Note that only set 3 is used for the Lorentz shaped wave function.

	m_u	m_d	m_s	β_N	$\beta_{\Sigma/\Lambda}$	β_Ξ	F_{2u}	F_{2d}	F_{2s}
Set 1	0.267	0.267	–	0.56	–	–	–0.0069	–0.028	–
Set 2	0.267	0.267	–	0.56	–	–	0.0	0.0	–
Set 3	0.263	0.263	–	0.607	–	–	0.0	0.0	–
Set 4	0.33	0.33	0.55	0.16	1.00	1.08	–0.0086	–0.034	0.077
Set 5	0.267	0.267	0.33	0.56	0.63	0.70	0.0	0.0	0.0
Set 6	0.267	0.267	0.40	0.56	0.60	0.62	0.0	0.0	0.0
Set 7	0.267	0.267	0.40	0.56	0.60	0.62	–0.0069	–0.028	0.056

Table 3.2: The quantity $F'(0)$ for the nucleons with parameter sets 1 and 2 of Table 3.1. The values for the Lorentz shaped wave function (set 3) are almost the same as the one from set 2.

Form factor	Set 1 [fm^2]	Set 2 [fm^2]	Expt. [fm^2]
F'_{1p}	0.0874	0.0924	0.0966
F'_{2p}	0.179	0.177	0.234
F'_{1n}	0.0027	0.012	0.0017
F'_{2n}	–0.186	–0.170	–0.236

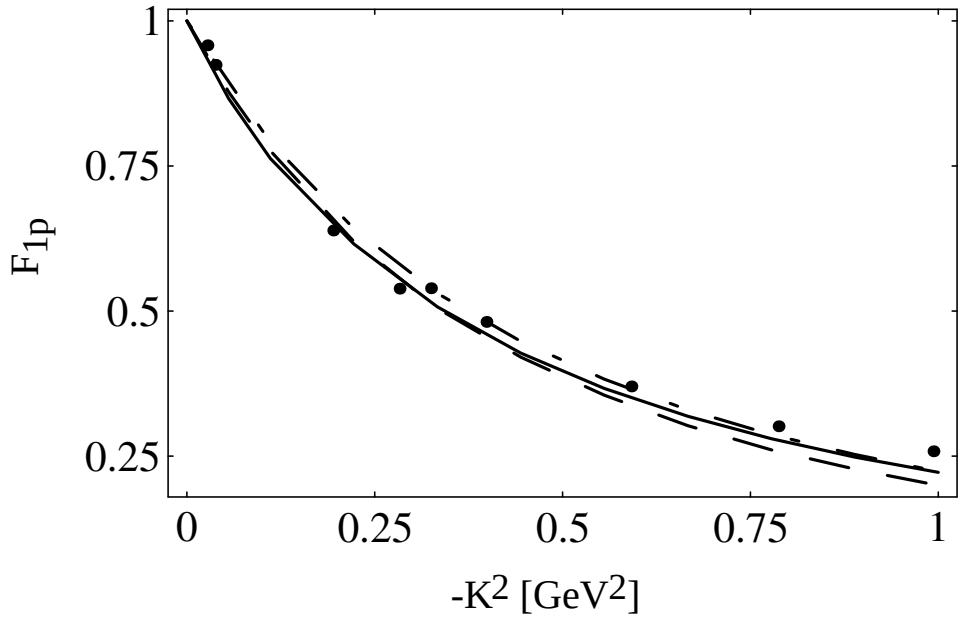

Figure 3.2: The proton form factor $F_{1p}(K^2)$. Continuous line, Parameter set 3; dashed line, parameter set 2; dashed-dotted line, parameter set 1. The experimental points are taken from Ref. [43, 44, 45].

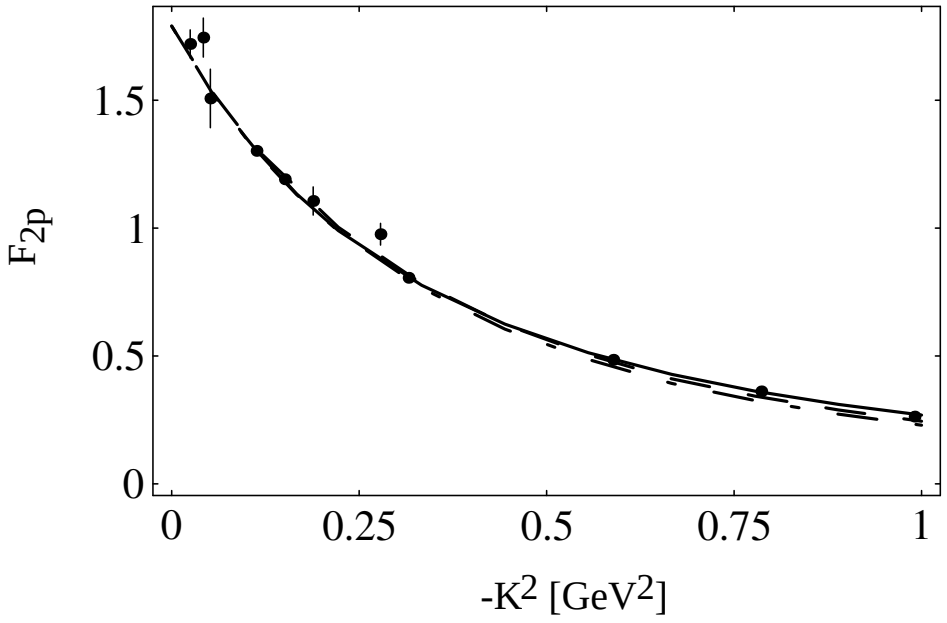

Figure 3.3: The proton form factor $F_{2p}(K^2)$. Continuous line, Parameter set 3; dashed line, parameter set 2; dashed-dotted line, parameter set 1. The experimental data are taken from Ref. [43, 44, 45].

corrections.

All data for form factors can be reproduced well up to 2 GeV^2 for both wave functions in Eq. (2.33). But only the Lorentz shaped wave function has a good high energy behavior up to more than 30 GeV^2. In this region we already have QCD predictions for G_M [46]. Note that this is an extremely large K^2 region, since other models can only fit the data up to 2.5 GeV^2 [47] and 6 GeV^2 [13]. Our fit is even better than the well known dipole formula

$$\frac{G_{Mp}}{\mu(p)} = \left(1 - \frac{K^2}{M_V^2}\right)^{-2} \quad , \quad M_V = 0.84 \ \text{GeV} \quad . \tag{3.9}$$

One can approximate our form factors with the parameterization of Eq. (4.23) on page 39. It is valid up to 3 GeV^2 with a deviation of less than 5%. This justifies the use of that parameterization in Chapter 4.

The values for magnetic moments derived with the parameter sets 1 and 2 have been collected in Table 3.3 and will be discussed further in Sec. 3.2. We do not consider the Lorentz shaped wave function (set 3) any further in this thesis, because the results for small momentum transfer or even static properties are almost the same for both types of wave functions.

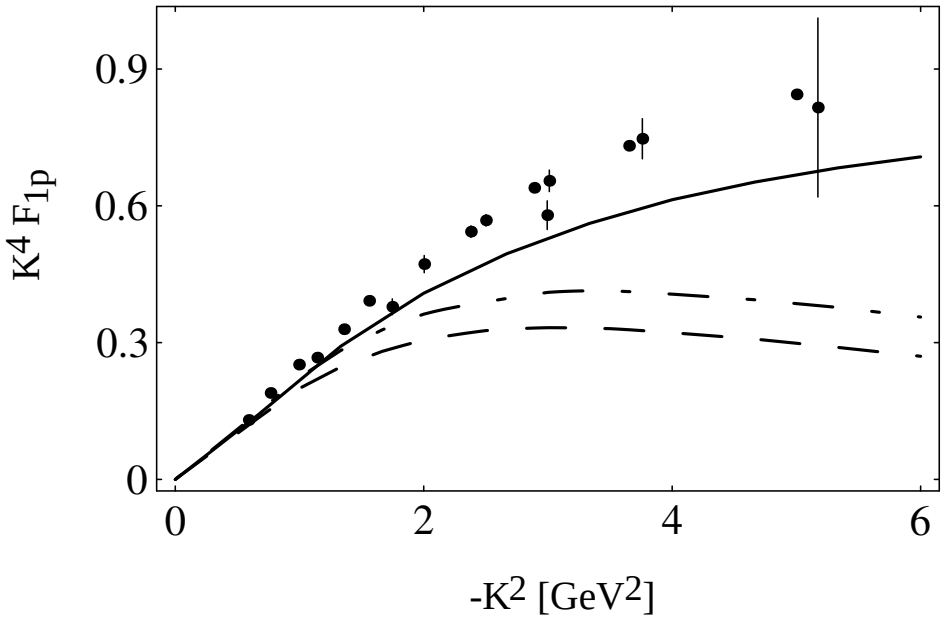

Figure 3.4: The proton form factor $F_{1p}(K^2)$. Continuous line, Parameter set 3; dashed line, parameter set 2; dashed-dotted line, parameter set 1. The experimental data are taken from Ref. [43, 44, 45].

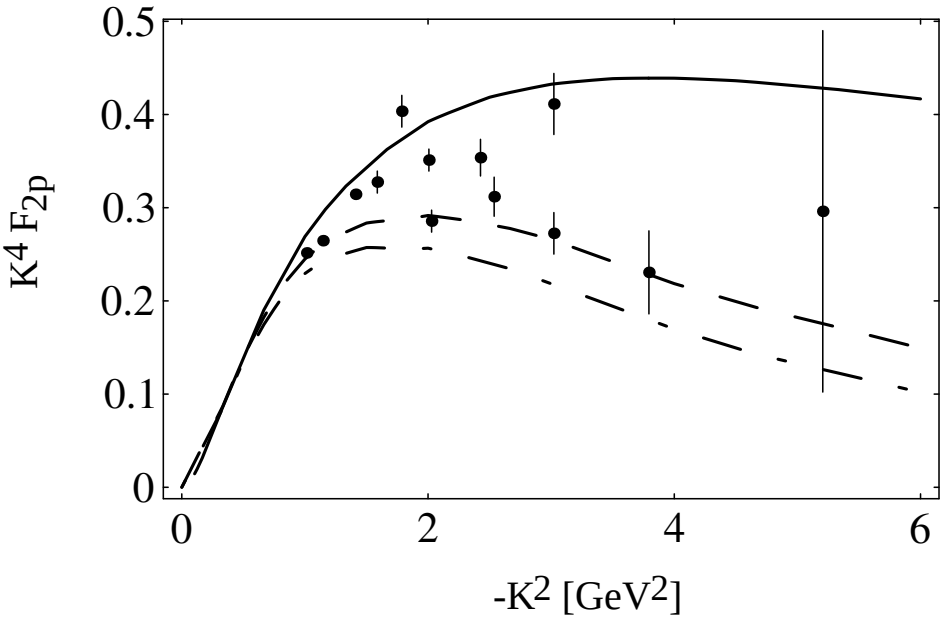

Figure 3.5: The proton form factor $F_{2p}(K^2)$. Continuous line, Parameter set 3; dashed line, parameter set 2; dashed-dotted line, parameter set 1. The experimental data are taken from Ref. [43, 44, 45].

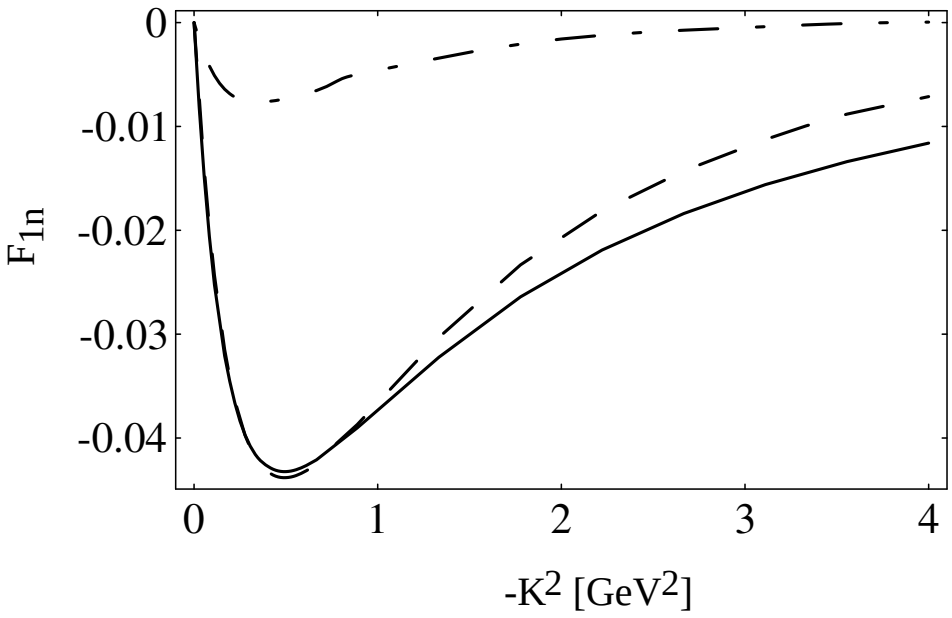

Figure 3.6: The neutron form factor $F_{1n}(K^2)$. Continuous line, Parameter set 3; dashed line, parameter set 2; dashed-dotted line, parameter set 1.

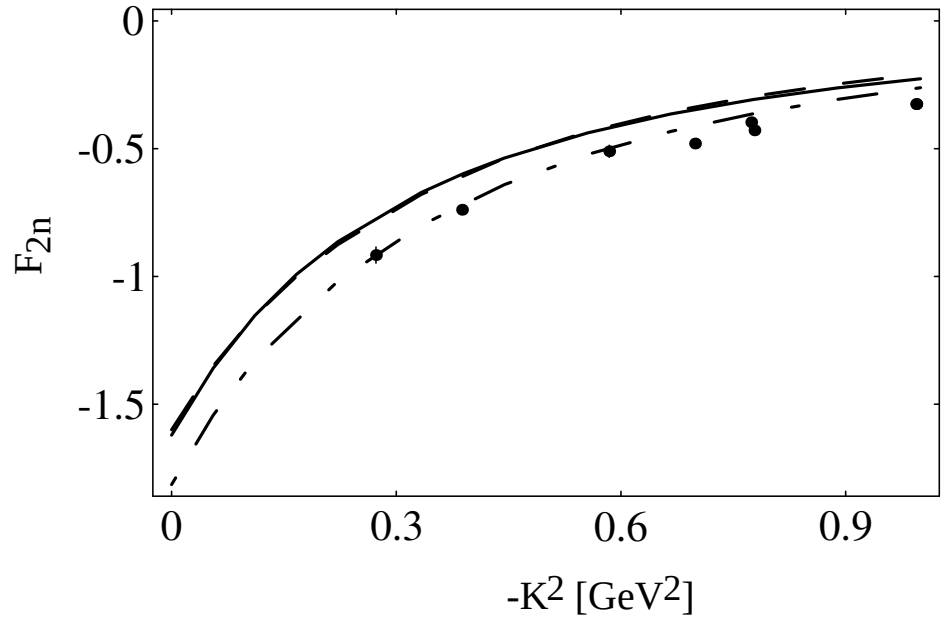

Figure 3.7: The neutron form factor $F_{2n}(K^2)$. Continuous line, Parameter set 3; dashed line, parameter set 2; dashed-dotted line, parameter set 1. The experimental data are taken from Ref. [48, 49, 50].

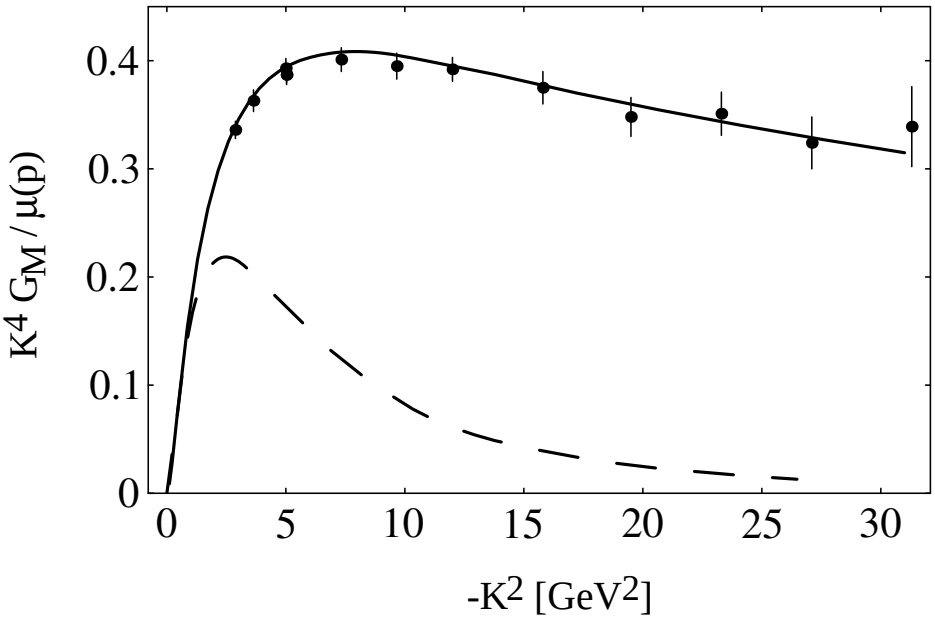

Figure 3.8: Proton form factor $G_{Mp}(K^2)$ for both wave functions in Eq. 2.33. Continuous line, Lorentz shaped wave function with parameter set 3; broken line; Gauss shaped wave function with parameter set 2. The experimental data are taken from Ref. [51].

3.2 Magnetic moment of the baryon octet

3.2.1 $F_2(0)$ in the quark model

According to Eq. (3.1) the magnetic moment of a baryon is $\mu = F_1(0) + F_2(0)$. The form factor $F_1(0)$ is equal to the charge, and $F_2(0)$ to the anomalous magnetic moment κ of the particle. We have [see Eqs. (2.25) and (3.5)]

$$M^+_{\lambda'\lambda} = 2P^+ \frac{N_c}{(2\pi)^6} \int d^3q d^3Q \left(\frac{E'_3 E'_{12} M}{E_3 E_{12} M'} \right)^{1/2} \Psi^\dagger(\mathbf{q}', \mathbf{Q}', \lambda') O \Psi(\mathbf{q}, \mathbf{Q}, \lambda) \; , \tag{3.10}$$

where O is given by:

$$O = 3\bar{u}_3 \left(F_{13}\gamma^+ + \frac{1}{2m_3} F_{23} i\sigma^{+\nu} K_\nu \right) u_3 \; .$$

We get for the baryon octet

$$\begin{aligned} \Psi^\dagger_\uparrow O \Psi_\uparrow (K^2 = 0) &= \sum_{i=1}^{3} F_{1i} \left\langle \chi^{bi}_\uparrow | \chi^{ai}_\uparrow \right\rangle |\phi|^2 \; , \\ \Psi^\dagger_\uparrow O \Psi_\downarrow &= \sum_{i=1}^{3} \phi^\dagger \phi \left(F_{1i} \left\langle \chi^{bi}_\uparrow | \chi^{ai}_\downarrow \right\rangle + \frac{K_\perp}{2m_i} F_{2i} \left\langle \chi^{bi}_\uparrow | O_3 | \chi^{ai}_\downarrow \right\rangle \right) \; , \end{aligned} \tag{3.11}$$

with $O_3 = \begin{pmatrix} 0 & -1 \\ 1 & 0 \end{pmatrix}$, and with

	p	n	Σ^+	Σ^-	Σ^0	Λ	Ξ^-	Ξ^0	$\Sigma^0\Lambda$
a/b	λ/λ	λ/λ	λ/λ	λ/λ	λ/λ	ρ/ρ	λ/λ	λ/λ	ρ/λ
i=1	u	d	u	d	(u+d)/2	(u+d)/2	s	s	(d–u)/2
i=2	u	d	u	d	(u+d)/2	(u+d)/2	s	s	(d–u)/2
i=3	d	u	s	s	s	s	d	u	–

In order to get $F_1(0)$ and $F_2(0)$ the matrix elements $\langle\chi_\uparrow|\chi_\uparrow\rangle$ and $\langle\chi_\uparrow|O_3|\chi_\downarrow\rangle$ have to be calculated to order 1, and $\langle\chi_\uparrow|\chi_\downarrow\rangle$ to order $K_\perp$:

$$\begin{aligned} \left\langle \chi^{\lambda}_\uparrow | \chi^{\lambda}_\uparrow \right\rangle &= \left\langle \chi^{\rho}_\uparrow | \chi^{\rho}_\uparrow \right\rangle = 1 \; , \\ \left\langle \chi^{\lambda 1}_\uparrow | O_3 | \chi^{\lambda 1}_\downarrow \right\rangle &= \left\langle \chi^{\lambda 2}_\uparrow | O_3 | \chi^{\lambda 2}_\downarrow \right\rangle = -\frac{2}{3} \frac{b^2}{b^2 + Q^2_\perp} \; , \\ \left\langle \chi^{\lambda 3}_\uparrow | O_3 | \chi^{\lambda 3}_\downarrow \right\rangle &= \frac{1}{3} \frac{b^2}{b^2 + Q^2_\perp} \; , \\ \left\langle \chi^{\rho 1}_\uparrow | O_3 | \chi^{\lambda 1}_\downarrow \right\rangle &= \left\langle \chi^{\rho 2}_\uparrow | O_3 | \chi^{\lambda 2}_\downarrow \right\rangle = \frac{1}{\sqrt{3}} \frac{b^2}{b^2 + Q^2_\perp} \; , \\ \left\langle \chi^{\rho 1}_\uparrow | O_3 | \chi^{\rho 1}_\downarrow \right\rangle &= \left\langle \chi^{\rho 2}_\uparrow | O_3 | \chi^{\rho 2}_\downarrow \right\rangle = 0 \; , \end{aligned}$$

$$
\begin{aligned}
\left\langle \chi_\uparrow^{\rho 3} | O_3 | \chi_\downarrow^{\rho 3} \right\rangle &= -\frac{b^2}{b^2+Q_\perp^2} \,, \\
\left\langle \chi_\uparrow^{\lambda 1} | \chi_\downarrow^{\lambda 1} \right\rangle &= \frac{1}{3} K_\perp (2A_1 + 2A_2 - A_3) \,, \\
\left\langle \chi_\uparrow^{\lambda 2} | \chi_\downarrow^{\lambda 2} \right\rangle &= \frac{1}{3} K_\perp (2A_1 + 2A_3 - A_2) \,, \\
\left\langle \chi_\uparrow^{\lambda 3} | \chi_\downarrow^{\lambda 3} \right\rangle &= \frac{1}{3} K_\perp (2A_2 + 2A_3 - A_1) \,, \\
\left\langle \chi_\uparrow^{\rho 1} | \chi_\downarrow^{\rho 1} \right\rangle &= K_\perp A_3 \,, \\
\left\langle \chi_\uparrow^{\rho 2} | \chi_\downarrow^{\rho 2} \right\rangle &= K_\perp A_2 \,, \\
\left\langle \chi_\uparrow^{\rho 3} | \chi_\downarrow^{\rho 3} \right\rangle &= K_\perp A_1 \,, \\
\left\langle \chi_\uparrow^{\rho 1} | \chi_\downarrow^{\lambda 1} \right\rangle &= \frac{1}{\sqrt{3}} K_\perp (A_2 - A_1) \,, \\
\left\langle \chi_\uparrow^{\rho 2} | \chi_\downarrow^{\lambda 2} \right\rangle &= \frac{1}{\sqrt{3}} K_\perp (A_2 - A_1) \,,
\end{aligned}
\tag{3.12}
$$

with

$$
\begin{aligned}
A_1 &= \frac{\frac{Q_\perp^2}{2M} - \eta b}{b^2+Q_\perp^2} \,, \\
A_2 &= \frac{\eta \left(a - \frac{Q_\perp^2}{2(1-\eta)M} \right)}{a^2+Q_\perp^2} \frac{d^2}{d^2+q_\perp^2} \,, \\
A_3 &= \frac{\eta \left(a - \frac{Q_\perp^2}{2(1-\eta)M} \right)}{a^2+Q_\perp^2} \frac{c^2}{c^2+q_\perp^2} \,.
\end{aligned}
$$

Eq. (3.10) together with Eqs. (3.11) and (3.12) is the most general formula for $F_2(0)$. Putting $m_u = m_d$ for the hyperons there is an equality $A_2 = A_3$ under the integral, which reduces the number of integrations. The simplified formulae read:

$$
\begin{aligned}
\kappa(p) &= -\frac{1}{3} S_N^{(3)} + \frac{4}{3} S_N^{(2)} + \frac{1}{3} \left(\frac{4F_{2u}}{2m_u} - \frac{F_{2d}}{2m_d} \right) Z_N \,, \\
\kappa(n) &= \frac{2}{3} S_N^{(3)} - \frac{2}{3} S_N^{(2)} - \frac{1}{3} \left(\frac{F_{2u}}{2m_u} - \frac{4F_{2d}}{2m_d} \right) Z_N \,, \\
\kappa(\Sigma^+) &= -\frac{1}{3} S_\Sigma^{(3)} + \frac{4}{3} S_\Sigma^{(2)} + \frac{4}{3} \frac{F_{2u}}{2m_u} Z_\Sigma^{(2)} - \frac{1}{3} \frac{F_{2s}}{2m_s} Z_\Sigma^{(3)} \,, \\
\kappa(\Sigma^-) &= -\frac{1}{3} S_\Sigma^{(3)} - \frac{2}{3} S_\Sigma^{(2)} - \frac{1}{3} \frac{F_{2s}}{2m_s} Z_\Sigma^{(3)} + \frac{4}{3} \frac{F_{2d}}{2m_d} Z_\Sigma^{(2)} \,, \\
\kappa(\Lambda) &= -\frac{1}{3} A_\Sigma^{(3)} + \frac{1}{3} A_\Sigma^{(2)} + \frac{F_{2s}}{2m_s} Z_\Sigma^{(3)} \,, \\
\kappa(\Xi^-) &= -\frac{1}{3} S_\Xi^{(3)} - \frac{2}{3} S_\Xi^{(2)} - \frac{1}{3} \frac{F_{2d}}{2m_d} Z_\Xi^{(3)} + \frac{4}{3} \frac{F_{2s}}{2m_s} Z_\Xi^{(2)} \,, \\
\kappa(\Xi^0) &= \frac{2}{3} S_\Xi^{(3)} - \frac{2}{3} S_\Xi^{(2)} - \frac{1}{3} \frac{F_{2u}}{2m_u} Z_\Xi^{(3)} + \frac{4}{3} \frac{F_{2s}}{2m_s} Z_\Xi^{(2)} \,,
\end{aligned}
\tag{3.13}
$$

$$
\begin{aligned}
\kappa(\Sigma^0\Lambda) &= \frac{\sqrt{3}}{2}\left(S_\Sigma^{(2)} - A_\Sigma^{(2)}\right) + \frac{1}{\sqrt{3}}\left(\frac{F_{2u}}{2m_u} - \frac{F_{2d}}{2m_d}\right) Z_\Sigma^{(2)} \ , \\
&\text{with} \\
S_B^{(2)} &= -2M_B \frac{N_c}{(2\pi)^6} \int d^3q d^3Q |\phi|^2 (2A_1 + A_2)/3 \ , \\
S_B^{(3)} &= -2M_B \frac{N_c}{(2\pi)^6} \int d^3q d^3Q |\phi|^2 (4A_2 - A_1)/3 \ , \\
A_B^{(2)} &= -2M_B \frac{N_c}{(2\pi)^6} \int d^3q d^3Q |\phi|^2 A_2 \ , \\
A_B^{(3)} &= -2M_B \frac{N_c}{(2\pi)^6} \int d^3q d^3Q |\phi|^2 A_1 \ , \\
Z_B &= 2M_B \frac{N_c}{(2\pi)^6} \int d^3q d^3Q |\phi|^2 \frac{b^2}{b^2 + Q_\perp^2} \ .
\end{aligned}
$$

The masses m_i are set as follows:

$$
\begin{aligned}
S_N^{(2)}, S_N^{(3)}, Z_N &: \quad m_1 = m_2 = m_3 = m \ , \\
S_\Sigma^{(2)}, A_\Sigma^{(2)}, Z_\Sigma^{(2)} &: \quad m_1 = m_3 = m, \quad m_2 = m_s \ , \\
S_\Sigma^{(3)}, A_\Sigma^{(3)}, Z_\Sigma^{(3)} &: \quad m_1 = m_2 = m, \quad m_3 = m_s \ , \\
S_\Xi^{(2)}, Z_\Xi^{(2)} &: \quad m_1 = m_3 = m_s, \quad m_2 = m \ , \\
S_\Xi^{(3)}, Z_\Xi^{(3)} &: \quad m_1 = m_2 = m_s, \quad m_3 = m \ ,
\end{aligned}
\tag{3.14}
$$

where $m = m_u = m_d$. In $\kappa(\Sigma^0\Lambda)$ the mass M_B is equal to $(M_\Lambda + M_\Sigma)/2$.

3.2.2 Results and conclusions

Table 3.3 shows the magnetic moments for all baryons and the transition moment $\Sigma^0 \to \Lambda\gamma$. For comparison we have chosen set 4 from Table 3.1.

These parameters are fitted to the magnetic moments and good agreement can be achieved even without anomalous quark magnetic moments. But we have

$$\beta_N \ll \beta_\Sigma \approx \beta_\Xi \ , \tag{3.15}$$

which cannot be reconciled with the weak beta decay, since the small wave function overlap would cause too large a suppression of the $\Delta S = 1$ transitions. Therefore, we reject the parameter set 4. In Chapter 4 it is shown that beta decay requires

$$\beta_N \approx \beta_\Sigma \approx \beta_\Xi \ . \tag{3.16}$$

So another set of parameters (set 6) will be considered in Chapter 4, but Table 3.3 shows that it leads to results which are in disagreement with experiment. Use of set 6 with non-zero quark anomalous magnetic moments (set 7) leads only to a slight improvement. For the quark form factor F_{2s} we get 0.056 GeV by fitting $\mu(\Lambda)$.

We did not used the Lorentz shaped wave function for the magnetic moments because this wave function is only important for high K^2-values.

Table 3.3: Magnetic moments of the baryon octet and transition moment for $\Sigma^0 \to \Lambda\gamma$ in units of the nuclear magneton.

Particle	Experiment [52]	Set 4	Set 6	Set 7
p	2.79 ± 10^{-7}	2.85	2.78	2.78
n	-1.91 ± 10^{-7}	–1.83	–1.62	–1.73
Σ^+	2.42 ± 0.05	2.59	3.23	3.15
Σ^-	-1.157 ± 0.025	–1.30	–1.36	–1.56
Λ	-0.613 ± 0.004	–0.48	–0.72	–0.58
Ξ^0	-1.250 ± 0.014	–1.25	–1.87	–1.64
Ξ^-	-0.679 ± 0.031	–0.99	–0.96	–0.71
$\Sigma^0\Lambda$	1.61 ± 0.08	1.22	1.74	1.79

We conclude that, within the symmetric wave function model, either the magnetic moments can be fitted and the weak decay parameters are poorly fitted or vice versa. The opposite statement in Ref. [9] has to be questioned, because their numerical results for the magnetic moments are wrong. Our results agree with Ref. [53] on this point. The inconsistency just described between the electromagnetic and the weak sector can be resolved by using asymmetric wave functions as described in Chapter 5.

Chapter 4

Hyperon semileptonic beta decay

There is evidence for SU(3) symmetry breaking in semileptonic beta decay of hyperons [2, 54]. Up to now one does not have any means to calculate such a behavior from first principles. Some symmetry breaking schemes have been proposed in the framework of bag models [55] and chiral perturbation theory [56]. Since they are different from each other we need some support from other models.

Another uncertainty in the analysis of data is the K^2 dependence of the form factors. Although it is generally small, a change of M_V or M_A by ± 0.15 GeV in the case $\Sigma^- \to ne\nu$ (which has the largest $K^2_{\rm max}$) causes a relative change of g_1/f_1 of $\pm 2\%$. Ignoring the K^2 dependence altogether would shift g_1/f_1 by 17%. Our quark model provides a unique scheme for the calculation of these form factors.

4.1 Hyperon semileptonic decay

In the low energy limit the standard model for semileptonic weak decays reduces to an effective current-current interaction Hamiltonian

$$H_{\rm int} = \frac{G}{\sqrt{2}} J_\mu L^\mu + \text{h.c.} \,, \tag{4.1}$$

where $G \simeq 10^{-5}/M_p^2$ is the weak coupling constant,

$$L^\mu = \bar{\psi_e}\gamma^\mu(1-\gamma_5)\psi_\nu + \bar{\psi_\mu}\gamma^\mu(1-\gamma_5)\psi_\nu \tag{4.2}$$

is the lepton current, and

$$J_\mu = V_\mu - A_\mu \,, \quad V_\mu = V_{ud}\bar{u}\gamma_\mu d + V_{us}\bar{u}\gamma_\mu s \,, \quad A_\mu = V_{ud}\bar{u}\gamma_\mu\gamma_5 d + V_{us}\bar{u}\gamma_\mu\gamma_5 s \,, \tag{4.3}$$

is the hadronic current, and V_{ud}, V_{us} are the elements of the Kobayashi-Maskawa mixing matrix. The τ-lepton current cannot contribute since m_τ is much too large.

The matrix elements of the hadronic current between spin-$\frac{1}{2}$ states are

$$\langle B', p' \,|V^\mu|\, B, p\rangle = V_{qq'}\bar{u}(p')\left[f_1(K^2)\gamma^\mu - \frac{f_2(K^2)}{M_i} i\sigma^{\mu\nu}K_\nu + \frac{f_3(K^2)}{M_i}K^\mu\right] u(p) \,, \tag{4.4}$$

$$\langle B', p' \left| A^\mu \right| B, p \rangle = V_{qq'} \bar{u}(p') \left[g_1(K^2)\gamma^\mu - \frac{g_2(K^2)}{M_i} i\sigma^{\mu\nu} K_\nu + \frac{g_3(K^2)}{M_i} K^\mu \right] \gamma_5 u(p) \ , \quad (4.5)$$

where $K = p - p'$ and M_i is the mass of the initial baryon. The quantities f_1 and g_1 are the vector and axial-vector form factors, f_2 and g_2 are the weak magnetism and electric form factors and f_3 and g_3 are the induced scalar and pseudoscalar form factors, respectively. T invariance implies real form factors. We do not calculate f_3 and g_3 since we put $K^+ = 0$ and their dependence on the decay spectra is of the order

$$\left(\frac{m_l}{M_i} \right)^2 \ll 1 \ , \quad (4.6)$$

where m_l is the mass of the final charged lepton. The other form factors are

$$\begin{aligned} 2P^+ f_1 &= \left\langle B', \uparrow \left| V^+ \right| B, \uparrow \right\rangle \ , \\ 2P^+ K_\perp f_2 &= M_i \left\langle B', \uparrow \left| V^+ \right| B, \downarrow \right\rangle \ , \\ 2P^+ g_1 &= \left\langle B', \uparrow \left| A^+ \right| B, \uparrow \right\rangle \ , \\ 2P^+ K_\perp g_2 &= -M_i \left\langle B', \uparrow \left| A^+ \right| B, \downarrow \right\rangle \ . \end{aligned} \quad (4.7)$$

What is usually measured is the total decay rate R, the electron-neutrino correlation $\alpha_{e\nu}$ and the electron α_e, neutrino α_ν and final baryon α_B asymmetries. The e-ν correlation is defined as

$$\alpha_{e\nu} = 2 \frac{N(\Theta_{e\nu} < \frac{1}{2}\pi) - N(\Theta_{e\nu} > \frac{1}{2}\pi)}{N(\Theta_{e\nu} < \frac{1}{2}\pi) + N(\Theta_{e\nu} > \frac{1}{2}\pi)} \ , \quad (4.8)$$

where $N(\Theta_{e\nu} < \frac{1}{2}\pi)$ is the number of e-ν pairs that form an angle $\Theta_{e\nu}$ smaller than 90°. The correlations α_e,α_ν and α_B are defined analogously with Θ_e,Θ_ν and Θ_B now being the angles between the e, ν, B directions and the polarization of the initial baryon.

Ignoring the lepton-mass one can calculate expressions for the measured quantities. We copy the expressions for R, $\alpha_{e\nu}$, α_e, α_ν and α_B from Ref. [57]:

$$\begin{aligned} R &= G^2 \frac{\Delta M^5 |V|^2}{60\pi^3} \Big[(1 - \frac{3}{2}\beta + \frac{6}{7}\beta^2) f_1^2 + \frac{4}{7}\beta^2 f_2^2 + (3 - \frac{9}{2}\beta + \frac{12}{7}\beta^2) g_1^2 \\ &\quad + \frac{12}{7}\beta^2 g_2^2 + \frac{6}{7}\beta^2 f_1 f_2 + (-4\beta + 6\beta^2) g_1 g_2 + \frac{4}{7}\beta^2 (f_1\lambda_f + 5 g_1 \lambda_g) \Big] \ , \quad (4.9) \\ R\alpha_{e\nu} &= G^2 \frac{\Delta M^5 |V|^2}{60\pi^3} \Big[(1 - \frac{5}{2}\beta + \frac{11}{7}\beta^2) f_1^2 - \frac{2}{7}\beta^2 f_2^2 + (-1 - \frac{3}{2}\beta + \frac{25}{7}\beta^2) g_1^2 \\ &\quad - 2\beta^2 g_2^2 - \frac{2}{7}\beta^2 f_1 f_2 + (4\beta - 2\beta^2) g_1 g_2 - \frac{24}{7}\beta^2 g_1 \lambda_g \Big] \ , \quad (4.10) \\ R\alpha_e &= G^2 \frac{\Delta M^5 |V|^2}{60\pi^3} \Big[(-\frac{1}{3}\beta + \frac{3}{14}\beta^2) f_1^2 - \frac{4}{21}\beta^2 f_2^2 + (-2 + \frac{8}{3}\beta - \frac{9}{14}\beta^2) g_1^2 - \frac{4}{3}\beta^2 g_2^2 \\ &\quad + (-\frac{2}{3}\beta + \frac{14}{21}\beta^2) f_1 f_2 + (2 - \frac{11}{3}\beta + \frac{15}{7}\beta^2) f_1 g_1 + (-\frac{2}{3}\beta + \frac{32}{21}\beta^2) f_1 g_2 \\ &\quad + (-\frac{2}{3}\beta + \frac{32}{21}\beta^2) f_2 g_1 + \frac{16}{21}\beta^2 f_2 g_2 + (\frac{10}{3}\beta - \frac{94}{21}\beta^2) g_1 g_2 \\ &\quad + \frac{4}{7}\beta^2 (g_1\lambda_f + f_1\lambda_g - 4 g_1 \lambda_g) \Big] \ , \quad (4.11) \end{aligned}$$

$$
\begin{aligned}
R\alpha_\nu &= G^2\frac{\Delta M^5|V|^2}{60\pi^3}\Big[(\frac{1}{3}\beta-\frac{3}{14}\beta^2)f_1^2+\frac{4}{21}\beta^2 f_2^2+(2-\frac{8}{3}\beta+\frac{9}{14}\beta^2)g_1^2+\frac{4}{3}\beta^2 g_2^2 \\
&\quad +(\frac{2}{3}\beta-\frac{14}{21}\beta^2)f_1f_2+(2-\frac{11}{3}\beta+\frac{15}{7}\beta^2)f_1g_1+(-\frac{2}{3}\beta+\frac{32}{21}\beta^2)f_1g_2 \\
&\quad +(-\frac{2}{3}\beta+\frac{32}{21}\beta^2)f_2g_1+\frac{16}{21}\beta^2 f_2g_2+(-\frac{10}{3}\beta+\frac{94}{21}\beta^2)g_1g_2 \\
&\quad +\frac{4}{7}\beta^2(g_1\lambda_f+f_1\lambda_g+4g_1\lambda_g)\Big]\ , \qquad (4.12)\\
R\alpha_B &= G^2\frac{\Delta M^5|V|^2}{60\pi^3}\frac{5}{2}\Big[(-1+\frac{11}{6}\beta-\beta^2)f_1g_1+(\frac{1}{3}\beta-\frac{5}{6}\beta^2)f_1g_2 \\
&\quad +(\frac{2}{3}\beta-\frac{7}{6}\beta^2)f_2g_1-\frac{2}{3}\beta^2 f_2g_2-\frac{1}{3}\beta^2(f_1\lambda_g+g_1\lambda_f)\Big]\ , \qquad (4.13)
\end{aligned}
$$

where β is defined as $\beta=(M_i-M_f)/M_i$, and $\Delta M=M_i-M_f$, M_i, M_f being the masses of the initial and final baryon, respectively. The K^2 dependence of f_2 and g_2 is ignored and f_1 and g_1 are expanded as

$$
f_1(K^2)=f_1(0)+\frac{K^2}{M_i^2}\lambda_f\ ,\quad g_1(K^2)=g_1(0)+\frac{K^2}{M_i^2}\lambda_g\ . \qquad (4.14)
$$

We get the corresponding expression for the dipole parameterization by putting

$$
\lambda_f=2M_i^2f_1/M_V^2\ ,\quad \lambda_g=2M_i^2g_1/M_A^2\ . \qquad (4.15)
$$

Two corrections have to be made to these quantities: (a) the correction due to the nonvanishing lepton mass and (b) the radiative corrections. To keep the lepton mass non-zero we integrate the differential decay rate for $f_2=g_2=0$:

$$
R=G^2\frac{M_i^5|V|^2}{32\pi^3}\int_{x_l^2}^{(1-x')^2}dz\left[\left(f_1^2+g_1^2\right)I_1+\left(f_1^2-g_1^2\right)I_2\right] \qquad (4.16)
$$

with

$$
\begin{aligned}
I_1 &= (z-x_l^2)(1+x'^2-z)f\ ,\\
I_2 &= -(z-x_l^2)x'f\ ,\\
f &= \lambda^{1/2}(1,z,x'^2)\lambda^{1/2}(z,x_l^2,0)/z\ ,\\
\lambda(x,y,z) &= x^2+y^2+z^2-2xy-2yz-2xz\ ,\\
x_l &= \frac{m_l}{M_i},\ x'=\frac{M_f}{M_i},\ K^2=zM_i^2\ .
\end{aligned}
$$

The ratio $R/R(m_l=0)$ for the various reactions is given in Table 4.1 for the e-mode ($l=e$) and the μ-mode ($l=\mu$).

The radiative corrections are well known [57]. The rate can be written as

$$
R'=R(1+\delta_a)(1+\delta_b)=R(1+\delta)\ , \qquad (4.17)
$$

where R is the rate defined in Eq. (4.9). The term δ_a comes from the model independent virtual corrections and the bremsstrahlung [58]. For the model dependent term δ_b one

Table 4.1: Ratio of the rate to the rate with vanishing lepton mass.

	$R/R(m_l = 0)$	
Reaction	e-mode	μ-mode
np	0.472	–
$\Sigma^+\Lambda$	1.000	–
$\Sigma^-\Lambda$	1.000	–
$\Sigma^-\Sigma^0$	0.955	–
$\Sigma^0\Sigma^+$	0.830	–
$\Xi^-\Xi^0$	0.971	–
Λp	1.000	0.161
$\Sigma^0 p$	1.000	0.431
$\Sigma^- n$	1.000	0.443
$\Xi^-\Lambda$	1.000	0.271
$\Xi^-\Sigma^0$	1.000	0.0136
$\Xi^0\Sigma^+$	1.000	0.00821

Table 4.2: Radiative corrections to the semileptonic decay rates.

	Reaction	δ_a	δ
e-mode	np	0.0486	0.0706
	$\Sigma^+\Lambda$	0.0015	0.0225
	$\Sigma^-\Lambda$	0.0012	0.0222
	$\Sigma^0\Sigma^+$	0.0226	0.0441
	$\Xi^-\Xi^0$	0.0104	0.0316
	Λp	0.0207	0.0421
	$\Sigma^0 p$	0.0196	0.0410
	$\Sigma^- n$	-0.0025	0.0184
	$\Xi^-\Lambda$	-0.0015	0.0195
	$\Xi^-\Sigma^0$	0.0000	0.0210
μ-mode	Λp	0.0468	0.0688
	$\Sigma^0 p$	0.0336	0.0553
	$\Sigma^- n$	-0.0022	0.0188
	$\Xi^-\Lambda$	-0.0013	0.0197
	$\Xi^-\Sigma^0$	0.0002	0.0212

takes the value 0.021 [59]. The δ term is the whole radiative correction given in Table 4.2 together with δ_a.

For the angular correlation $\alpha_{e\nu}$ and the asymmetries α_e and α_ν the model dependent corrections vanish and the model independent corrections are of the order of 0.001 [57]. We therefore do not include these corrections.

Table 4.3: Matrix elements for weak beta decay.

Reaction	
np	$-\left(\left\langle \chi^{\lambda 2}\left\vert O_3\right\vert \chi^{\lambda 1}\right\rangle + \left\langle \chi^{\lambda 1}\left\vert O_3\right\vert \chi^{\lambda 2}\right\rangle\right)$
$\Sigma^+\Lambda$	$-\frac{1}{\sqrt{2}}\left(\left\langle \chi^{\rho 1}\left\vert O_3\right\vert \chi^{\lambda 1}\right\rangle + \left\langle \chi^{\rho 2}\left\vert O_3\right\vert \chi^{\lambda 2}\right\rangle\right)$
$\Sigma^-\Lambda$	$-\frac{1}{\sqrt{2}}\left(\left\langle \chi^{\rho 1}\left\vert O_3\right\vert \chi^{\lambda 1}\right\rangle + \left\langle \chi^{\rho 2}\left\vert O_3\right\vert \chi^{\lambda 2}\right\rangle\right)$
$\Sigma^-\Sigma^0$	$\frac{1}{\sqrt{2}}\left(\left\langle \chi^{\lambda 1}\left\vert O_3\right\vert \chi^{\lambda 1}\right\rangle + \left\langle \chi^{\lambda 2}\left\vert O_3\right\vert \chi^{\lambda 2}\right\rangle\right)$
$\Sigma^0\Sigma^+$	$-\frac{1}{\sqrt{2}}\left(\left\langle \chi^{\lambda 1}\left\vert O_3\right\vert \chi^{\lambda 1}\right\rangle + \left\langle \chi^{\lambda 2}\left\vert O_3\right\vert \chi^{\lambda 2}\right\rangle\right)$
$\Xi^-\Xi^0$	$-\left\langle \chi^{\lambda 3}\left\vert O_3\right\vert \chi^{\lambda 3}\right\rangle$
Λp	$\frac{1}{\sqrt{2}}\left\langle \chi^{\lambda 2}-\chi^{\lambda 1}\left\vert O_3\right\vert \chi^{\rho 3}\right\rangle$
$\Sigma^0 p$	$\frac{1}{\sqrt{2}}\left\langle \chi^{\lambda 1}+\chi^{\lambda 2}\left\vert O_3\right\vert \chi^{\lambda 3}\right\rangle$
$\Sigma^- n$	$-\left\langle \chi^{\lambda 3}\left\vert O_3\right\vert \chi^{\lambda 3}\right\rangle$
$\Xi^-\Lambda$	$\frac{1}{\sqrt{2}}\left(\left\langle \chi^{\rho 2}\left\vert O_3\right\vert \chi^{\lambda 1}\right\rangle + \left\langle \chi^{\rho 1}\left\vert O_3\right\vert \chi^{\lambda 2}\right\rangle\right)$
$\Xi^-\Sigma^0$	$-\frac{1}{\sqrt{2}}\left(\left\langle \chi^{\lambda 1}\left\vert O_3\right\vert \chi^{\lambda 2}\right\rangle + \left\langle \chi^{\lambda 2}\left\vert O_3\right\vert \chi^{\lambda 1}\right\rangle\right)$
$\Xi^0\Sigma^+$	$-\left(\left\langle \chi^{\lambda 1}\left\vert O_3\right\vert \chi^{\lambda 2}\right\rangle + \left\langle \chi^{\lambda 2}\left\vert O_3\right\vert \chi^{\lambda 1}\right\rangle\right)$

4.2 The form factors in the quark model

The basic formula for the matrix elements in Eq. (4.7) is Eq. (2.25). The Dirac quark current

$$\bar{q}\Gamma^\mu q\ , \quad \Gamma^\mu = \gamma^\mu(1-\gamma_5) \tag{4.18}$$

can be generalized by the Ansatz

$$\Gamma^\mu = f_{1q}\gamma^\mu - \frac{f_{2q}}{m_q}i\sigma^{\mu\nu}K_\nu + \frac{f_{3q}}{m_q}K^\mu + g_{1q}\gamma^\mu\gamma_5 - \frac{g_{2q}}{m_q}i\sigma^{\mu\nu}K_\nu\gamma_5 + \frac{g_{3q}}{m_q}K^\mu\gamma_5\ . \tag{4.19}$$

The subscript 'q' stands for a transition on the quark level. The form factor f_{2q} is determined by the anomalous quark moments through CVC. But f_{2q} as well as f_{3q}, g_{2q} and g_{3q} do not contribute to $f_1(0)$ and $g_1(0)$ because of their factor K. Since K^2 is small and contributions different from $f_1(0)$ and $g_1(0)$ are of higher order in β we put $f_{2q} = f_{3q} = g_{2q} = g_{3q} = 0$ without loss of generality. For the form factors f_{1q} and g_{1q} we shall distinguish between the transitions $d \to u$ and $s \to u$. In the last Chapter we have put the parameters f_{1ud} and g_{1ud} equal to one. For the $s \to u$ transition we note that we have to put $f_{1us} = 1$, if we wish to predict V_{us}, since the rate is proportional to $f_{1us}^2|V_{us}|^2$. The determination of g_{1us} is discussed in the next Section. Notice that we would have to put $f_{1us} \sim g_{1us} \sim 5$, if we liked to fit the weak sector with parameter set 4 (see Table 5.2).

As seen from Eq. (4.7) we have to calculate $\langle\chi_\uparrow\left\vert V^+\right\vert\chi_\uparrow\rangle$, $\langle\chi_\uparrow\left\vert V^+\right\vert\chi_\downarrow\rangle$, $\langle\chi_\uparrow\left\vert A^+\right\vert\chi_\uparrow\rangle$ and $\langle\chi_\uparrow\left\vert A^+\right\vert\chi_\downarrow\rangle$. Table 4.3 gives the matrix elements for the various reactions with $O_3 = V^+, A^+$.

Table 4.4: Parameters in Eq. (4.20).

Reaction	$A(f_1)$	$A(f_2)$	$A(g_1)$
np	1	$(2A_2 - 5A_1)/3$	$\frac{5}{3}$
$\Sigma^+\Lambda$	0	$(A_2 + A_3 - 2A_1)/\sqrt{6}$	$\sqrt{\frac{2}{3}}$
$\Sigma^-\Lambda$	0	$(A_2 + A_3 - 2A_1)/\sqrt{6}$	$\sqrt{\frac{2}{3}}$
$\Sigma^-\Sigma^0$	$\sqrt{2}$	$-(4A_1 + A_2 + A_3)/(3\sqrt{2})$	$\frac{2\sqrt{2}}{3}$
$\Sigma^0\Sigma^+$	$-\sqrt{2}$	$(4A_1 + A_2 + A_3)/(3\sqrt{2})$	$-\frac{2\sqrt{2}}{3}$
$\Xi^-\Xi^0$	–1	$(2A_2 + 2A_3 - A_1)/3$	$\frac{1}{3}$

For $K^2 = 0$ we have for $\Delta S = 0$ transitions

$$\begin{aligned} f_1 &= A(f_1)\,, \\ f_2 &= \frac{N_c}{(2\pi)^6}\int d^3q d^3Q |\Phi|^2 A(f_2)\,, \\ g_1 &= g_{1ud}A(g_1)\frac{N_c}{(2\pi)^6}\int d^3q d^3Q |\Phi|^2 \frac{b^2 - Q_\perp^2}{b^2 + Q_\perp^2}\,, \\ g_2 &\simeq 0\,, \end{aligned} \tag{4.20}$$

with As given in Table 4.4. The values $A(f_1)$ and $A(g_1)$ are the values in the nonrelativistic quark model.

The $\Delta S = 1$ transitions for $K^2 = 0$ are

$$f_1 = \frac{N_c}{(2\pi)^6}\int d^3q d^3Q \left(\frac{E_3' E_{12}' M}{E_3 E_{12} M'}\right)^{1/2} \frac{\Phi^\dagger(M')\Phi(M)B(f_1)}{(a'^2 + Q_\perp^2)(a^2 + Q_\perp^2)\sqrt{b'^2 + Q_\perp^2}\sqrt{b^2 + Q_\perp^2}}\,, \tag{4.21}$$

$$g_1 = \frac{N_c}{(2\pi)^6}\int d^3q d^3Q \left(\frac{E_3' E_{12}' M}{E_3 E_{12} M'}\right)^{1/2} \frac{\Phi^\dagger(M')\Phi(M)B(g_1)}{(a'^2 + Q_\perp^2)(a^2 + Q_\perp^2)\sqrt{b'^2 + Q_\perp^2}\sqrt{b^2 + Q_\perp^2}}\,,$$

$$\begin{aligned} B(f_1) &= B_1(a'a + Q_\perp^2)^2(b'b + Q_\perp^2) \\ &\quad + B_2(a' - a)^2 Q_\perp^2 (b'b + Q_\perp^2)\frac{(cd - q_\perp^2)^2}{(c^2 + q_\perp^2)(d^2 + q_\perp^2)} \\ &\quad + B_3(a' - a)(b' - b)Q_\perp^2(a'a + Q_\perp^2)\left(\frac{c^2}{c^2 + q_\perp^2} + \frac{d^2}{d^2 + q_\perp^2}\right)\,, \end{aligned} \tag{4.22}$$

$$B(g_1) = B_4(b'b - Q_\perp^2)\left[(a'a + Q_\perp^2)^2 + (a' - a)^2 Q_\perp^2 \frac{(cd - q_\perp^2)^2}{(c^2 + q_\perp^2)(d^2 + q_\perp^2)}\right]$$

Table 4.5: Parameters in Eq. (4.22).

Reaction	B_1	B_2	B_3	B_4	B_5	B_6
Λp	$-\sqrt{\frac{3}{2}}$	$-\sqrt{\frac{3}{2}}$	0	$-\sqrt{\frac{3}{2}}$	0	0
$\Sigma^0 p$	$-\frac{1}{\sqrt{2}}$	$\frac{1}{3\sqrt{2}}$	$\frac{\sqrt{2}}{3}$	$\frac{1}{3\sqrt{2}}$	$\frac{4\sqrt{2}}{3}$	$\frac{\sqrt{2}}{3}$
$\Sigma^- n$	–1	$\frac{1}{3}$	$\frac{2}{3}$	$\frac{1}{3}$	$\frac{8}{3}$	$\frac{2}{3}$
$\Xi^-\Lambda$	$\sqrt{\frac{3}{2}}$	$\frac{1}{\sqrt{6}}$	$-\frac{1}{\sqrt{6}}$	$\frac{1}{\sqrt{6}}$	$-2\sqrt{\frac{2}{3}}$	$-\frac{1}{6}$
$\Xi^-\Sigma^0$	$\frac{1}{\sqrt{2}}$	$\frac{5}{3\sqrt{2}}$	$\frac{1}{3\sqrt{2}}$	$\frac{5}{3\sqrt{2}}$	$\frac{4}{3\sqrt{2}}$	$\frac{\sqrt{2}}{6}$
$\Xi^0\Sigma^+$	1	$\frac{5}{3}$	$\frac{1}{3}$	$\frac{5}{3}$	$\frac{4}{3}$	$\frac{1}{3}$

$$+B_5(a'-a)^2Q_\perp^2(b'b-Q_\perp^2)\frac{cdq_\perp^2}{(c^2+q_\perp^2)(d^2+q_\perp^2)}$$
$$+B_6(a'-a)Q_\perp^2(b'+b)(a'a+Q_\perp^2)\left(\frac{c^2}{c^2+q_\perp^2}+\frac{d^2}{d^2+q_\perp^2}\right) .$$

The B_i for the different decays are given in Table 4.5.

Eqs. (4.21) and (4.22) confirm the Ademollo-Gatto theorem [60]. Since $(a'-a)\sim\Delta m$ and $(b'-b)\sim\Delta m$ the symmetry breaking for f_1 is of the order $(\Delta m)^2$ whereas it is of the order Δm for g_1 owing to the term containing B_6. In addition to Ademollo-Gatto we see that the symmetry breaking for $g_1(\Lambda\to p)$ is also of second order.

The full formulae for $K^2\leq 0$ are longer than the ones for $K^2=0$; they are given in Appendix **??**.

4.3 Results

The form factors can be determined by the generalization of Eqs. (4.20) and (4.21). With the parameterization of the form factor $f(K^2)$:

$$f(K^2) \simeq \frac{f(0)}{1 - K^2/\Lambda_1^2 + K^4/\Lambda_2^4} \,, \tag{4.23}$$

we get the result shown in Tables 4.6 and 4.7 together with the rates, angular correlation and asymmetries from Eqs. (4.9)–(4.13). The parameters Λ_n are determined by the calculation of the appropriate derivatives of $f(K^2)$ at $K^2 = 0$. The rates have been corrected taking into account the non-vanishing lepton mass and radiative corrections.

4.3.1 The rates and $f_1(0), g_1(0)$

We fit our remaining parameters m_s and $\beta_\Sigma = \beta_\Lambda$ to the rate R and the ratio g_1/f_1 for the processes $\Lambda \to pe^-\bar{\nu}_e$ and $\Sigma^- \to ne^-\bar{\nu}_e$, and β_Ξ is fitted to the rate for $\Xi^- \to \Lambda e^-\bar{\nu}_e$. We find parameter set 5 of Table 3.1 and get

$$\begin{aligned} R(\Lambda \to pe^-\bar{\nu}_e) &= 3.38 \times 10^6 \mathrm{s}^{-1} \,, \\ R(\Sigma^- \to ne^-\bar{\nu}_e) &= 5.79 \times 10^6 \mathrm{s}^{-1} \,, \\ g_1/f_1(\Lambda \to pe^-\bar{\nu}_e) &= 0.782 \,, \\ g_1/f_1(\Sigma^- \to ne^-\bar{\nu}_e) &= -0.261 \,. \end{aligned}$$

But the value for m_s seems to be too small if we compare it with the well confined value in the meson sector of the same model [10]. By considering the constraints $\Delta m = m_s - m_{u/d} \simeq 140$ MeV and $m_s/m_{u/d} \simeq 1.4$ [63] we choose $m_s = 0.40$ GeV (set 6). The results with set 6 have been collected in Tables 4.6 and 4.7.

The largest discrepancy between theory and experiments comes from the rates and g_1/f_1 for the processes $\Lambda \to pe^-\bar{\nu}_e$ and $\Sigma^- \to ne^-\bar{\nu}_e$. By changing the axial couplings of the quarks, i.e. $g_{1us} \simeq 0.9$, we could improve the rates of both reactions, but the ratios g_1/f_1 clearly force us to use $g_{1us} = 1$. Another modification could be the $\Lambda - \Sigma^0$-mixing. Let us write

$$\Lambda_{\mathrm{phys}} = A\,\Lambda + B\,\Sigma^0 \,, \quad \Sigma^0_{\mathrm{phys}} = -B\,\Lambda + A\,\Sigma^0 \,, \quad A^2 + B^2 = 1 \,. \tag{4.24}$$

From the measurement $f_1/g_1(\Sigma^- \to \Lambda e^-\bar{\nu}_e)$ we get a constraint $A \geq 0.9961,\ B \leq 0.0078$ which gives

$$f_1/g_1(\Lambda \to pe^-\bar{\nu}_e) \geq 0.773 \quad (\geq 0.73 \text{ for } \Delta m = 63 \text{ MeV}) \,, \tag{4.25}$$

and reduces the rate by about 1 %. Therefore, $\Lambda - \Sigma^0$-mixing only improves one of the four values for which theory and experiment differ. Actually, this inconsistency of our values is a general feature of quark models with a SU(6) flavor-spin symmetry.[1] The ratio

[1] The bag model calculation [55] gives similar results: $g_1/f_1(\Lambda \to pe^-\bar{\nu}_e) = 0.84$, and $g_1/f_1(\Sigma^- \to ne^-\bar{\nu}_e) = -0.28$.

Table 4.6: Results for $\Delta S = 0$ weak beta decay with parameter set 6. Experimental data are from PDG [52].

		np	$\Sigma^+\Lambda$	$\Sigma^-\Lambda$	$\Sigma^-\Sigma^0$	$\Sigma^0\Sigma^+$	$\Xi^-\Xi^0$
f_1	$f_1(0)$	1.00	0	0	1.41	–1.41	–1.00
	Λ_1 [GeV]	0.69	–0.32[a]	–0.32[a]	0.60	0.60	0.56
	Λ_2 [GeV]	0.96	–1.72[a]	–1.72[a]	0.81	0.81	0.71
g_1	$g_1(0)$	1.25	0.60	0.60	0.69	–0.69	0.24
	Λ_1 [GeV]	0.76	0.77	0.77	0.77	0.77	0.76
	Λ_2 [GeV]	1.04	1.05	1.05	1.04	1.04	1.04
g_1/f_1	Theor.	1.252	0.736[b]	0.736[b]	0.491	0.491	–0.244
	Expt.	1.261	0.742[b]	–	–	–	$< 2 \times 10^3$
		±0.004	±0.018				
$\frac{f_2}{M}$ [GeV^{-1}]	Theor.	1.81	1.04	1.04	0.76	–0.76	0.73
	CVC	1.85	1.17	1.17	0.60	–0.60	1.00
$\frac{g_2}{M}$ [GeV^{-1}]		0	0	0	0	0	0
Rate [$10^6 s^{-1}$]	Theor.	1.152×10^{-9}	0.24	0.389	1.47 [c]	3.65[d]	1.55[c]
e-mode	Expt.	1.125×10^{-9}	0.25	0.387	–	–	–
		±0.004	±0.06	±0.018			
$\alpha_{e\nu}$	Theor.	–0.101	–0.404	–0.412	0.436	0.438	0.793
	Expt.	–0.102	–0.35	–0.404			
		±0.005	±0.15	±0.044			
α_e	Theor.	–0.112	–0.701	–0.704	0.287	0.288	–0.514
	Expt.	–0.083					
		±0.002					
α_ν	Theor.	0.989	0.647	0.645	0.850	0.850	–0.314
	Expt.	0.998					
		±0.025					
α_B	Theor.	–0.548	0.070	0.077	–0.710	–0.711	0.518
	Expt.						

[a] Instead of Λ_i we list $f_1^{(i)}$. [b] Instead of g_1/f_1 we list $\sqrt{3/2}g_1$. [c] $\times 10^{-6}$. [d] $\times 10^{-8}$.

Table 4.7: Results for $\Delta S = 1$ weak beta decay with parameter set 6. Experimental data are from PDG [52].

		Λp	$\Sigma^0 p$	$\Sigma^- n$	$\Xi^-\Lambda$	$\Xi^-\Sigma^0$	$\Xi^0\Sigma^+$
f_1	$f_1(0)$	–1.19	–0.69	–0.97	1.19	0.69	0.98
	Λ_1 [GeV]	0.71	0.64	0.64	0.68	0.75	0.75
	Λ_2[GeV]	0.98	0.84	0.90	0.89	1.05	1.05
g_1	$g_1(0)$	–0.99	0.19	0.27	0.33	0.94	1.33
	Λ_1 [GeV]	0.81	0.83	0.83	0.81	0.81	0.81
	Λ_2 [GeV]	1.12	1.16	1.16	1.10	1.12	1.12
g_1/f_1	Theor.	0.826	–0.275	–0.275	0.272	1.362	1.362
	Expt.	0.718	–	–0.340	0.250	1.287	< 2.93
		± 0.015		± 0.017	± 0.042	± 0.158	
$\frac{f_2}{M}$[GeV^{-1}]	Theor.	–0.85	0.44	0.62	0.070	0.98	1.38
	CVC	–1.19	–	1.12	–0.080	1.38	1.95
$\frac{g_2}{M}$ [GeV^{-1}]		–0.025	0.0043	0.0061	–[a]	–[a]	–[a]
Rate [$10^6 s^{-1}$]	Theor.	3.51	2.72	5.74	2.96	0.549	0.942
e-mode	Expt.	3.170	–	6.88	3.36	0.53	–
		± 0.058		± 0.26	± 0.19	± 0.10	
Rate [$10^6 s^{-1}$]	Theor.	0.58	1.18	2.54	0.80	7.47×10^{-3}	7.74×10^{-3}
μ-mode	Expt.	0.60	–	3.04	2.1	–	–
		± 0.13		± 0.27	± 2.1		
$\alpha_{e\nu}$	Theor.	–0.100	0.443	0.437	0.531	–0.252	–0.248
	Expt.	–0.017[b]		0.279	0.53		
		± 0.023		± 0.026	± 0.1		
α_e	Theor.	–0.021	–0.536	–0.537	0.236	–0.226	–0.223
	Expt.	0.125		–0.519[c]			
		± 0.066		± 0.104			
α_ν	Theor.	0.992	–0.318	–0.318	0.592	0.973	0.973
	Expt.	0.821		–0.230[c]			
		± 0.066		± 0.061			
α_B	Theor.	–0.582	0.568	0.569	–0.519	–0.437	–0.439
	Expt.	–0.508		0.509[c]			
		± 0.065		± 0.102			

[a] $\frac{g_2}{g_1 M} \simeq 0.023$ since $\frac{g_2}{g_1} \simeq$ constant. [b] From Ref. [61]. [c] From Ref. [62].

g_1/f_1 can generally be written as

$$\frac{g_1}{f_1} = \rho\eta \left(\frac{g_1}{f_1}\right)_{\rm non-rel} , \tag{4.26}$$

where $(g_1/f_1)_{\rm non-rel}$ is the non-relativistic value. The quantity ρ is a relativistic suppression factor due to the " small " components in the quark spinors (in the bag-model) or due to the Melosh-transformation (in our model). The quantity η is an enhancing factor due to SU(3) symmetry breaking in $\Delta S = 1$ transitions. From Tables 4.6 and 4.7 we see that $\rho \simeq 0.73 - 0.76$ depending on the strangeness content of the wave functions and $\eta \simeq 1.11$. This simple estimate shows that every quark model is *a priori* constrained to

$$\frac{g_1/f_1(\Lambda \to pe^-\bar{\nu}_e)}{g_1/f_1(\Sigma^- \to ne^-\bar{\nu}_e)} = -3 \tag{4.27}$$

in contrast to the experimental value -2.11 ± 0.15 for $g_2 = 0$. For $g_2 \neq 0$ it is measured that [64]

$$\left|\frac{g_1}{f_1}\right|_{\Lambda p} = 0.715 + 0.28\frac{g_2}{f_1} , \tag{4.28}$$

and [62]

$$\left|\frac{g_1}{f_1} - 0.237\frac{g_2}{f_1}\right|_{\Sigma^- n} = 0.34 \pm 0.017 , \tag{4.29}$$

which will bring the data closer to -3, but in our model $g_2/g_1 \simeq 0.025$ which is much too small to remove the discrepancy.

4.3.2 $f_2(0)$ and $g_2(0)$

Our model agrees with the conserved vector current (CVC) hypothesis. The deviations have the same origin as the too small neutron magnetic moment since f_2 and the magnetic moments have similar analytic forms. If we take μ_p as in Sec. 3.2, CVC will reproduce our values. The experimental situation is not yet clear, some experiments confirm [62] and some disprove [61] CVC.

For $\Delta S = 1$ transitions the prediction of g_2/g_1 for nonrelativistic quark models is ~ 0.37 and for the bag model ~ 0.15 [55]. Our model gives also a constant value [2]

$$\left(\frac{g_2}{g_1}\right)_{\Delta S=1} \simeq 0.025 . \tag{4.30}$$

For $\Delta S = 0$ transitions we get

$$\left(\frac{g_2}{g_1}\right)_{\Delta S=0} \simeq 0.0033 , \tag{4.31}$$

if we put $m_d - m_u = 7$ MeV. This confirms the viewpoint of the PDG [52] which fixes $g_2 = 0$. Experiments also find a vanishing or small g_2 [57].

With CVC and the absence of g_2 we reach the same conclusion that was reached in nuclear physics.

[2] $(g_2)_{\Xi\Lambda}$ and $(g_2)_{\Xi\Sigma}$ could only be calculated for $\Delta m = 63$ MeV and we get $(g_2/g_1)_{\Delta S=1} \simeq 0.11$.

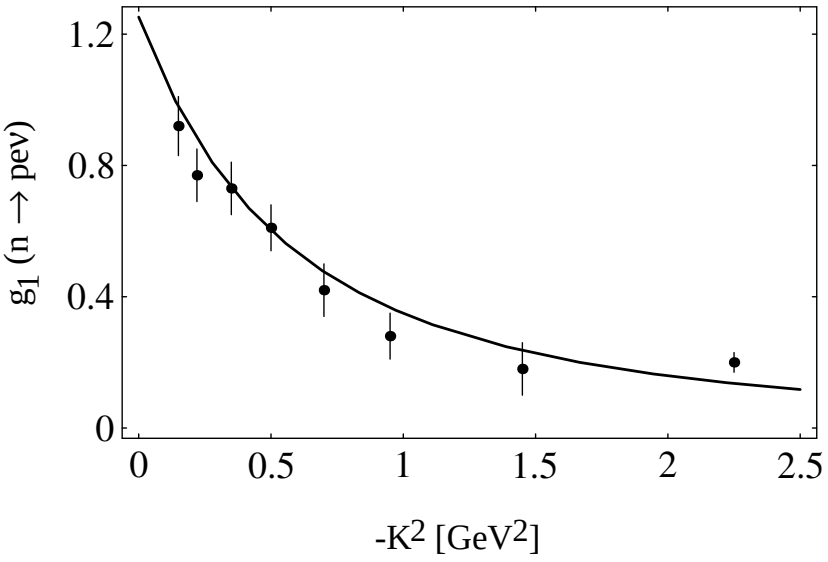

Figure 4.1: The axial vector form factor $g_1(K^2)$ for the np-transition. The dipole formula is compared with the experimental data taken from Ref. [65].

4.3.3 K^2-dependence of the form factors

Tables 4.6 and 4.7 suggest that the form factor of Eq. (4.23) can be approximated by the dipole form

$$f(K^2) \simeq \frac{f(0)}{\left(1 - K^2/\Lambda_2^2\right)^2} \,. \tag{4.32}$$

The axial vector form factor g_1 for the neutron decay gives a value $M_A = \Lambda_2 = 1.04$ GeV compared to the experimental value $M_A = (1.00 \pm 0.04)$ GeV [65, 66]. Figure 4.1 compares the dipole-fit with experimental points [65].

If we take the dipole Ansatz we can compare our values for M_V and M_A with the results of other work (see Table 4.8).

The contribution of M_V and M_A to the rate and to $x = g_1/f_1$ to first order is

$$\begin{aligned} \frac{\Delta R}{R} &= \frac{8}{7}\frac{\beta^2 M^2}{(1+3x^2)}\left(\frac{1}{M_V^2} + \frac{5x^2}{M_A^2}\right) \\ \frac{\Delta x^2}{x^2} &= -\frac{8}{7}\beta^2 M^2\left[\frac{(1-\alpha_{e\nu})\alpha_{e\nu}}{M_V^2} + \frac{6+5\alpha_{e\nu}}{M_A^2}\right] \end{aligned} \tag{4.33}$$

which shows that our parameters give for the decay $\Sigma^- \to ne^-\bar{\nu}_e$ a 0.3% larger rate and a 5% smaller g_1/f_1 than with the parameters of Gaillard et al. that are often used for the experimental analysis. Although this does not explain the inconsistency of the data with our calculation, it shows that future high-statistics experiments should pay more attention to M_V and M_A in analyzing g_1/f_1.

Table 4.8: The parameters M_V and M_A for various models.

	This work		Gaillard et al.[59]		Garcia et al. [57]		Gensini [54]	
	M_V	M_A	M_V	M_A	M_V	M_A	M_V	M_A
np	0.96	1.04	0.84	1.08	0.84	0.96	0.84	1.08
$\Sigma\Lambda$	-	1.05	-	1.08	-	0.96	-	1.08
$\Sigma\Sigma$	0.81	1.04	0.84	1.08	0.84	0.96	0.84	1.08
$\Xi\Xi$	0.71	1.04	0.84	1.08	0.84	0.96	0.84	1.08
Λp	0.98	1.12	0.98	1.25	0.97	1.11	0.94	1.16
Σp	0.84	1.16	0.98	1.25	0.97	1.11	0.94	1.16
Σn	0.90	1.16	0.98	1.25	0.97	1.11	0.94	1.16
$\Xi\Lambda$	0.89	1.10	0.98	1.25	0.97	1.11	0.94	1.16
$\Xi\Sigma$	1.05	1.12	0.98	1.25	0.97	1.11	0.94	1.16

4.4 Cabibbo fit and V_{us}

There are at present some questions concerning flavor SU(3) breaking in semileptonic weak hyperon decay [2, 3, 54]. This symmetry breaking is included to all orders in our approach. We can extract this effect from our model and fit the experimental values within the Cabibbo model. This has been done for the bag model in 1987 [55, 67], but since then some of the experimental data have changed. The main difficulty is the rate for $\Xi^- \to \Lambda e^- \bar{\nu}_e$, which comes out too small and is made even worse by their symmetry breaking scheme.

The reason for using the Cabibbo model is the bad fit for the relevant data in Table 4.7. The experimental deviations are as large as 17% and do not permit a precise determination of the Kobayashi-Maskawa matrix element V_{us}.

The Cabibbo model analyses the experimental results in terms of three parameters V_{us}, F, and D. The form factor $f_1(0)$ is given by SU(3) symmetry, $f_2(0)$ by its CVC-values and $g_1(0)$ as follows:

np	Λp	Σn	$\Sigma^{\pm}\Lambda$	$\Xi\Lambda$	$\Xi^-\Sigma$
$F+D$	$-\sqrt{3/2}(F+D/3)$	$-F+D$	$\sqrt{2/3}D$	$\sqrt{3/2}(F-D/3)$	$1/\sqrt{2}(F+D)$

The purpose of a Cabibbo fit is to determine the values of V_{us}, F, and D corresponding to the best agreement between experiment and theory.

We choose the value $V_{ud} = 0.9735$ of Ref. [68], and perform a least-squares χ^2-fit. Radiative corrections are taken into account.

Table 4.9 gives the residuals $R_i = [x_i(\text{fit}) - x_i(\text{meas})]/\delta x_i(\text{meas})$ for each reaction, $\chi^2 = \sum_i R_i^2$ for 11 degrees of freedom, and the fit variables.

Two fits have been made without symmetry breaking. Fit 1 uses the commonly used values of $M_{V/A}$ given in Ref. [59] and fit 2 uses our masses, which gives a slightly improved χ^2. Therefore, we use our values for all the other fits. The rate for $\Sigma^- \to \Lambda e^- \bar{\nu}$ produces

Table 4.9: Fits to the Cabibbo model. The decay rates are given in units of $10^6 s^{-1}$, except for the neutron decay with $10^3 s^{-1}$. The residuals are given by $[x_i(\text{fit}) - x_i(\text{meas})]/\delta x_i(\text{meas})$.

	Expt.	Residuals of fit no.						
		1	2	3	4	5	6	7
$R(n \to pe\nu)$	1.125 ± 0.013	-1.1	-1.1	-1.2	-1.5	-1.2	-1.2	-1.1
$R(\Lambda \to pe\nu)$	3.170 ± 0.058	0.9	0.8	1.0	1.5	1.2	0.3	0.4
$R(\Sigma \to ne\nu)$	6.88 ± 0.26	–0.5	–0.3	–0.3	–1.1	–0.5	–0.5	–0.7
$R(\Sigma^- \to \Lambda e\nu)$	0.387 ± 0.018	2.7	2.7	1.1	2.2	0.4	1.2	1.1
$R(\Sigma^+ \to \Lambda e\nu)$	0.25 ± 0.06	0.2	0.2	–0.1	0.1	–0.2	–0.1	–0.1
$R(\Xi^- \to \Lambda e\nu)$	3.36 ± 0.19	–2.2	–2.1	–2.8	–3.5	–3.3	1.1[a]	1.1[a]
$R(\Xi^- \to \Sigma e\nu)$	0.53 ± 0.10	0.0	–0.1	–0.2	0.2	–0.3	–0.3	–0.3
$R(\Lambda \to p\mu\nu)$	0.60 ± 0.13	–0.3	–0.3	–0.3	–0.3	–0.3	–0.4	–0.4
$R(\Sigma \to n\mu\nu)$	3.04 ± 0.27	–0.2	–0.1	–0.1	–0.4	–0.2	–0.2	–0.3
$R(\Xi^- \to \Lambda\mu\nu)$	2.1 ± 2.1	–0.6	–0.6	–0.6	–0.6	–0.6	–0.6	–0.6
$g_1(n \to pe\nu)$	1.261 ± 0.004	–0.1	–0.1	–0.2	–0.9	–0.3	–0.1	0.1
$\frac{g_1}{f_1}(\Lambda \to pe\nu)$	0.718 ± 0.015	0.9	1.0	2.8	5.2	3.5	2.7	1.1[b]
$\frac{g_1}{f_1}(\Sigma \to ne\nu)$	-0.340 ± 0.017	0.9	1.0	–0.6	–1.8	–1.4	–0.8	–0.5
$\frac{g_1}{f_1}(\Xi^- \to \Lambda e\nu)$	0.25 ± 0.05	–0.9	–0.9	–1.1	–0.8	–1.1	–1.1	–1.1
F		0.468	0.469	0.461	0.458	0.457	0.460	0.462
D		0.793	0.792	0.799	0.800	0.802	0.801	0.799
$V_{us}[\pm 0.003]$		0.227	0.226	0.226	0.222	0.223	0.225	0.225
χ^2		17.5	16.9	21.4	54.8	30.3	14.3	7.7

[a]We take the experimental value 1.83 ± 0.79 [69]. [b]The effective value 0.744 ± 0.015 is taken.

Table 4.10: Symmetry breaking for f_1. The ratio $f_1/f_1^{\text{SU(3)}}$ is shown.

	This work		Donoghue	Krause
	$\Delta m = 63$MeV	$\Delta m = 133$MeV		
$\Delta S = 0$	1	1	1	1
Λp	0.978	0.976	0.987	0.943
Σp	0.979	0.975	0.987	-
Σn	0.978	0.975	0.987	0.987
$\Xi\Lambda$	0.981	0.976	0.987	0.957
$\Xi\Sigma$	0.982	0.976	0.987	0.943

Table 4.11: Symmetry breaking for g_1. The ratio $g_1/g_1^{\mathrm{SU(3)}}$ is shown.

	This work		Donoghue
	$\Delta m = 63$MeV	$\Delta m = 133$MeV	
np	1.000	1.000	1.000
$\Sigma\Lambda$	0.959	0.981	0.9383/0.9390
$\Sigma\Sigma$	0.955	0.982	-
$\Xi\Xi$	0.916	0.977	-
Λp	1.021	1.072	1.050
Σp	1.011	1.051	-
Σn	1.012	1.056	1.040
$\Xi\Lambda$	0.987	1.072	1.003
$\Xi\Sigma$	0.981	1.061	0.9954

the largest deviation, indicating SU(3) symmetry breaking. Using Tables 4.10 and 4.11 we fit using $\Delta m = 63$ MeV (fit 3), $\Delta m = 133$ MeV (fit 4), and the results of Donoghue (fit 5). The symmetry breaking scheme for $\Delta m = 133$ MeV cannot be correct. We improved the above deviation at the cost of introducing a large contribution to χ^2 from the rate $\Xi^- \to \Lambda e^- \bar{\nu}$ and the ratio g_1/f_1 for $\Lambda \to p e^- \bar{\nu}$. Fit 3 performs best, but is still worse than no symmetry breaking. Since there are doubts about the experimental rate for $\Xi^- \to \Lambda e^- \bar{\nu}$ [2] we use $(1.83 \pm 0.79) \times 10^6 s^{-1}$ [69] for fit 6 with $\Delta m = 63$ MeV. This case is nearly as good as no symmetry breaking, which gives $\chi^2 = 13.8$. We have to remember Eq. (4.28) and footnote 2 on page 42, and the nonvanishing g_2 gives an effective $g_1/f_1 = 0.744 \pm 0.015$. With these data, fit 7 is in excellent agreement with experiment ($\chi^2 = 7.7$ for 11 DF). We observe that V_{us} lowers its value from fit 1 to 7, so that we get closer to the one derived from the meson sector. The analysis of K_{e3} decays yields

$$V_{us} = \begin{cases} 0.2196 \pm 0.0023 & \text{(Ref. [32])} , \\ 0.2199 \pm 0.0017 & \text{(Refs. [12, 70])}. \end{cases} \tag{4.34}$$

Other values from hyperon beta decay are

$$V_{us} = \begin{cases} 0.2258 \pm 0.0027 & \text{(Ref. [4])} , \\ 0.222 \pm 0.003 & \text{(Ref. [52])} . \end{cases} \tag{4.35}$$

The last value is derived from WA2 data [71] with the symmetry breaking scheme from Ref. [67]. Our result is in excellent agreement with the recent value from Ref. [4], and it is also consistent with the other baryonic value [52]. But the discrepancy with the meson sector still remains.

In conclusion, there is evidence for symmetry breaking from the rate $\Sigma^- \to \Lambda e^- \bar{\nu}$. But symmetry breaking alone makes the fit even worse. We also have to use a new value of $M_{V/A}$ and a small second-class axial coupling as given by our model. In this Section, we considered symmetry breaking due to the mass difference $m_s - m_{u/d}$ alone, but an asymmetric wave function as treated in Chapter 5 breaks SU(3) symmetry as well.

4.5 Conclusions

Parameter set 6 yields the best fit for the semileptonic weak decays in the MQM. It agrees with the data within 17%, except for some of the correlations and asymmetries. The main discrepancy with experiments lies with the decays $\Lambda \to pe^-\bar{\nu}_e$, and $\Sigma^- \to ne^-\bar{\nu}_e$, which are the main sources for determining the Kobayashi-Maskawa mixing matrix element V_{us}. This is the reason why we switched over to the Cabibbo model in calculating V_{us}.

The parameter set 6 is quite different from the set 4 found by a comparison with the baryon magnetic moments. This result shows that the representation of the model discussed up to now does not give a consistent picture of the u, d, and s sector of the baryons. A consistent picture can be achieved with the help of asymmetric wave functions as shown in the next Chapter. Even the fit within the weak sector improves dramatically.

Chapter 5

Asymmetric wave functions

5.1 The diquark model

In this Chapter we investigate the effects of an asymmetric wave function. Since the early days of the quark model diquark clustering has been studied. In Gell-Mann's original paper on quarks [1], he mentions the term diquark in a footnote. Refs. [72, 73] first took the idea seriously, and in both papers, a baryon is described as a bound state of a quark and a diquark. A recent review with many references can be found in Ref. [74]. It has even been seen that many gluon effects can be simulated by diquarks [75].

The concept of diquarks is also useful in treating deep-inelastic electron scattering. Feynman [76] observed that the experimental ratio of the neutron to proton structure function can be qualitatively explained if nearly all the momentum is carried by a leading quark, which is a u quark in the case of a proton and a d quark in the case of a neutron. In both cases a scalar diquark with isospin zero remains. Close [77] includes both scalar and vector diquarks, which have the same probability within SU(6) symmetry. The conclusion from the analysis [77] is that a scalar diquark is more probable than a vector one at large momentum transfer. This is in agreement with the fact that the QCD spin-spin force, originally introduced into the quark model in Ref. [78], is attractive and strongest in the spin-0 quark-quark state.

Most generally the proton can be composed of the four combinations for spin and isospin either equal to zero or one:

$$\begin{aligned} |p\rangle &= \mathrm{A}\; u(ud)_0\phi + \mathrm{B}\; d(uu)_0\phi + \mathrm{C}\; u(ud)_1\phi + \mathrm{D}\; d(uu)_1\phi + \text{ perm.}\,, \\ & \quad \mathrm{A}^2 + \mathrm{B}^2 + \mathrm{C}^2 + \mathrm{D}^2 = 1\,, \end{aligned} \tag{5.1}$$

where the parentheses indicate the diquark clustering and the spin of the quark pair is given as a subscript. A preliminary calculation for the magnetic moments of the baryon octet suggests that C and D are small or zero. The fit shows that if we put B = –0.2 the parameters β_q and β_Q, discussed below, can be chosen to be equal. Note that SU(6) is still broken in this case.

Considering the number of the parameters and because of the picture from deep-inelastic electron scattering we only keep the spin-isospin-0 part. To implement this feature we have to modify the wave functions in Section 2.3. In order to get a spin-

isospin-0 clustering we write the proton wave function as

$$\frac{-1}{\sqrt{18}}\left[-uud\left(\phi_1\chi^{\rho 1}+\phi_2\chi^{\rho 2}\right)+udu\left(\phi_1\chi^{\rho 1}-\phi_3\chi^{\rho 3}\right)+duu\left(\phi_2\chi^{\rho 2}+\phi_3\chi^{\rho 3}\right)\right] . \quad (5.2)$$

The wave functions for the Σs and Ξs are obtained by changing the flavor wave function accordingly. The Λ wave function is given by

$$\frac{-1}{\sqrt{12}}\left[\phi_3\chi^{\rho 3}\left(uds-dus\right)+\phi_2\chi^{\rho 2}\left(usd-dsu\right)+\phi_1\chi^{\rho 1}\left(sud-sdu\right)\right] . \quad (5.3)$$

The function ϕ_i is the momentum wave function with symmetry in the quarks different from i. We choose

$$\phi_i = N_i e^{-X_i} , \quad (5.4)$$

where the normalization factor N_i is given below and the X_i are the generalized forms of $M^2/2\beta$:

$$\begin{aligned}
X_3 &= \frac{Q_\perp^2}{2\eta(1-\eta)\beta_Q^2}+\frac{q_\perp^2}{2\eta\xi(1-\xi)\beta_q^2}+\frac{m_1^2}{2\eta\xi\beta_q^2}+\frac{m_2^2}{2\eta(1-\xi)\beta_q^2}+\frac{m_3^2}{2(1-\eta)\beta_Q^2} ,\\
X_2 &= q_\perp^2\frac{(1-\eta)(1-\xi)\beta_Q^2+\xi\beta_q^2}{2\beta_Q^2\beta_q^2\eta\xi(1-\xi)(1-\eta+\xi\eta)}+Q_\perp^2\frac{(1-\xi)(1-\eta)\beta_q^2+\xi\beta_Q^2}{2\beta_Q^2\beta_q^2\eta(1-\eta)(1-\eta+\xi\eta)}\\
&\quad +q_\perp Q_\perp\frac{\beta_Q^2-\beta_q^2}{\beta_Q^2\beta_q^2\eta(1-\eta+\xi\eta)}+\frac{m_1^2}{2\eta\xi\beta_q^2}+\frac{m_2^2}{2\eta(1-\xi)\beta_Q^2}+\frac{m_3^2}{2(1-\eta)\beta_q^2} ,\\
X_1 &= q_\perp^2\frac{(1-\xi)\beta_q^2+\xi(1-\eta)\beta_Q^2}{2\beta_Q^2\beta_q^2\eta\xi(1-\xi)(1-\xi\eta)}+Q_\perp^2\frac{(1-\xi)\beta_Q^2+\xi(1-\eta)\beta_q^2}{2\beta_Q^2\beta_q^2\eta(1-\eta)(1-\xi\eta)}\\
&\quad -q_\perp Q_\perp\frac{\beta_Q^2-\beta_q^2}{\beta_Q^2\beta_q^2\eta(1-\xi\eta)}+\frac{m_1^2}{2\eta\xi\beta_Q^2}+\frac{m_2^2}{2\eta(1-\xi)\beta_q^2}+\frac{m_3^2}{2(1-\eta)\beta_q^2} .
\end{aligned} \quad (5.5)$$

There is a special form of N_i with $N_1 = N_2 = N_3$:

$$N_i^2 = \left[\int e^{-2X_3}\frac{d\xi dq_\perp d\eta dQ_\perp}{\xi\eta(1-\xi)(1-\eta)}\right]^{-1} . \quad (5.6)$$

However, this normalization gives too small rates for the semileptonic decays. We use instead our usual normalization

$$\frac{N_c}{(2\pi)^6}\int d^3q d^3Q|\phi_i|^2 = 1 . \quad (5.7)$$

5.2 Results and discussions

The calculations of the matrix elements are similar to those in the symmetric case, but they are more involved because the wave function is no longer symmetric. We give an example for the vector current ($K^2 = 0$) [see Eq. **??**]

$$\langle\uparrow\uparrow\downarrow \mid \uparrow\uparrow\downarrow\rangle_{\rm asym} = \langle\uparrow\uparrow\downarrow \mid \uparrow\uparrow\downarrow\rangle_{\rm sym} - \frac{2(a-a')^2(bb'+Q_\perp)cd(q_LQ_R)^2}{(a'^2+Q_\perp^2)(a^2+Q_\perp^2)\sqrt{b'^2+Q_\perp^2}\sqrt{b^2+Q_\perp^2}(c^2+q_\perp^2)(d^2+q_\perp^2)} \,. \tag{5.8}$$

For the numerical calculation it is important to simplify the additional term to reduce the six-dimensional integral to a five-dimensional one (see Appendix A.2).

Before presenting the results we give some general considerations. To take an asymmetric wave function is the most natural extension to the minimal model. Since we do not have this possibility in the meson sector, this extension does not contradict the minimal meson model [10, 12]. Another question concerns the ratio in Eq. (4.27). It is in principle possible to improve this value drastically to give -2.26 ($m_{u/d} = 0.26$ GeV, $m_s = 0.39$ GeV, $\beta_{QN} = 0.3$ GeV, $\beta_{qN} = 0.7$ GeV, $\beta_{Q\Sigma} = 0.7$ GeV, $\beta_{q\Sigma} = 0.3$ GeV), which shows great flexibility compared to other models.

We minimize the function $\Delta = \sum_i |x_i(\text{fit}) - x_i(\text{meas})|$ for the fit. The details of the fit are described in Appendix A.3. Figure 5.1 shows Δ as a function of the various parameters. The black areas in the density plots indicate the minimum, the white areas the maximum of the function Δ. The fixed values of the parameters in the plots are the ones in Table 5.1. The figures (a) and (b) show the fit for the magnetic moments of the proton and neutron, and the weak axial form factor $g_1(n \to pe^-\bar{\nu}_e)$. We can see that there is no large diquark clustering in the nucleon sector ($\beta_{QN} = \beta_{qN}$). The magnetic moments of the hyperons are fitted in figures (c), (d) and (e). There is a strong diquark clustering in the strange baryon sector ($\beta_q \sim 2\beta_Q$). The mass of the u and d quarks is (0.26 ± 0.20) GeV for both the nucleons and hyperons. The strange quark mass is fixed to be 1.5 times $m_{u/d}$. Figure (f) gives the fit to the rates and the axial form factors for the decays $\Lambda \to pe^-\bar{\nu}_e$ and $\Sigma \to ne^-\bar{\nu}_e$ as a function of the weak quark form factors.

We summarize the results for the asymmetric parameter set in Table 5.2. There is a considerable improvement for the magnetic moments of the neutron, the Σs and Ξs, and for the rates and the ratios g_1/f_1 of the semileptonic decays. Non-zero quark anomalous magnetic form factors could even give better results for the magnetic moments of the neutron and the Ξ^- (see Table 3.3). Parameter set 8 fits both electromagnetic and weak

Table 5.1: The parameters of the asymmetric constituent quark model. All numbers are given in GeV.

	$m_{u/d}$	m_s	β_{QN}	β_{qN}	$\beta_{Q\Sigma/\Lambda}$	$\beta_{q\Sigma/\Lambda}$	$\beta_{Q\Xi}$	$\beta_{q\Xi}$	f_{1us}	g_{1us}
Set 8	0.26	0.395	0.55	0.55	0.35	0.65	0.34	0.65	1.32	1.17

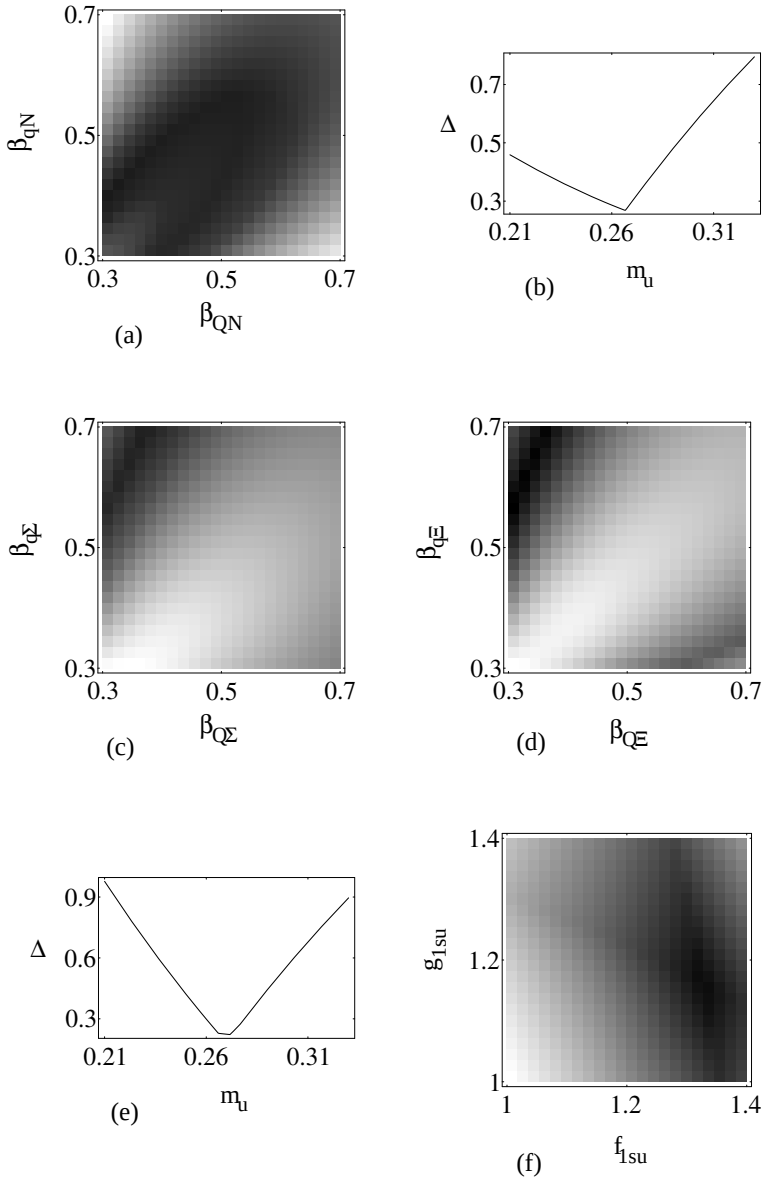

Figure 5.1: Parameter space of the asymmetric wave function fit. The deviation from the experimental data is plotted against the various parameters. The black areas in the density plot show the minimum, the white areas the maximum of the difference between the experimental values and those given by the fit. The βs and the masses are given in units of GeV.(a), (b) nucleon sector; (c), (d), (e) magnetic moments of the hyperons; (f) semileptonic, strangeness changing, weak decay.

Table 5.2: Electroweak properties of the baryon octet. The calculations with parameter sets 4, 6 and 8 are compared. We see that set 4 is only able to fit the magnetic moments (see Section 3.2), set 6 fits the weak sector (see Chapter 4), and set 8 can fit both sectors simultaneously. The magnetic moments are given in units of the nuclear magneton, the decay rates are given in $10^6 s^{-1}$.

Particle	Experiment [52]	Set 4	Set 6	Set 8
$\mu(p)$	2.79 ± 10^{-7}	2.85	2.78	2.82
$\mu(n)$	-1.91 ± 10^{-7}	–1.83	–1.62	–1.66
$\mu(\Sigma^+)$	2.42 ± 0.05	2.59	3.23	2.48
$\mu(\Sigma^-)$	-1.157 ± 0.025	–1.30	–1.36	–1.09
$\mu(\Lambda)$	-0.613 ± 0.004	–0.48	–0.72	–0.64
$\mu(\Xi^0)$	-1.250 ± 0.014	–1.25	–1.87	–1.28
$\mu(\Xi^-)$	-0.679 ± 0.031	–0.99	–0.96	–0.78
$\frac{g_1}{f_1}(np)$	1.261 ± 0.004	1.63	1.252	1.25
$\frac{g_1}{f_1}(\Lambda p)$	0.718 ± 0.015	0.957	0.826	0.760
$\frac{g_1}{f_1}(\Sigma n)$	-0.340 ± 0.017	–0.319	–0.275	–0.238
$\frac{g_1}{f_1}(\Xi^-\Lambda)$	0.250 ± 0.042	0.319	0.272	0.190
$\frac{g_1}{f_1}(\Xi^-\Sigma^0)$	1.287 ± 0.158	1.594	1.362	1.13
$R(\Lambda p)$	3.17 ± 0.058	0.14	3.51	3.20
$R(\Sigma n)$	6.88 ± 0.26	0.16	5.74	6.68
$R(\Xi^-\Lambda)$	3.36 ± 0.19	0.10	2.96	3.61
$R(\Xi^-\Sigma^0)$	0.53 ± 0.10	0.02	0.55	0.48

properties of the baryon octet. Weak form factors of the quarks are needed for the strangeness changing transition $s \to u$. Since the rate is proportional to $|V_{us}|^2 f_{1us}^2$ and we have to fit both values, we cannot predict an accurate value for V_{us}.

General features exhibited by these results are

- In the nucleon sector, there is no diquark clustering ($\beta_{QN} = \beta_{qN}$).
- There is a strong diquark clustering in the strange baryon sector ($2\beta_Q \sim \beta_q$).
- The momentum scale parameter for the diquark pair is about the same for all baryons ($\beta_{QN} = \beta_{qN} \sim \beta_{q\Sigma/\Lambda} = \beta_{q\Xi}$).

Table 5.3 compares the results of this work with other models. The nonrelativistic quark model yields accurate magnetic moments, but fails in the weak decay sector. The results derived from QCD sum rules and the bag model are comparable to those from our model. Nevertheless, some of the data are reproduced best within our model. The fits from the lattice simulation and the Skyrme model are too small.

Table 5.3: Electroweak properties of the baryon octet. The calculations of the present work with parameter set 8 are compared with the static nonrelativistic quark model (NQM), QCD sum rule (SR) [79], lattice simulations (Latt.) [80], bag model (Bag) [81], and Skyrme model (Skyr.) [82, 83]. The magnetic moments are given in units of the nuclear magneton.

Particle	Experiment [52]	Set 8	NQM	SR	Latt.	Bag	Skyr.
$\mu(p)$	2.79 $\pm 10^{-7}$	2.82	2.82	3.04	2.3	2.78	1.97
$\mu(n)$	–1.91 $\pm 10^{-7}$	–1.66	–1.88	–1.79	–1.3	–1.83	–1.24
$\mu(\Sigma^+)$	2.42 ± 0.05	2.48	2.70	2.73	1.9	2.65	2.25
$\mu(\Sigma^-)$	–1.157 ± 0.025	–1.09	–1.05	–1.26	–0.88	–1.40	–0.88
$\mu(\Lambda)$	–0.613 ± 0.004	–0.64	–0.60	–0.50	–0.41	–0.60	–0.59
$\mu(\Xi^0)$	–1.250 ± 0.014	–1.28	–1.43	–1.32	–0.96	–1.40	–1.42
$\mu(\Xi^-)$	–0.679 ± 0.031	–0.78	–0.49	–0.93	–0.42	–0.53	–0.40
$\frac{g_1}{f_1}(np)$	1.261 ± 0.004	1.25	1.67			1.224	0.61
$\frac{g_1}{f_1}(\Lambda p)$	0.718 ± 0.015	0.760	1.00			0.757	
$\frac{g_1}{f_1}(\Sigma n)$	–0.340 ± 0.017	–0.238	–0.33			–0.252	
$\frac{g_1}{f_1}(\Xi^-\Lambda)$	0.250 ± 0.042	0.190	0.33			0.167	
$\frac{g_1}{f_1}(\Xi^-\Sigma^0)$	1.287 ± 0.158	1.13	1.67			1.256	

Chapter 6

Discussion and conclusions

We have considered a relativistic model for the three-quark core of the baryons. A field-theory calculation of matrix elements between bound states is given with the help of the quasipotential reduction of the Bethe-Salpeter equation.

The input to our model fits is the constituent quark masses and the momentum range parameters. They are essentially free parameters in the framework of spectroscopic models, but they are kept fixed for the entire set of reactions. This is not an easy task because the minimal model will not do the job. The physical picture that emerges in our analysis is an asymmetric three quark state with a spin-isospin-0 diquark for the hyperons and a symmetric wave function for the nucleons, which is Lorentz shaped in the momentum distribution. Only for the strangeness-changing weak decay do we need nontrivial form factors. With this input we can fit almost every measurement within 6%; many fits are even more accurate (see Table 5.2).

There is no need for quark form factors in the electromagnetic sector except for fine tuning. Wave functions can be described without admixtures of mixed permutation symmetry. In fact, a slight asymmetry in the wave function does correspond to a nonvanishing mixed permutation symmetry, but we need a large diquark clustering, as we have seen in the previous Chapter.

The symmetry breaking scheme and the M_V and M_A of our model can explain all present data for the weak beta decay of the hyperons within the Cabibbo theory (see Sec. 4.4). The value for $V_{us} = 0.225 \pm 0.003$ that we get has recently been confirmed in a different analysis [4]. But a discrepancy with the meson sector still remains.

We list some features of our model, which have not been looked at before in this framework:

1. Asymmetric wave functions.
2. Wave functions with admixture of mixed permutation symmetry.
3. Wave functions with realistic high-momentum features up to more than 30 GeV^2.
4. Comprehensive calculations for both the electromagnetic and the weak sector.
5. Consistent symmetry breaking scheme for the Cabibbo theory.

6. Derivatives of the weak form factors.

It is interesting to note that the mass parameters in this work are similar to those in the meson sector of the same model [12]. This gives us confidence concerning the generality of the model.

We conclude with some remarks on how to improve the model described in this thesis.

1. In addition to the three valence quarks, one should consider the effects of higher Fock states (valence quarks, gluons).

2. The momentum wave function should be derived from a potential.

3. Gluon corrections should be calculated.

4. A different diquark clustering should be investigated.

Points 1 and 3 have been considered to some extent in our model because diquark clustering simulates gluon effects and these also give rise to higher Fock states. Point 2 should justify the choice of our wave function.

Appendix A

Computational methods

The main programs for this thesis are written in FORM [84], MATHEMATICA [85], FORTRAN [86], and C [87], together with the NAG LIBRARY [88]. They run on an Alliant FX/80, a Sun SPARC station, a Macintosh Classic, and a Macintosh IIsi. The final version of the programs are written in MATHEMATICA and C to meet two goals:

1. The software should be easy to modify and to maintain since we want to check many different flavors of the quark model.

2. Because the formulae are large, there should be a way to check their correctness easily.

The general design philosophy is given in Fig. A.1. The input, the description of the process, should be small and similar to the physical notation. The properties of the Melosh transform and of the various wave functions should be kept in a database, so that they have to be typed only once and can be thoroughly checked. From this starting point, the symbolic program should produce the large formulae in an automated way and splice them into the C program. With this method it is easy to achieve the two above mentioned goals, because the input is short and can be given in a physical language.

The rest of Appendix A is organized as follows: In Sec. A.1 we give details of the symbolic implementation. Numerical questions are treated in Sec. A.2, in Sec. A.3 we show our procedure for the multidimensional fit, and in the last Section some parts of the program are listed.

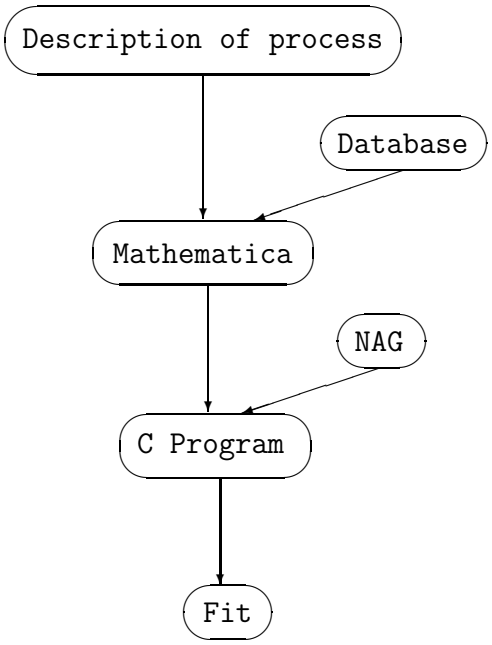

Figure A.1: Flow chart of the basic steps for this thesis. The aim was to keep the input for the programs as small and simple as possible to make sure to get correct results. The steps in between have been automated to minimize typographical errors.

A.1 Symbolic calculation

In implementing the wave functions of Eqs. (2.34), (5.2), and (5.3) we use some simple relations between them. For instance:

$$\begin{aligned} |n\rangle &= -|p\rangle\,(u \leftrightarrow d)\ , \\ |\Sigma^+\rangle &= -|p\rangle\,(d \to s)\ , \\ |p\downarrow\rangle &= -|p\uparrow\rangle\,(\uparrow\leftrightarrow\downarrow)\ . \end{aligned} \tag{A.1}$$

The wave functions in the MATHEMATICA program are written in an obvious notation. The flavors up, down, and strange are denoted by their initials `u`, `d`, `s`. The functions in Eq. (5.4) are `p1`, `p2`, and `p3`, respectively. Spin up and spin down are denoted by `a` and `b` respectively. This part of the MATHEMATICA program reads:

```
prot = -(uud (p1(aba-aab)+p2(baa-aab))
        +udu (p1(aab-aba)+p3(baa-aba))
        +duu (p2(aab-baa)+p3(aba-baa)))/Sqrt[18];
lam = (sud p1(aba-aab)+usd p2(baa-aab)
      +sdu p1(aab-aba)+uds p3(baa-aba)
      +dsu p2(aab-baa)+dus p3(aba-baa))/Sqrt[12];

ab = {aab -> -bba,aba -> -bab,baa -> -abb};
```

```
ud = {uud -> -ddu,udu -> -dud,duu -> -udd};
us = {uud -> -ssd,udu -> -sds,duu -> -dss};
ds = {uud -> -uus,udu -> -usu,duu -> -suu};
udds = {uud -> dds,udu -> dsd,duu -> sdd};
usdu = {uud -> ssu,udu -> sus,duu -> uss};
sigma = {uud->(uds+dus)/Sqrt[2],udu->(usd+dsu)/Sqrt[2],
       duu->(sud+sdu)/Sqrt[2]};

proton[spin_] := If[spin==1/2,prot,prot /. ab];
neutron[spin_] := If[spin==1/2,prot /. ud,
                                prot /. ud /.ab];
sigmaP[spin_] := If[spin==1/2,prot /. ds,
                                prot /. ds /.ab];
sigma0[spin_] := If[spin==1/2,prot /. sigma,
                                prot /. sigma /.ab];
sigmaM[spin_] := If[spin==1/2,prot /. udds,
                                prot /. udds /.ab];
xi0[spin_] := If[spin==1/2,prot /. usdu,
                                prot /. usdu /.ab];
xiM[spin_] := If[spin==1/2,prot /. us,
                                prot /. us /.ab];
lambda[spin_] := If[spin==1/2,lam,lam /.ab];
```

The wave function of the $|\Xi^0 \downarrow\rangle$ baryon for example can now be called by `xi0[-1/2]`. The transition matrix elements for the weak decay in Eq. (4.7) can be defined by a function `transition[.,.]`.

```
transition[b2_,b1_] :=
     Block[{b},b=b2 /. bar;
         Expand[3 b b1] /. flavourWeak /. spin
     ]
```

This function needs some additional definitions for the spin and flavor part.

```
flavourWeak ={udu udd -> 1,dud duu -> 1,ssd ssu -> 1,
              dsd dsu -> 1,sdd sdu -> 1,usd usu -> 1,
              sud suu -> 1,usu usd -> 1,
              uds udu -> 1,dus duu -> 1,dds ddu -> 1,
              sds sdu -> 1,dss dsu -> 1,sus suu -> 1,
              uss usu -> 1,sdu sdd -> 1,dsu dsd -> 1,
              uud->0,udu->0,duu->0,ddu->0,dud->0,udd->0,
              uds->0,dus->0,usd->0,dsu->0,sud->0,sdu->0,
              uus->0,usu->0,suu->0,dds->0,dsd->0,sdd->0,
              ssu->0,sus->0,uss->0,ssd->0,sds->0,dss->0};

spin = {aabs aab->aabaab,aabs aba->aababa,aabs baa->
```

```
        aabbaa,abas aab->abaaab,abas aba->abaaba,
        abas baa->ababaa,baas aab->baaaab,
        baas aba->baaaba,baas baa->baabaa};
bar = {aab->aabs,aba->abas,baa->baas,p1->p1s,
       p2->p2s,p3->p3s};
```

We now turn to the spin part of the bracket and write the Melosh transform in Eq. (2.29) as:

```
Melosh={{{a c-qr Ql,-a ql-c Ql},{c Qr +a qr,a c-ql Qr}},
        {{a d+qr Ql,a ql-d Ql},{d Qr-a qr,a d+ql Qr}},
        {{b,Ql},{-Qr,b}}} ;

aab = {Melosh[[1]].{1,0},Melosh[[2]].{1,0},
       Melosh[[3]].{0,1}};
aba = {Melosh[[1]].{1,0},Melosh[[2]].{0,1},
       Melosh[[3]].{1,0}};
baa = {Melosh[[1]].{0,1},Melosh[[2]].{1,0},
       Melosh[[3]].{1,0}};
abb = {Melosh[[1]].{1,0},Melosh[[2]].{0,1},
       Melosh[[3]].{0,1}};
bab = {Melosh[[1]].{0,1},Melosh[[2]].{1,0},
       Melosh[[3]].{0,1}};
bba = {Melosh[[1]].{0,1},Melosh[[2]].{0,1},
       Melosh[[3]].{1,0}};
```

For calculating the spin bracket we define the function `bracket[.,.]`, e.g. the transition $\langle\uparrow\downarrow\uparrow |A^+| \uparrow\downarrow\uparrow\rangle$ can be computed by `bracket[aba,aba]`.

```
o = {{{1,0},{0,1}},{{1,0},{0,1}},{{1,0},{0,-1}}};
qQrule1={qr->qt2/ql,Qr->Qt2/Ql};
qQrule2={ql^n_Integer?Negative->(qt2/qr)^n,
         Ql^n_Integer?Negative->(Qt2/Qr)^n}
qQrule3={ql Qr->qtQt,(ql Qr)^2->qlQr2,(ql Qr)^3->qlQr3,
        qr Ql->qtQt,(qr Ql)^2->qlQr2,(qr Ql)^3->qlQr3};
conjugate={qr->ql,ql->qr,Qr->Ql,Ql->Qr,a->as,b->bs};
bracket[x_,y_] :=
   Block[{z},z = x /. conjugate;
      Factor[ReplaceAll[ReplaceAll[ReplaceAll[Expand[
         Product[z[[i]].o[[i]].y[[i]],{i,1,3}]],qQrule1],
         qQrule2],qQrule3]]
        ]
```

The computation of `bracket[aba,aba]` takes 40 seconds on a Macintosh IIsi for $K^2 = 0$:

```
In = bracket[aba,aba]//Timing
```

```
Out = {39.23333333333333333*Second,
   (b*bs - Qt2)*(a^2*as^2*c^2*d^2 +
      2*a^2*c*d*qlQr2 - 4*a*as*c*d*qlQr2 +
      2*as^2*c*d*qlQr2 + a^2*as^2*c^2*qt2 +
      a^2*as^2*d^2*qt2 + a^2*as^2*qt2^2 +
      2*a*as*c^2*d^2*Qt2 + 2*a*as*c^2*qt2*Qt2 -
      2*a^2*c*d*qt2*Qt2 + 4*a*as*c*d*qt2*Qt2 -
      2*as^2*c*d*qt2*Qt2 + 2*a*as*d^2*qt2*Qt2 +
      2*a*as*qt2^2*Qt2 + c^2*d^2*Qt2^2 +
      c^2*qt2*Qt2^2 + d^2*qt2*Qt2^2 + qt2^2*Qt2^2
      )}
```

In order to obtain a convenient form for the numerical implementation in Sec. A.2 we define the function `list`, which gives a list of the coefficients of the spin parts.

```
coeff[a_,b_]:=Block[{x},x=Coefficient[a,b];
      {Coefficient[x,p1*p1s],Coefficient[x,p1*p2s],
      Coefficient[x,p1*p3s],Coefficient[x,p2*p1s],
      Coefficient[x,p2*p2s],Coefficient[x,p2*p3s],
      Coefficient[x,p3*p1s],Coefficient[x,p3*p2s],
      Coefficient[x,p3*p3s]}]
list[a_]:=Block[{x},x=Expand[N[a]];
  Flatten[{coeff[x,aabaab],coeff[x,aababa],coeff[x,aabbaa],
           coeff[x,abaaab],coeff[x,abaaba],coeff[x,ababaa],
           coeff[x,baaaab],coeff[x,baaaba],coeff[x,baabaa]}]]
```

A.2 Numerical calculation

The integrals to be handled are normally six dimensional. In some special cases, such as for $K^2 = 0$ and for a symmetric wave function, we have only four dimensional integrals to do. But it is obvious that a fast and accurate integration routine is crucial for our analysis. After testing various library and self-written routines we use the routine `d01fcf` from the NAG LIBRARY [88]. `d01fcf` is based on the `half` subroutine [89] and uses the basic rule described by Ref. [90]. The routine attempts to evaluate a multidimensional integral, with constant and finite limits, to a specified relative accuracy, using a repeated subdivision of the hyper-rectangular region into smaller hyper-rectangles. In each subregion, the integral is estimated using a seventh-degree rule, and an error estimate is obtained by comparison with a fifth-degree rule, which uses a subset of the same points. The error estimate is therefore less time consuming than for the Gauss integration. The fourth differences of the integrand along each coordinate axis are evaluated, and the subregion is marked for possible future subdivision in half along that coordinate axis which has the largest absolute fourth difference.

For a multidimensional integral it is important to keep the dimensionality of the integrals as small as possible. By introducing cylindrical coordinates we can easily reduce the six dimensions to five. Defining new variables by

$$\begin{aligned} q_1 &= q\cos\theta\ , & Q_1 &= Q\cos\phi\ , \\ q_2 &= q\sin\theta\ , & Q_2 &= Q\sin\phi\ , \\ q_3 &= q_3\ , & Q_3 &= Q_3\ , \\ 0 &< \theta < 2\pi\ , & 0 &< \phi < 2\pi\ , \end{aligned} \tag{A.2}$$

we can write the difficult parts of the formulae [e.g. (5.5) and (5.8)] as follows:

$$\begin{aligned} q_\perp Q_\perp &= qQ\cos(\theta-\phi)\ , \\ (q_L q_R)^2 &= q^2Q^2\cos[2(\theta-\phi)]\ , \\ (q_L q_R)^3 &= q^3Q^3\cos(\theta-\phi)\left\{2\cos[2(\theta-\phi)]-1\right\}\ . \end{aligned} \tag{A.3}$$

Since the integrand depends only on $(\theta-\phi)$, one integral is trivial. This is crucial because the routine `d01fcf` looses much efficiency for more than five integrations. In some cases the $(\theta-\phi)$-integration can also be done yielding modified Bessel functions of the first kind, but the speed of the routine `d01fcf` would not increase.

A.3 Fitting procedures

The procedure to fit our variables to the experimental data is rather involved since the number of variables is high for some versions of our model. One way to go is to fit some subset of the experiments, e.g. the nucleon sector, and fix the values of the parameters so obtained when fitting the rest of the data. The other way is to define a function that measures the error of the fit. The MATHEMATICA function for the magnetic moments of the octet could be written as:

```
f[mu_,bQs_,bqs_,bQx_,bqx_]:=
    Abs[1.42-sP[mu,bQs,bqs]]+
    Abs[-0.16-sM[mu,bQs,bqs]]+
    Abs[-0.61-ml[mu,bQs,bqs]]+
    Abs[-1.25-x0[mu,bQx,bqx]]+
    Abs[0.32-xM[mu,bQx,bqx]];
```

The calls `sP`, `sM`, `ml`, `x0`, and `xM` give the magnetic moments of the Σ^+, Σ^0, Λ, Ξ^0, and Ξ^- respectively as a function of the mass of the u quark (`mu`), and the scale factors $\beta_{q\Sigma}$ (`bqs`), $\beta_{Q\Sigma}$ (`bQs`), $\beta_{q\Xi}$ (`bqx`), and $\beta_{Q\Xi}$ (`bQx`). Because of speed considerations we do not directly compute the magnetic moments at runtime, but we build a lookup table, which we interpolate with the MATHEMATICA function `Interpolate`, e.g.

```
sP=Interpolation[data_sP,InterpolationOrder->3].
```

A local minimum of the function `f` can be found by the MATHEMATICA command

```
FindMinimum[f[mu,bQs,bqs,bQx,bqx],
    {mu,{.25,.26},.21,.33},{bQs,{.5,.52},.3,.7},
    {bqs,{.5,.52},.3,.7},{bQx,{.5,.52},.3,.7},
    {bqx,{.5,.52},.3,.7}]
```

To search for a global minimum we use the graphics capability of MATHEMATICA. The command

```
DensityPlot[f[.25,.35,.65,bQx,bqx],{bQx,.3,.7},{bqx,.3,.7}]
```

produces the plot in Fig. A.2. The black areas show the minimum, the white areas the maximum of the function `f` mentioned above. We can easily see in Fig. A.2 that an asymmetric wave function is strongly favored.

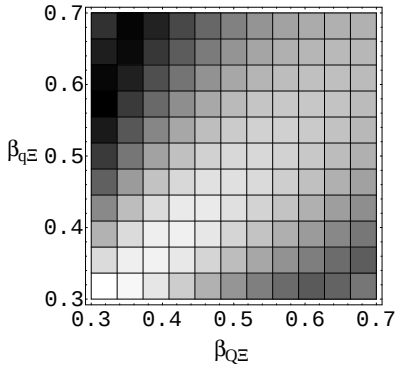

Figure A.2: Example of a density plot for the magnetic moments of the baryon octet. The black areas show the minimum, the white areas the maximum of the deviation from the experimental data. The βs are given in units of GeV. One can easily see that an asymmetric wave function is strongly favored.

A.4 Program listing

In this Section we present some parts of the listing of the C program for the strangeness-changing weak semileptonic decay with no momentum transfer ($K^2 = 0$). The programs for $K^2 \neq 0$ are larger, and the one for electromagnetic properties is shorter. We will not present the entire program, but simply comment on some of its parts. The aim was to keep the program modular and flexible.

The FORTRAN routine `d01fcf` can be called from within a C program in the following way:

```
d01fcf_(&ndim,a,b,&minpts,&maxpts,g1sn_,&eps,&acc,&lenwrk,
        wrkstr,&sum_g1sn,&ifail);
```

The routine names must be extended by an underscore, and the variables must be called by addresses. In the above call we evaluate the form factor g_1 for the process $\Sigma^- \to n$ and store its value in the variable `sum_g1sn`. The function `g1sn` is given below, and the parameters are fixed by experience as follows:

```
#define LENWRK 100000
#define N      5
#define PI2    6.283185308
...
  int ndim=N,ifail=1,minpts=0,maxpts=(int)(93*LENWRK/7),lenwrk=LENWRK;
  static double a[N]={0.,-3.,0.,-3.,0.},b[N]={3.,3.,3.,3.,PI2};
  double eps,acc,wrkstr[LENWRK], ...
```

The succeeding parts of the C program are directly produced by the MATHEMATICA programs explained in Sec. A.1. The MATHEMATICA command

```
FactorTerms[transition[sigmaM[.5],neutron[.5]]]//list
```

produces the array in the function `g1sn`.

```
double g1sn_(ndim,z)
int *ndim;
double *z;
{
double trans[81]={-0.1666666666666666667, -0.1666666666666666667, 0,
  -0.1666666666666666667, -0.1666666666666666667, 0, 0, 0,
  0, 0.1666666666666666667, 0.1666666666666666667, 0, 0, 0,
  0, 0, 0, 0, 0, 0, 0, 0.1666666666666666667,
  0.1666666666666666667, 0, 0, 0, 0, 0.1666666666666666667,
  0, 0, 0.1666666666666666667, 0, 0, 0, 0, 0,
  -0.1666666666666666667, 0, 0, 0, 0, 0, 0, 0, 0, 0, 0, 0,
  -0.1666666666666666667, 0, 0, 0, 0, 0, 0,
  0.1666666666666666667, 0, 0, 0.1666666666666666667, 0, 0,
  0, 0, 0, -0.1666666666666666667, 0, 0, 0, 0, 0, 0, 0, 0,
  0, 0, 0, -0.1666666666666666667, 0, 0, 0, 0},axial();
return(axial(z,trans));
}
```

The function `axial`, called on the last line, contains the entire implementation of the Melosh transform, the kinematics, and the variable transform discussed in the proceeding Section. The wave functions are taken from Eq. (5.5). The spin transitions `aabaab, aababa, ...` are calculated with MATHEMATICA as shown in Sec. A.1:

```
aabaab=bracket[aab,aab];
aababa=bracket[aab,aba];
...
Splice["weak.mc"]
```

The last command `Splice` splices MATHEMATICA output into an external file. The output looks as follows:

```
double axial(z,t)
double *z,*t;
{
  double q,qt2,Q,Qt2,theta,M,M3,xi,eta,p1,p2,p3,p1s,p2s,p3s,
         alpha2,beta2,alpha2s,beta2s,m12,m22,m32,m32s,aabaab,aababa,
         aabbaa,abaaab,abaaba,ababaa,baaaab,baaaba,baabaa,res,qtQt,
         qlQr2,qlQr3,Ms,Q3,Q3s,Q_2,Q_2s,e3,e3s,e12,e12s,a,as,b,bs,c,d,
         X1,X2,X3,X1s,X2s,X3s,q_2,e1,e2,q3;
  q=z[0]; q3=z[1]; Q=z[2]; Q3=z[3]; theta=z[4];

  qt2 = q*q; Qt2 = Q*Q;
  q_2 = qt2 + q3 * q3; Q_2 = Qt2 + Q3 * Q3;
  qtQt = q*Q*cos(theta);
  qlQr2 = q*q*Q*Q*cos(2.*theta);
```

```
  qlQr3 = q*q*q*Q*Q*Q*cos(theta)*(2.*cos(2.*theta)-1);

  e1 = sqrt(q_2 + m1 * m1); e2 = sqrt(q_2 + m2 * m2); M3 = e1 + e2;
  e3 = sqrt(Q_2 + m3 * m3); e12 = sqrt(Q_2 + M3 * M3);M = e3 + e12;
  xi = (e1 + q3)/M3; eta = (e12 + Q3)/M;
  Ms = sqrt((Qt2+(1-eta)*M3*M3+eta*m3s*m3s)/eta/(1-eta));
  Q3s = (eta-0.5)*Ms-(M3*M3-m3s*m3s)/2.0/Ms;
  Q_2s = Qt2 + Q3s * Q3s;
  e3s = sqrt(Q_2s + m3s * m3s); e12s = sqrt(Q_2s + M3 * M3);

  a = M3 + eta * M;       as = M3 + eta * Ms;
  b = m3 + (1 - eta) * M; bs = m3s + (1 - eta) * Ms;
  c = m1 + xi * M3;
  d = m2 + (1 - xi) * M3;

  alpha2 = alpha*alpha; beta2 = beta*beta;
  alpha2s = alphas*alphas; beta2s = betas*betas;
  m12=m1*m1; m22=m2*m2; m32=m3*m3; m32s=m3s*m3s;
  X3=(Qt2/eta/(1-eta)/alpha2+qt2/eta/xi/(1-xi)/beta2+
      m12/eta/xi/beta2+m22/eta/(1-xi)/beta2+m32/(1-eta)/alpha2);
  X2=qt2*((1-eta)*(1-xi)*alpha2+xi*beta2)/alpha2/beta2
     /eta/xi/(1-xi)/(1-eta+xi*eta)+Qt2*((1-xi)
     *(1-eta)*beta2+xi*alpha2)/alpha2/beta2/eta
     /(1-eta)/(1-eta+xi*eta)+2.*(alpha2-beta2)/alpha2
     /beta2/eta/(1-eta+xi*eta)*q*Q*cos(theta)+
     m12/eta/xi/beta2+m22/eta/(1-xi)/alpha2+m32/(1-eta)/beta2;
  X1=qt2*((1-xi)*beta2+xi*(1-eta)*alpha2)/alpha2/beta2
     /eta/xi/(1-xi)/(1-xi*eta)+Qt2*((1-xi)*alpha2+xi*(1-eta)*
     beta2)/alpha2/beta2/eta/(1-eta)/(1-xi*eta)-2.*(alpha2-beta2)
     /alpha2/beta2/eta/(1-xi*eta)*q*Q*cos(theta)+
     m12/eta/xi/alpha2+m22/eta/(1-xi)/beta2+m32/(1-eta)/beta2;
#ifdef GAUSS
  p3=N3*exp(-X3/2.); p2=N2*exp(-X2/2.); p1=N1*exp(-X1/2.);
#else
  p3=N3*pow((X3+1),-4); p2=N2*pow((X2+1),-4); p1=N1*pow((X1+1),-4);
#endif
  X3s=(Qt2/eta/(1-eta)/alpha2s+qt2/eta/xi/(1-xi)/beta2s+
      m12/eta/xi/beta2s+m22/eta/(1-xi)/beta2s+m32s/(1-eta)/alpha2s);
  X2s=qt2*((1-eta)*(1-xi)*alpha2s+xi*beta2s)/alpha2s/beta2s
     /eta/xi/(1-xi)/(1-eta+xi*eta)+Qt2*((1-xi)
     *(1-eta)*beta2s+xi*alpha2s)/alpha2s/beta2s/eta
     /(1-eta)/(1-eta+xi*eta)+2.*(alpha2s-beta2s)/alpha2s
     /beta2s/eta/(1-eta+xi*eta)*q*Q*cos(theta)+
     m12/eta/xi/beta2s+m22/eta/(1-xi)/alpha2s+m32s/(1-eta)/beta2s;
  X1s=qt2*((1-xi)*beta2s+xi*(1-eta)*alpha2s)/alpha2s/beta2s
```

```
     /eta/xi/(1-xi)/(1-xi*eta)+Qt2*((1-xi)*alpha2s+xi*(1-eta)*
     beta2s)/alpha2s/beta2s/eta/(1-eta)/(1-xi*eta)-2.*(alpha2s-beta2s)
     /alpha2s/beta2s/eta/(1-xi*eta)*q*Q*cos(theta)+
     m12/eta/xi/alpha2s+m22/eta/(1-xi)/beta2s+m32s/(1-eta)/beta2s;
#ifdef GAUSS
  p3=N3*exp(-X3s/2.); p2=N2*exp(-X2s/2.); p1=N1*exp(-X1s/2.);
#else
  p3=N3*pow((X3s+1),-4); p2=N2*pow((X2s+1),-4); p1=N1*pow((X1s+1),-4);
#endif

  aabaab=(Qt2 - b*bs)*(Qt2*Qt2*c*c*d*d + 2*Qt2*a*as*c*c*d*d +
    a*a*as*as*c*c*d*d - 2*a*a*c*d*qlQr2 + 4*a*as*c*d*qlQr2 -
    2*as*as*c*d*qlQr2 + Qt2*Qt2*c*c*qt2 + 2*Qt2*a*as*c*c*qt2 +
    a*a*as*as*c*c*qt2 + 2*Qt2*a*a*c*d*qt2 -
    4*Qt2*a*as*c*d*qt2 + 2*Qt2*as*as*c*d*qt2 + Qt2*Qt2*d*d*qt2 +
    2*Qt2*a*as*d*d*qt2 + a*a*as*as*d*d*qt2 + Qt2*Qt2*qt2*qt2 +
    2*Qt2*a*as*qt2*qt2 + a*a*as*as*qt2*qt2);
  aababa=(a - as)*(b + bs)*(Qt2*Qt2*c*c*d*d + Qt2*a*as*c*c*d*d +
    ...
    28 lines omitted
    These formulae are given in Eqs. (B.41) - (B.57)
    ...
  baabaa = -((Qt2 - b*bs)*(Qt2*Qt2*c*c*d*d + 2*Qt2*a*as*c*c*d*d +
      a*a*as*as*c*c*d*d + 2*a*a*c*d*qlQr2 - 4*a*as*c*d*qlQr2 +
      2*as*as*c*d*qlQr2 + Qt2*Qt2*c*c*qt2 + 2*Qt2*a*as*c*c*qt2 +
      a*a*as*as*c*c*qt2 - 2*Qt2*a*a*c*d*qt2 +
      4*Qt2*a*as*c*d*qt2 - 2*Qt2*as*as*c*d*qt2 +
      Qt2*Qt2*d*d*qt2 + 2*Qt2*a*as*d*d*qt2 + a*a*as*as*d*d*qt2 +
      Qt2*Qt2*qt2*qt2 + 2*Qt2*a*as*qt2*qt2 + a*a*as*as*qt2*qt2));

  res = t[0]*aabaab*p1*p1s + t[1]*aabaab*p1*p2s + t[2]*aabaab*p1*p3s +
        t[3]*aabaab*p2*p1s + t[4]*aabaab*p2*p2s + t[5]*aabaab*p2*p3s +
        t[6]*aabaab*p3*p1s + t[7]*aabaab*p3*p2s + t[8]*aabaab*p3*p3s +
        ...
        22 lines omitted
        ...
        t[75]*baabaa*p2*p1s + t[76]*baabaa*p2*p2s + t[77]*baabaa*p2*p3s +
        t[78]*baabaa*p3*p1s + t[79]*baabaa*p3*p2s + t[80]*baabaa*p3*p3s;
  res /= (a*a+Qt2)*(d*d+qt2)*(as*as+Qt2)*(c*c+qt2)*
         sqrt(b*b+Qt2)*sqrt(bs*bs+Qt2);
  res *= sqrt(e3s*e12s*M/e3/e12/Ms);
  return(q*Q*res);
}
```

The C preprocessor directives `#ifdef GAUSS, #else, #endif` give us the possibility of choosing either the Gauss shaped wave function or the Lorentz shaped one by simply

typing the line

```
#define GAUSS
```

or by commenting it out.

The weak vector form factor is calculated in an analogous way; the line

```
o = {{{1,0},{0,1}},{{1,0},{0,1}},{{1,0},{0,-1}}};
```

on page 60 has just to be replaced by

```
o = {{{1,0},{0,1}},{{1,0},{0,1}},{{1,0},{0,1}}};
```

The listings for the calculation for $K^2 \neq 0$ are longer, so we omit them here.

Acknowledgments

It is a pleasure to acknowledge the kind help of the following persons:

- Especially, I would like to thank my advisor *Prof. Dr. W. Jaus* for suggesting the problem of this thesis, for many stimulating discussions, and for carefully reading the manuscript. His advice and criticism proved to be indispensable.
- Furthermore, I am indebted to *Prof. Dr. G. Rasche* for his continuous interest in this thesis and his kind help.
- I would like to thank *Kurt Sonnenmoser* for many helpful discussions about computer problems.
- I am grateful to the members of the Institute for Theoretical Physics of the University of Zurich for the friendly atmosphere.
- Finally, I would like to express my profound gratitude towards my dear *wife* for her encouragement and her interest in my thesis.

This work was supported by the Canton of Zurich and the Swiss National Science Foundation.

Bibliography

[1] M. Gell-Mann. *Phys. Lett.* **8**, 214, (1964).

[2] M. Roos. *Phys. Lett. B* **246**, 179, (1990).

[3] P. G. Ratcliffe. *Phys. Lett. B* **242**, 271, (1990).

[4] A. García, R. Huerta, and P. Kielanowski. *Phys. Rev. D* **45**, 879, (1992).

[5] V. B. Berestetskii and M. V. Terent'ev. *Yad. Fiz.* **24**, 1044, (1976). [Sov. J. Nucl. Phys. **24**, 547 (1976)].

[6] V. B. Berestetskii and M. V. Terent'ev. *Yad. Fiz.* **25**, 653, (1977). [Sov. J. Nucl. Phys. **25**, 347 (1977)].

[7] I. G. Aznauryan, A. S. Bagdasaryan, and N. L. Ter-Isaakyan. *Phys. Lett. B* **112**, 393, (1982).

[8] I. G. Aznauryan, A. S. Bagdasaryan, and N. L. Ter-Isaakyan. *Yad. Fiz.* **36**, 1278, (1982). [Sov. J. Nucl. Phys. **36**, 743 (1982)].

[9] I. G. Aznauryan, A. S. Bagdasaryan, and N. L. Ter-Isaakyan. *Yad. Fiz.* **39**, 108, (1984). [Sov. J. Nucl. Phys. **39**, 66 (1984)].

[10] W. Jaus. *Phys. Rev. D* **41**, 3394, (1990).

[11] W. Jaus and D. Wyler. *Phys. Rev. D* **41**, 3405, (1990).

[12] W. Jaus. *Phys. Rev. D* **44**, 2851, (1991).

[13] P. L. Chung and F. Coester. *Phys. Rev. D* **44**, 229, (1991).

[14] Z. Dziembowski. *Phys. Rev. D* **37**, 778, (1988).

[15] Z. Dziembowski, T. Dzurak, A. Szczepaniak, and L. Mankiewicz. *Phys. Lett. B* **200**, 539, (1988).

[16] Z. Dziembowski. *Phys. Rev. D* **37**, 768, (1988).

[17] H. J. Weber. *Ann. Phys. (N. Y.)* **177**, 38, (1987).

[18] W. Konen and H. J. Weber. *Phys. Rev. D* **41**, 2201, (1990).

[19] S. Godfrey. *Nuovo Cim. A* **102**, 1, (1989).

[20] W. Lucha, F. F. Schöberl, and D. Gromes. *Physics Reports* **200**, 127, (1991).

[21] J.-M. Richard. *Physics Reports* **212**, 1, (1992).

[22] S. Capstick and N. Isgur. *Phys. Rev. D* **34**, 2809, (1986).

[23] S. Capstick. *Phys. Rev. D* **36**, 2800, (1987).

[24] A. W. Thomas and B. H. J. McKellar. *Nucl. Phys. B* **227**, 206, (1984).

[25] P. A. M. Dirac. *Rev. Mod. Phys.* **21**, 392, (1949).

[26] H. Leutwyler and J. Stern. *Ann. Phys. (N. Y.)* **112**, 94, (1978).

[27] L. Susskind. *Phys. Rev.* **165**, 1535, (1968).

[28] S. Weinberg. *Phys. Rev.* **150**, 1313, (1966).

[29] H. J. Melosh. *Phys. Rev. D* **9**, 1095, (1974).

[30] V. L. Chernyak and I. R. Zhitnitsky. *Nucl. Phys. B* **246**, 52, (1984).

[31] G. P. Lepage and S. J. Brodksy. *Phys. Rev. D* **22**, 2157, (1980).

[32] H. Leutwyler and M. Roos. *Z. Phys. C* **25**, 91, (1984).

[33] P. L. Chung et al. *Phys. Rev. C* **37**, 2000, (1988).

[34] B. L. G. Bakker, L. A. Kondratyunk, and M. V. Terent'ev. *Nucl. Phys. B* **158**, 497, (1979).

[35] O. C. Jacob and L. S. Kisslinger. *Phys. Lett. B* **243**, 323, (1990).

[36] J. R. Hiller. *Phys. Rev. D* **41**, 937, (1990).

[37] J. G. Koerner F. Hussain and G. Thompson. *Ann. Phys. (N. Y.)* **206**, 334, (1991).

[38] C. Michael and F. P. Payne. *Z. Phys. C* **12**, 145, (1982).

[39] F. E. Close. *An Introduction to Quarks and Partons*. Academic Press, (1979).

[40] N. Isgur, G. Karl, and R. Konjuk. *Phys. Rev. D* **25**, 2394, (1982).

[41] R. K. Bhaduri. *Models of the Nucleon*. Addison-Wesley Publishing Company, Inc., (1988).

[42] N. Isgur and C. H. Llewellyn Smith. *Phys. Rev. Lett.* **52**, 1080, (1984).

[43] J. Litt et al. *Phys. Lett. B* **31**, 40, (1970).

[44] G. Höhler et al. *Nucl. Phys. B* **114**, 505, (1976).

[45] R. C. Walker et al. *Phys. Lett. B* **224**, 353, (1989).

[46] C.-R. Ji. In M. B. Johnson and L. S. Kisslinger, editors, *Nuclear and particle physics on the light cone*, (1990).

[47] M. Warns, H. Schröder, W. Pfeil, and H. Rollnik. *Z. Phys. C* **45**, 45, (1990).

[48] W. Albrecht et al. *Phys. Lett. B* **26**, 642, (1968).

[49] W. Bartel et al. *Nucl. Phys. B* **58**, 429, (1973).

[50] K. M. Hanson et al. *Phys. Rev. D* **8**, 753, (1973).

[51] R. G. Arnold et al. *Phys. Rev. Lett.* **57**, 176, (1986).

[52] J. J. Hernández et al. Particle data group, review of particle properties. *Phys. Lett. B* **239**, 1, (1990).

[53] N. E. Tupper, B. H. J. McKellar, and R. C. Warner. *Aust. J. Phys.* **41**, 19, (1988).

[54] P. M. Gensini. *Nuovo Cim.* **103 A**, 303, (1990).

[55] J. F. Donoghue and B. R. Holstein. *Phys. Rev. D* **25**, 206, (1982).

[56] A. Krause. *Helv. Phys. Acta* **63**, 3, (1990).

[57] A. García and P. Kielanowski. *The Beta Decay of Hyperons*. Lecture Notes in Physics Vol. **222**. Springer-Verlag, (1985).

[58] A. García. *Phys. Rev. D* **25**, 1348, (1982).

[59] J.-M. Gaillard and G. Sauvage. *Ann. Rev. Nucl. Part. Sci.* **34**, 351, (1984).

[60] M. Ademollo and K. Gatto. *Phys. Lett.* **13**, 264, (1964).

[61] J. Dworkin et al. *Phys. Rev. D* **41**, 780, (1990).

[62] S. Y. Hsueh et al. *Phys. Rev. D* **38**, 2056, (1988).

[63] M. D. Scadron. *Rep. Prog. Phys.* **44**, 213, (1981).

[64] D. Jensen et al. In *Proc. Conf. High-Energy Physics, Brighton*, 255, (1983).

[65] S. V. Belikov et al. *Z. Phys. A* **320**, 625, (1985).

[66] J. Brunner et al. *Z. Phys. C* **45**, 551, (1990).

[67] J. F. Donoghue, B. R. Holstein, and S. W. Klimt. *Phys. Rev. D* **35**, 934, (1987).

[68] W. Jaus and G. Rasche. *Phys. Rev. D* **41**, 166, (1990).

[69] J. A. Thompson et al. *Phys. Rev. D* **21**, 25, (1980).

[70] F. C. Barker, B. A. Brown, W. Jaus, and G. Rasche. *Nucl. Phys. A.* (to be published).

[71] M. Bourquin et al. *Z. Phys. C* **21**, 27, (1983).

[72] M. Ida and R. Kobayashi. *Prog. Theor. Phys.* **36**, 846, (1966).

[73] D. B. Lichtenberg and L. J. Tassie. *Phys. Rev.* **115**, 1601, (1967).

[74] M. Anselmino and E. Predazzi, editors. *Workshop on diquarks*, Torino, 1988. World Scientific, Singapore.

[75] S. Fredriksson. In M. Anselmino and E. Predazzi, editors, *Workshop on diquarks*, Torino, 1988. World Scientific, Singapore.

[76] R. P. Feynman. *Photon-Hadron Interaction.* Benjamin, New York, (1972). p. 150.

[77] F. E. Close. *Phys. Lett. B* **43**, 422, (1973).

[78] A. De Rújula, H. Georgi, and S. L. Glashow. *Phys. Rev. D* **12**, 147, (1970).

[79] C. B. Chiu, S. L. Wilson, and J. Pasupathy. *Phys. Rev. D* **36**, 1553, (1987).

[80] D. B. Leinweber, R. M. Woloshyn, and T. Draper. *Phys. Rev. D* **43**, 1659, (1991).

[81] N. Barik, S. N. Jena, and D. P. Rath. *Phys. Rev. D* **41**, 1568, (1990).

[82] J. Kunz and P. J. Mulders. *Phys. Rev. D* **41**, 1578, (1990).

[83] G. S. Adkins, C. R. Nappi, and E. Witten. *Nucl. Phys. B* **228**, 552, (1983).

[84] J. A. M. Vermaseren. *FORM*, 1989.

[85] S. Wolfram. *Mathematica, a System for Doing Mathematics by Computer.* Addison-Wesley Publishing Company, Inc., (1991).

[86] American National Programming Language FORTRAN. Technical Report ANSI X 3.9, American National Standards Institute, Inc., 1978.

[87] B. W. Kernighan and D. M. Ritchie. *The C Language, Second Edition, ANSI C.* Prentice-Hall International, (1988).

[88] Numerical Algorithms Group Ltd, UK. *NAG Fortran Library Manual Mark 14.*

[89] P. Van Dooren and L. De Ridder. *J. Comput. Appl. Math.* **2**, 207, (1976).

[90] A. C. Genz and A. A. Malik. *J. Comput. Appl. Math.* **6**, 295, (1980).

Index

Ademollo-Gatto theorem
    extension of, 38
Alliant, 57
angular correlation, 32

bag model, 2, 31, 42, 44, 53
Berestetskii, 1
Bethe-Salpeter equation, 2, 3, 6, 55
bound state, 2, 6, 10, 21, 49, 55
bracket[.,.], 60
bremsstrahlung, 33

C, 57
Cabibbo model, 44–46, 55
center of mass motion, 2, 5, 10
charge radius, 19
Chernyak, 16
chiral perturbation theory, 31
Chung, 1, 13
Coester, 1, 13
color, 9
confinement scale, 11, 13
conserved vector current, 42
current-current interaction Hamiltonian, 31

d01fcf, 62, 65
DensityPlot, 64
diquark, 3, 15, 49, 55
Donoghue, 46
Dziembowski, 1

Faddeev equation, 2, 6, 7
FindMinimum, 63
fit, 44, 63
form, 57
FORTRAN, 57

Gaillard, 43
Gell-Mann, 1, 49

Heitler, 2
hyperon decay, 1, 3, 30–46
    angular correlation, 32
    decay rate, 32

Interpolate[.], 63

Jaus, 1

kinematic subgroup, 5
Kobayashi-Maskawa matrix, 1, 3, 31

ladder approximation, 6
lattice simulation, 53, 54
light front, 1–3, 9, 15, 16
    variables, 10

Macintosh, 57
magnetic moments, 1, 13, 21, 27–30, 42, 63
many-particle system, 5
mass operator, 5, 7, 10
Mathematica, 57, 63
Melosh rotation, 1, 10, 42, 57, 60
modified Bessel function, 62
multidimensional integral, 62

NAG, 57
neutron beta decay, 21, 43
nucleons
    diquark clustering, 53
    electromagnetic form factors, 19–24

Poincaré group, 2, 5

QCD spin-spin force, 49
QCD sum rule technique, 16, 53
quark structure, 13, 20, 21, 30, 36

radiative corrections, 33
residual, 44

Sachs form factors, 19
Skyrme model, 53, 54
software, 57
Splice[.], 66
Sun SPARC, 57
symmetry breaking, 31, 38, 42, 44

Terent'ev, 1
transition[.,.], 59

uncertainty principle, 1

vector
    four-vector, 5
    light-front vectors, 5
vertex function, 6, 7, 9

wave function, 2, 7, 12–17
    asymmetric, 15, 49
    baryon octet, 11, 50
    configuration mixing, 14
    from vertex functions to, 9
weak magnetism, 32
Weber, 1

Zhitnitsky, 16